A LOCALIZATION SYSTEM FOR AUTONOMOUS GOLF COURSE MOWERS.

Evgeni Kiriy

Electrical and Computer Engineering
McGill University, Montréal

November 2002

A Thesis submitted to the Faculty of Graduate Studies and Research
in partial fulfilment of the requirements for the degree of
Master of Science

To my family.

Abstract

This thesis outlines the problem of outdoor autonomous robot localization. A comprehensive literature survey develops the place of the Kalman filtering in the general framework of the Bayesian recursive estimation algorithms and describes some of the successful industrial and research autonomous platforms to date. The test vehicles and their pertinent characteristics for the localization problem are discussed. The localization system design process is described showing the necessary compromises that were made in the choice of the platform sensor suit. The extended Kalman filter with measurement gaiting is implemented as a core of the Landmark Density Evaluator and is used to test various localization scenarios. The Evaluator is applied to analysis of combinations of experimental and simulated data. A sensor suite for outdoor robust localization is proposed and partially implemented.

Résumé

Cette thèse décrit le problème de la localisation d'un robot autonome à l'extérieure. Une enquête complète de littérature discute les filtres Kalman par rapport au cadre général des algorithmes récursifs bayésiens et fourni le lecteur avec un résumé de systèmes industriels et académiques concernant ce sujet et celui de la localisation en général. Le processus de conception d'un système de localisation est décrit montrant les compromis nécessaires qui ont été faits dans le choix de capteurs. Le filtre étendu de Kalman avec la mesure "gaiting" est appliqué à un algorithme qui évalue la densité de bornes et est utilisé pour tester de divers scénarios de localisation. L'algorithme est appliqué à l'analyse des combinaisons des données expérimentales et simulées. Une liste de capteurs pour la localisation extérieure robuste est proposée et partiellement mis en application.

Acknowledgements

This work would not be possible without the genuine input of many individuals. I would like to thank:

- Martin Buehler for his patience and guidance, for giving me the opportunity to work in the ARL with its magic combination of great people and machines.
- Sanjiv Singh, Stephan Roth and Parag Batavia for their software expertise and valuable technical input on my work. The experiments with the visual markers became possible because of them.
- Jeff Mishler for doing the video data processing.
- Dana Lonn for general support and encouragement.
- Mark Anderson for consulting me on the mower hydraulics.
- James Smith for introducing me to Latex, electronics discussions, proofreading the thesis, resourcefulness, and his readiness to help selflessly.
- Genevieve Vinois for the administrative support and cheerful attitude.
- Don Campbell for his expert advise on electronics design and software debugging.
- Danny Chouinard for his expert help with Linux and his deep hands-on knowledge of computing and electronics.
- Neal Neville for proofreading the thesis.
- Dave McMordie for his electronics expertise.

- Ioannis Rekleitis for the discussions on MCL localization, the laser experiments, and the modern Greek history.
- Ioannis Poulakakis for the philosophical disputes and monologues, mobile robotics and other discussions, but most importantly his dynamics advice.
- Charles Steeves III for mobile robotics and other discussions and for advising me on a mountain bike selection.
- Neal Wiper for sharing his deep knowledge of electronics and computing.
- Chris Prahacs and Matt Smith for their exemplary engineering work.
- Aki Sato for the stories about Japan and the Japanese characters.
- Ned Moor and other ARLers I had a good fortune to know.
- Alexei Morozov and Svetlana Ostrovskaya for their valuable consultations and recommendations.
- Jakov Gelfandbein for the localization and signal processing discussions.
- Igor Borissov for his English humor, video projects, and many long discussions, technical and not.
- Eliza Maria Haseganu for her teaching dedication and big heart.
- Marlene Grey, Jan Binder, and Cynthia Davidson for keeping CIM operational.
- Angelo Tambasco for generously providing the storage space for the mower.

I would like to acknowledge NSERC and The Toro Company for financially supporting this project. I would like to thank my loving wife Galina Charitonov for assisting in the experiments, editing, entering and verification of the bibliography and her understanding and support throughout this project. I want to specially thank my grandmother Izabella Grebeshenko and my parents Galina Grebeshenko and Anatoli Kiriy for their love, support and advise.

TABLE OF CONTENTS

LIST OF FIGURES

LIST OF TABLES

CHAPTER 1

Introduction

1. Motivation

Turf management in general and golf course maintenance in particular is time and labor intensive and therefore is an attractive area for introducing automation. Recent advances in robotics research and technology make it possible to automate routine golf course maintenance tasks such as daily grass mowing. Autonomous robot mowing may improve the quality and repeatability or variation, if desired, of the mowing patterns, increases the overall control of the operations on the golf course by, for example, gathering visual grass health information and associated location for timely spot-treatment and preventive care (part of The Toro Company's concept of precision turf management [105]), increases the availability of the golf courses by operating at night or at any convenient time, and reduces the operating costs in the long run. Almost all autonomous robotic applications depend on accurate localization for navigation,[1] control, and ultimately for the mission task accomplishment. Golf course mowers operate in an outdoor semi-structured environment where accurate localization is required for efficient area coverage, safety and control. A typical golf course is spread over fifty to two hundred thousand square meters of mildly cross-country terrain: clear patches of fairways and greens surrounded by trees, lakes,

[1]Navigation subsumes all aspects of guiding robot through the environment

and rolling hills[2]. Large and heterogeneous operating area presents the principal difficulty for reliable and accurate localization by a single localization modality and requires multisensor schemes. Commercial application of the system, on the other hand, implies reliability, low cost and integration with the existing infrastructure. A compromise solution that balances the localization system performance and cost has to be found.

The obstacle detection and control algorithms and their implementation for the autonomous mower are presented in the publications of the project's Carnegie Mellon University collaborators [90, 89, 41].

2. Author's Contribution

The purpose of this thesis is to investigate various possible solutions to the robust outdoor localization problem and apply conventional technologies to the proof of concept localization system. Issues related to sensor fusion in the Kalman filter framework and various sensor configurations are discussed.

- A localization testbed Toby-2 (see Chapter 3) is instrumented with the localizztion sensors.
- A Landmark Density Evaluator is developed (see Chapter 5 and Appendix B.)
- Field testing of the various localization sensor suites is performed (see Chapter 6.)
- An outdoor localization system composed entirely of off the shelf components is proposed (see Chapter 7.)

3. Structure of the Thesis

The thesis is organized as follows.

Chapter 2 presents the problem of mobile robot localization. It develops the place of the Kalman filtering in the general framework of the Bayesian recursive estimation

[2]The different terrain types are shown in Figure 1.1

(a) Bird's eye view

(b) Flat terrain

(c) "No Go" areas

(d) Hilly terrain

(e) Tree cover overhead

FIGURE 1.1. Golf course terrain types [21, 22, 23] (a) The bird's eye view of the fairway and the green. (b) The flat portion of the green bordered by trees. (c) The part of the course with multiple obstructions: the brook, the pond, the large rock and the bridge itself. (d) The hilly part of the fairway with steeply banked sandtraps. (e) The portion the fairway with overhanging branches.

algorithms and describes some of the successful industrial and research autonomous platforms to date. Chapter 3 discusses the mower platforms used in the experiments and their pertinent characteristics for localization. Chapter 4 describes the hardware and the extended Kalman filter implementation for localization data fusion. Chapter 5 describes the Landmark Density Evaluator used for the evaluation of the sensor architectures. Chapter 6 shows the application of the Landmark Density Evaluator to the localization data analysis. Chapter 7 presents the conclusions and sensor suite design recommendations.

CHAPTER 2

Literature Survey

1. Localization

Mobile robots are becoming a more significant segment of the field of robotics. An autonomous mobile robot needs the ability to estimate its pose (position and attitude) in order to navigate and perform required tasks. Localization is the process by which the robot determines its pose on the basis of the sensory measurements. The desired minimum accuracy of localization is dictated by the application, while the attainable accuracy depends on a complex interaction of individual sensor accuracies, sensor types, system dynamics[52], localization algorithms[38], and even trajectories to be taken[57], among other factors. Accurate localization is a primary requirement for any autonomous system and the design of an adequate localization system in terms of accuracy, cost, and other design criteria is a nontrivial task. For the terrestrial navigation, however, the planar subset of the pose - the Cartesian position and orientation - is often sufficient for mobile robot localization. Localization sensing approaches can generally be subdivided into relative and absolute by the type of the sensor devices used.

1.1. Relative Localization. Relative localization (RL), often called Dead Reckoning (DR), provides localization solution by *integrating* the available proprioceptive measurements, usually obtained from quadrature wheel encoders, gyroscopes,

and accelerometers. The relative sensing is self-contained and allows high accuracy and high bandwidth for short-term localization. However, inherent dead reckoning signal integration results in an unbounded error accumulation, which precludes the use of relative sensing as a sole mean of localization for autonomous robots - there is no error recovery mechanism in dead reckoning [1]. Dead reckoning may also be viewed, in terms of control theory terminology, as an open loop (OL) localization.

1.2. Absolute Localization. Absolute localization (AL), provides the localization solution based on the exteroceptive sensing of current environmental features or landmarks and without using the previous sensor information. The measurements are taken in the absolute coordinate frame directly. In general, the localization problem is solved if every position in the environment could be marked in a distinct way. On the other hand the robot's position in an absolute frame can be deduced from sensing a finite number of fixed environmental landmarks. The accuracy of the absolute localization is time-independent and is bounded by sensor accuracy and bandwidth; however it is sensitive to both the geometrical arrangement of the landmarks with respect to the robot and the changes in the environment [74, 55, 101, 80] that degrade or prevent landmark sensing altogether. Any machine-recognizable element can play the role of the landmark, natural[2] (the trees, boulders or other protruding (positive) movable and immovable obstacles on the ground[53, 63, 72], or stars in the sky[24]), or artificial (GPS or other navigational satellites, radio beacons, high visibility video or laser beacons and markers, magnetic markers, or a guide path [3]) Absolute position of the landmarks may be known to the robot, in which case it "only" has to identify

[1]Deduced or dead reckoning is the process of estimating position using heading, speed, time and distance traveled. The unforgiving nature of this localization technique is illustrated by the saying "you're dead if you don't reckon right" which possibly gave it is popular name – dead reckoning.

[2]There are two distinct natural landmark representations in the localization: dense sensor representation, in which a feature is described by its raw sensor impression[71], and the topological representation, in which a feature is described by a simple geometrical shape extracted from the raw sensor data[84].

[3]A mobile robot may resort to the use of a conventional visible, electromagnetic, or magnetic guide path if need be; the localization principle reappeared in the form of olfactory navigation of indoor robots [91], currently possible in almost "clean room" environments, in the along-the-edge-of-the-crop navigation of the harvester [78], and in highway lane following by tracking dicrete embedded magnets [113].

the perceived markers and localize itself with respect to them. The more difficult problem is localization with respect to unsurveyed landmarks. Thus the robot has to localize the perceived landmarks first (i.e. to build the local map with the observable features) and simultaneously use it in its proper localization. This approach is called Simultaneous Localization And Map building (SLAM) [72, 30, 71, 84]. A robust SLAM solution is highly desirable since it would allow the use of unsurveyed landmark grid and could naturally accommodate any changes to it due to loss or addition of the landmarks [28]. Currently only localization techniques that rely on the known artificial landmarks provide sufficient accuracy and reliability for the commercial outdoor localization.

2. Sensor fusion

Both relative and absolute localization approaches can be used with an advantage if properly combined. High fidelity and bandwidth localization can be obtained by merging measurements from the high-bandwidth relative and low-bandwidth absolute sensors. The absolute localization observes, directly or indirectly, at least part of the robot's pose and therefore is used as a feedback that bounds the relative localization error. Combining the sensor measurements from the relative and absolute localization systems results in redundancy of at least some of the information. The process of extraction of the desired estimates from redundant measurements is called sensor fusion. The fusion process can be done in the time or frequency domains. Fusion in the time domain is a switching procedure between the redundant inputs, so that the most "trustworthy", according to some, possibly heuristic, criterion measurement is used in the localization solution[34]. Fusion can also be accomplished by classical

frequency domain filtering [4] or recursive Bayesian estimation algorithms [5] which, in principle, can be considered as frequency domain filters. Some representative localization algorithms from the Bayesian estimation family are going to be briefly introduced in the following paragraphs.

2.1. Bayesian Recursive (Sequential) Estimation applied to localization. Raw sensor readings are often too noisy and inaccurate to be directly used for localization. Moreover, the sensors usually do not provide the information of interest directly. However, prior knowledge about the process is usually available and the initial belief can be represented in terms of prior distributions of the unknown quantities. As the new data from measurements arrives, its likelihood function is combined with the prior probability density function according to Bayes' theorem [4, 9] and the posterior distribution is obtained. Motivation to use the recursive (or sequential) estimation methods is given by the time-sequential nature of observations that require increasing amount of storage space and processing time for batch estimation. It is desirable to process the measurements on-line and shed the processed data immediately hence keeping the data storage and computational effort to minimum. The estimated quantity is obtained along with its estimation error measure in the form of full error probability distribution or its moments, depending on the algorithm. The system model in these algorithms infers the information that may be not directly measurable (but observable.) The general prediction-correction leitmotif is seen in all algorithms. Prediction phase: the process model estimates the system state open loop; Correction phase: the estimate is corrected by merging it with the measurement, thus closing the loop. As a result the recursive estimation algorithms

[4]The classical frequency domain filtering can be applied [33], for example, the fusion of heading from a fluxgate compass (a low bandwidth absolute measurement reliable at low frequencies) and a rate gyro (a high bandwidth relative measurement reliable at moderately high frequency, but exhibiting a slow drift at low frequencies). A complimentary filter [9] can be designed to attenuate the compass at high frequencies while letting the more reliable gyro rate pass.

[5]there exist many recursive estimation algorithms, but only Bayesian approach (nonlinear filtering) - to which extended Kalman filtering and Sequential Monte Carlo methods belong - offers a formal solution to the problem [67, 26].

distill raw measurements so that higher accuracy and reliability of information is attained.

2.1.1. *The Extended Kalman Filter.* The extended Kalman filter (EKF) is a nonlinear generalization of a linear Kalman filter [6] [83, 9] . The EKF has been used for over four decades in such applications as missile tracking and guidance, marine and aeronautical navigation, as well as for the localization of the indoor and outdoor mobile robots [27]. The extended Kalman filter maintains the same compact error distribution representation as the linear Kalman filter and thus is computationally efficient. The first order[7] linear KF framework requires that the Jacobians of the non-linear system and measurement equations be evaluated at the state estimate. It is assumed that the filter will maintain the estimate close to the true state so that the linearization will remain valid. The Jacobians substitute the system and measurement matrices in the KF algorithm. Since the assumption above is not guaranteed to hold and due to bias introduced by the nonlinearity of the system, EKF estimates can be suboptimal or even diverging [9] *i.e.* giving an unbounded estimation error. The filter error covariance[8] as well as the covariance of the innovation sequence has to be constantly monitored to prevent unrecoverable divergence [10, 66, 65]. The error probability distribution[9] is not limited to Gaussian, with no pretence on optimality. The filter however can only accurately model single-mode distributions due to its modest (mean and variance only) distribution representation vocabulary. The EKF

[6]The Kalman filter [83, 9, 81, 3] (KF) is *the optimal recursive linear minimum mean square error estimator* that models the uncertainties of the estimated random variables by their means and variances. Such a compact representation of the state error probability distribution makes the algorithm computationally efficient. At the same time, since the noise variables are assumed to be zero mean Gaussian [4] , the above error representation models the distribution exactly[9].

[7]Second order KF makes use of the second term of the Taylor expansion and calls for calculation of Hessians in addition to Jacobians.

[8]The terms *covariance of the state* and *covariance of the estimation error* are equivalent because the state estimate is a conditional mean.

[9]Gaussian error distribution is primarily used to model the spatial uncertainty for traditional wheel locomotion. "Maximum range" distribution can be used in the legged locomotion process modeling where an equal probability is assigned to all positions between the current and commanded positions and zero probability is assigned for all other positions. A "kidnapped robot" process is modeled by a uniform distribution with a spike at the last estimated position. The uniform portion represents the unknown position of the robot in case it is kidnapped, while the spike reflects the belief that the robot will not be kidnapped[38].

is widely used in mobile robotics to estimate the pose of the vehicle [42, 65, 17]. Multiple filters (filter banks) are required[10] for multiple hypothesis testing.

2.1.2. *Markov Localization.* Markov localization (ML) methods estimate the robot's position by discretization of the space of the possible robot positions. The probability distribution of the robot position[11] is approximated by assigning an "occupancy" probability to every point of the discretization. The successive prediction grids are combined (by element-by-element multiplication, for example) with the measurement grids using Bayes' rule[37, 38, 56]. Global search space of the ML algorithm makes it robust. At the same time global search space becomes prohibitive for large areas and/or small grid resolutions.

2.1.3. *Monte Carlo Localization.* Monte Carlo localization [26] (MCL) or *particle filtering* family of algorithms represent the position probability distribution by a finite (on the order of tens to tens of thousands [38, 84], depending on localization system[12] weighted samples. A general MCL algorithm consists of the following steps: *Initialization, Importance Sampling, Selection*, and *Markov Transition.* Particle filter is usually *initialized* to a uniform distribution (to reflect total initial localization uncertainty) with equal *importance weight* assigned to every particle. The sequential operation begins with the *Importance Sampling step* in which the particles are weighted according to the probability distribution of the measurement and then resampled, so that the total particle weight is unity. In the *Selection step* the particles with large importance weight are multiplied while the particles with the low weight are discarded, so that the total number of particles remains the same. The sequence is closed by the *Markov Transition step* in which the particles are propagated according to the process model (dead reckoning, for example). Any kind of distribution can be represented by MCL in its discrete model, making it robust, but is less computationally intensive than ML. Moreover, the computational intensity remains the

[10]The recently developed Combined Bayesian hypothesis testing and Kalman filtering [48] technique allows to do Multiple Hypothesis Tracking with a single EKF.

[11]The multidimensional ML that includes heading or even the full pose is possible but is extremely computationally expensive[39].

[12]Here localization system denotes the interaction of sensors, system dynamics, and environment

same irrespective of the localization area – only the particles with large emphimportance weight are maintained by the algorithm - making it suitable for the outdoor navigation. [56, 100, 37]

2.1.4. *The Distribution Approximation Filter.* The Distribution Approximation Filter (DAF) [51] is another generalization of the Kalman Filter for nonlinear systems. The method combines the analytical KF and the numerical MC approaches to approximate the process and observation models. As opposed to the MCL, the DAF algorithm chooses the samples of the distributions deterministically. Nonlinear, instead of linear covariance transformation is performed that insures the unbiased and converging filter performance.

2.1.5. *Combined Markov Localization and EKF.* Recently several hybrid methods, combining both EKF and ML were developed. Combined Bayesian hypothesis testing and Kalman filtering [48] and ML-EKF [38] allow Multiple Hypothesis Tracking (operate on multi-modal probability density functions) to be done, and thus it does not to discard even inconclusive landmark information[13] until clarification becomes possible. The new framework also treats the absence of the new observations as information useful for elimination of weak hypothesis and thus keeping the overall number of hypothesis small.

2.1.6. *Localization Techniques Summary.* The traditional EKF appears to be the most efficient and very precise, but at the same time the most sensitive to the sensor noise method. Sequential (recursive) Monte Carlo and Markov localization methods are more robust (since they model the whole probability distribution, and not just approximate it with a covariance matrix) but less accurate than EKF. With the development of the highly robust combined methods that improve the robustness of the EKF, these algorithms seem to be the most desirable. However they are only at the initial stages of development and are not efficient for high dimension

[13]Inconclusive information is rejected by the uni-modal (presumably Gaussian) distribution assumption in the regular KF framework. Bayesian hypothesis testing (ML) is applied to merge the KF displacement estimates with the discrete landmark measurements. Until recently multi-modal representation in the realm of Kalman filtering was accomplished by using multiple Kalman filters (filter banks) operating simultaneously with a filter for each mode – computationally intensive.

or for large area sensor fusion [39]. Thus Markov localization algorithms are not suitable for localization over large areas – a must for an outdoor robot – leaving the tested arsenal of Kalman filtering techniques and relatively novel MCL approach. Overall the algorithms give comparable precision and require tuning for best results. It should be noted that filter robustness [10, 9, 66] only guarantees consistency of the filter state error estimates (covariances for KF or probability distributions for MCL) under all realistic measurement conditions but does not affect the localization accuracy – the main goal of the mobile robot localization. The filter works on noisy and sometimes biased sensor measurements[14] and signal processing algorithm cannot substitute for the quality of the raw sensor data, it can only make the best (in terms of some optimality criterion) out of the information it is supplied. Should the robot find itself with the localization estimate accuracy significantly below the desired limit and thus potentially not following the specified trajectory, the robustness of the low accuracy estimate – so valuable from the theoretical point of view – becomes of no avail from the practical, user's point of view. The localization system – the sensor suite and the measurement processing algorithm – should be designed in a such a way that the required pose estimation accuracy is maintained at all realistic operating conditions robustly. The explicitly distinguishable (cooperating) artificial landmarks approach[56] eliminate the complex data association problem and allow using relatively simple and computationally efficient algorithms, EKF for example.

3. The Vehicles and Their Localization Systems

Recently a few robotic systems have become commercially available or are rapidly approaching the requirements of a commercial product, in difference to being strictly research platforms. Some of the systems that can localize themselves, even roughly, will be considered in this section. Some of the representative contemporary applications and the research platforms are discussed. A necessity for the development of a robust absolute localization system for autonomous mobile robot navigation, as

[14]The filter may also be working open loop (without exteroceptive observation) most of the time due to unavailability of landmarks.

well as the possibility of application-correlated simplifications is inferred from the discussion.

3.1. Commercial Platforms. **iMow** manufactured by The Toro Company[107] (see Figure 2.1) is a household autonomous mower based on a differential drive platform. The removable 24-volt lead-acid battery pack positioned between the driving wheels is sufficient for over two hours of autonomous operation with the maximum speed 0.5 m/s. iMow senses the magnetic field created by the perimeter wire with two Hall effect sensors located in the front of the mower and stays within the staked out area. The mowing starts by following the perimeter wire; once the perimeter is trimmed along, the rest of the lawn is covered in a zigzag pattern[15] changing the direction of motion every time the perimeter wire is sensed (see Figure 18.) The absolute localization is limited to orientation sensing via the electronic compass, sensing the work area boundaries, and bumper tactile sensors while the relative localization is done by dead reckoning with hall effect wheel encoders. Manual control of the mower is possible with the *operator control unit* (OCU)[16] (see Figure 2.1.)

Intelecaddy manufactured by GolfPro International (USA) [70] (see Figure 2.2) is a robotic golf club toter that follows the golfer and avoids impassable and restricted (greens, for example) areas by comparing the GPS-derived position with the map of the environment. The caddy is equipped with a cemi-circular ultrasonic array that establishes the direction to the pager-sized ultrasonic beacon/OCU worn by the golfer. The pursuit behavior can be stopped and resumed from the OCU. The two absolute sensor modalities (ultrasonic sensors and GPS) available to the robot are exploited as follows [17]. The robot follows the golfer in a *pure pursuit* manner , that is it tracks the desired trajectory directly using the ultrasonic sensor array[18] The robot

[15]In order to use an area coverage scheme with less overlap iMow has to localize with precision higher than is achievable with the existing sensor suit.

[16]The wired operator control unit is located in the docking port on top of the mower plastic shell. It can be removed from the dock for manual control of the mower.

[17]The following is the author's opinion. Official information was unavailable at the time of publication.

[18]Each of the ultrasonic sensors provides the range, while the signal strength distribution between the sensors in the array resolves the heading to the waypoint.

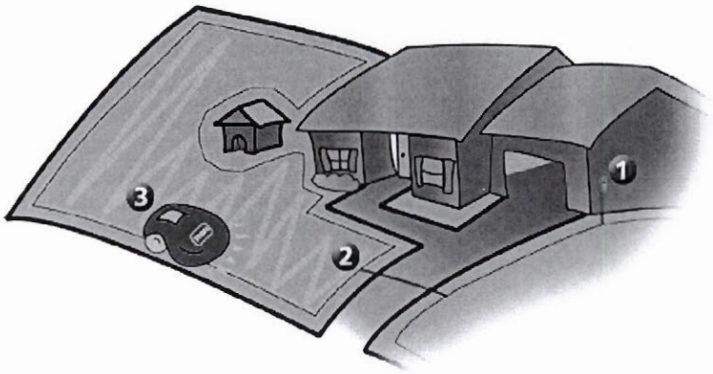

(a) Yard installation: 1 - perimeter switch, 2 - perimeter wire, 3 - iMow inside the perimeter

(b) iMow

(c) The operator control unit

FIGURE 2.1. iMow design and functionality [107]

tracks the cooperative waypoint (beacon) absolutely and requires fused DR (from the wheel encoders) and GPS position estimates only in order to discriminate between the allowed and restricted areas. GPS could also become useful for this "carrot following" navigation if the waypoint (the "carrot") had an independent GPS. The vector defined by the positions of the robot and its master would define the range and heading for the pure pursuit. The pursuit vector will be calculated in the virtually differential mode since similar absolute errors will be incurred by both receivers in close proximity to each other; the GPS position uncertainty, however, would have to be small with respect to the look-ahead distance chosen for the pursuit algorithm.

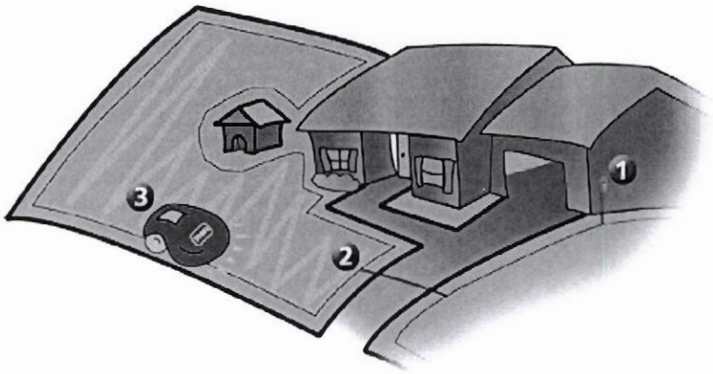

(a) Yard installation: 1 - perimeter switch, 2 - perimeter wire, 3 - iMow inside the perimeter

(b) iMow

(c) The operator control unit

FIGURE 2.1. iMow design and functionality [107]

tracks the cooperative waypoint (beacon) absolutely and requires fused DR (from the wheel encoders) and GPS position estimates only in order to discriminate between the allowed and restricted areas. GPS could also become useful for this "carrot following" navigation if the waypoint (the "carrot") had an independent GPS. The vector defined by the positions of the robot and its master would define the range and heading for the pure pursuit. The pursuit vector will be calculated in the virtually differential mode since similar absolute errors will be incurred by both receivers in close proximity to each other; the GPS position uncertainty, however, would have to be small with respect to the look-ahead distance chosen for the pursuit algorithm.

FIGURE 2.2. Intelecaddy by GolfPro International [70]

HelpMate [82] by Pyxis Corporation (USA) (see Figure 2.3 is a differentially driven robotic courier for the hospital environment. The robot is equipped with a rich sensor suite for navigation and interaction with the manned and structured hospital environment. The human interface is composed of the LCD display with a telephone-style keypad, manual steering handles, three emergency stop buttons positioned for easy accessibility about the robot, and turn signals. The two forward-directed infrared strobe lights and the contact bumper wrapped around the robot's base are used for obstacle detection and avoidance. The sensors that follow can all be used for localization/navigation purposes. The ultrasonic sensors – eighteen primary, positioned on the front and side panels of the robot, and six secondary transducers on the bumper - provide object detection in the front and to the sides of the robot. Wall following, as well as more sophisticated *dense sensor matching* localization or *topological navigation* (see section 1.2) can be achieved by the use of the sonar sensor. The video camera in the circular opening of the front of the robot is directed along the direction of motion and registers distant (over six feet away) obstacles [19]. The robot communicates with the other robots and possibly with a master station via a wireless radio frequency (RF) Ethernet modem whose antenna placed on top of the robot. The Ethernet link is also used to control the hospital elevators. The strength

[19]The obstacle identification is possibly done by combining the angular measurements from video with the sonar range scans for the range overlap interval of the two sensor modalities.

of the RF signal received from an identifiable stationary Ethernet hub (hub's ID encoded in the message) can also be used as a measure of distance to the surveyed hub location [7] for subsequent *trilateration*[20]. The infrared (IR) transmitter controls the automatic doors. It can also be used as a beacon to be localized in the stationary video cameras [21] positioned along the robot's workspace.

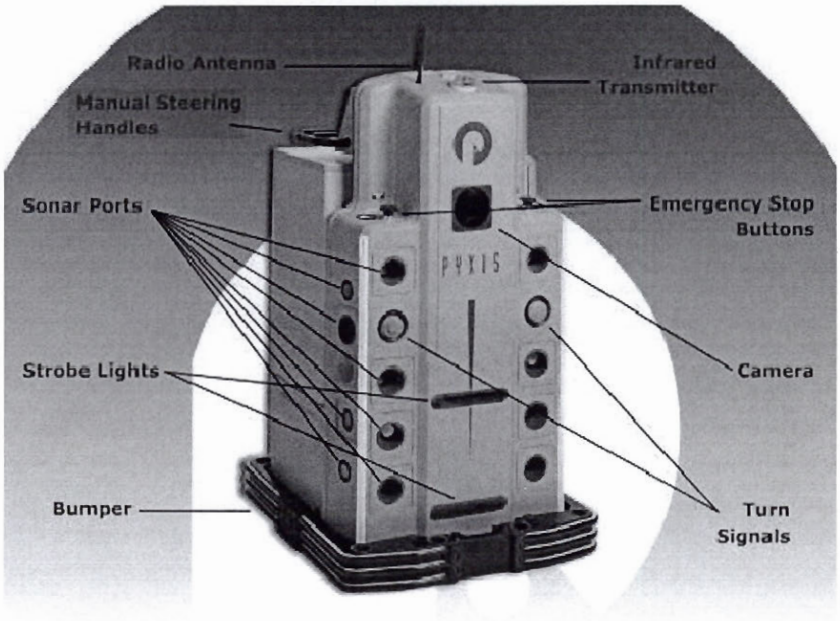

FIGURE 2.3. HelpMate by Pyxis Corporation [82]

AutoVacC 6 manufactured by ROBOSOFT (France) depicted on Figure 2.4 is an autonomous industrial vacuum cleaner [87] on a differentially steered platform that can be operated remotely (for dangerous areas or white room cleaning.) The desired path is taught by example via a joystick. Ultrasonic sensors positioned in the openings around the perimeter of the robot are used for dynamic obstacle avoidance [22], while the optical wheel encoders and the laser range finder are employed for the

[20]Trilateration - the localization of an unknown point by calculations involving *distance measurements* to distinguishable and localized landmarks.

[21]Infrared filters can be successfully used indoors, in the areas with no direct sun light, to simplify the image processing - the infrared diode/beacon is seen as a bright spot on the grayish ambient IR background.

[22]The range of the ultrasonic sensors is insufficient for detection of walls or columns in the large indoor spaces, thus these sensors are used for the obstacle avoidance only.

relative (DR) and absolute localization respectively. The fused measurements result in robust localization in structured environments (airports, shopping centers) that allows efficient (with minimal overlaps) floor coverage. The maximum speed of the platform is $0.75m/s$.

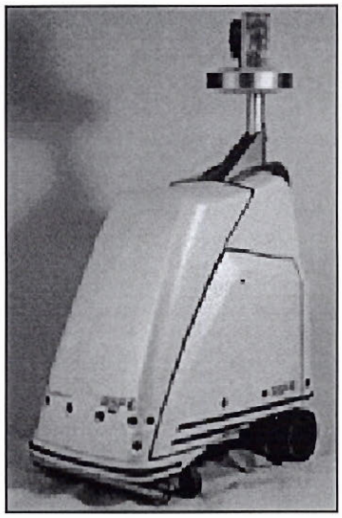

FIGURE 2.4. AutoVacC 6 by ROBOSOFT [87]

The Automation Kit [86], by the same company (ROBOSOFT) allows to automate the mass-produced manned machines without alteration of the original design. Due to security and legal concerns the automated heavy equipment will remain human driven during the day, when the traffic in the work area is at its peak, demanding fail-safe (unrealistic, for the time being) obstacle avoidance system. The machines are operated in the autonomous mode during the night, in the minimally populated [23] environment (see Figure 25.) The different trajectories and phases of the work cycle are recorded when the platform is in the manual mode with the help of the joystick and programming console. The recorded trajectories are played back in the autonomous mode. The kit consists of the following modular components depicted on Figure 25: A - the programming console, B - tactile bumper (0.25 m extended beyond the frontal extremity of the vehicle), C - low-range (0.5 to 4 m)

[23] "People are typical obstacles. Because they are difficult to label, they are detected by onboard sensors."[40]

laser rangefinder, D - programming joystick, E - sonar obstacle detection array (up to 0.5 m), F - side-mountable low-ranege laser rangefinder. The laser rangefinders require the use of retro reflective markers (0.40 m wide and 0.12 m tall) approximately every 10 m. Five-centimeter accuracy is achieved in the structured indoor (smooth concrete floors) warehouse environment at the maximum speed of 0.55 m/s.

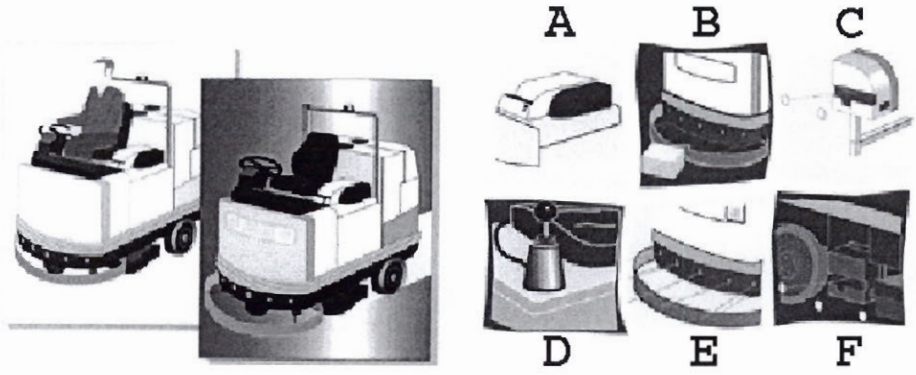

(a) Day and Night operation. (b) Modules.

FIGURE 2.5. The Automation Kit by ROBOSOFT [86]

NY city Vehicle Integrated Navigation System developed by the Fibersense Technology Corporation integrates INS and GPS for bus localization in urban environments. According to the Americans with Disabilities Act the location of the upcoming bus stop must be announced in city buses. In practice transit personnel are reluctant to alert the passengers. In order to improve the dependability of announcement service it was decided to develop an automatic passenger notification system. As a side benefit of automation the status of the buses is available at each bus stop [45]. The "urban canyon" environment of New York City is very challenging for GPS blockage and multipath. Unaided GPS is not suitable for the bus localization with the accuracy required for the error-free passenger notification. The GPS was augmented by the MEMS[24] gyro and the vehicle odometer in the EKF framework. Filtering the raw GPS range and range rate measurements from the proprietary GPS

[24]Micro-Electro-Mechanical System

message and immediate rejection of the outlier data from individual satellites allows to improve localization accuracy to the desired [25] (unreported) accuracy. The authors emphasize that a moving platform can benefit from the intermittent GPS fixes, say at intersections, when the view of the sky improves in the direction transverse to the direction of motion.

In 1999 Australian Centre for Field Robotics (ACFR) in partnership with Patrick Stevedores completed an **automated straddle carrier** for automated container handling at seaports. The 65 ton carrier shown in Figure 2.6 and has a top operating speed of 30km/h. For increased robustness and automatic fault detection in the localization system it employs twin-redundant guidance using GPS/INS and MMWR[26]/encoder system [99]. The project is wholly industry-funded and geared towards commercialization by the world's largest straddle carrier manufacturer, Kalmar Industries of Finland.

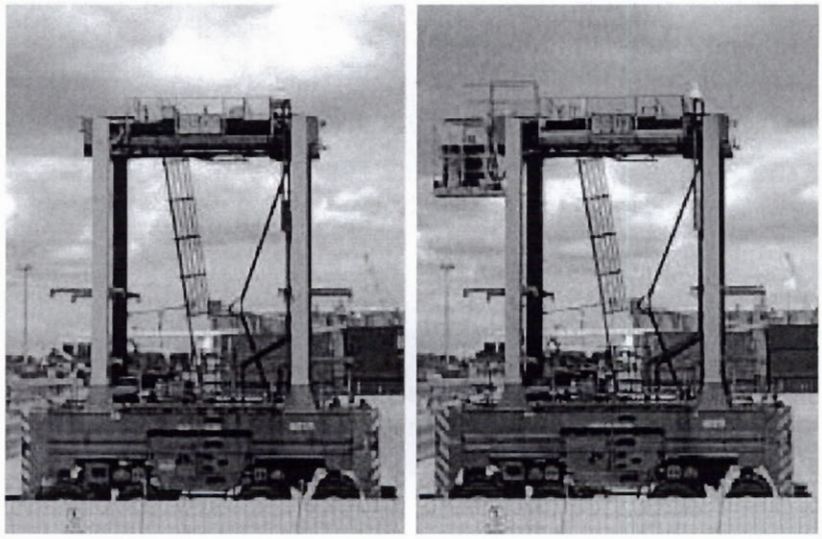

FIGURE 2.6. The autonomous straddle carrier: left – autonomous, right – prior to automation, with the driver's cabin [28]

The Centre has also developed other automated vehicles in the past, including the **autonomous flatbed** (See Figure 2.7) for cargo handling applications [42]. The

[25] As it is the case with the suboptimal estimation, extensive filter tuning and application of heuristic procedures was required to achieve the desired system performance.
[26] MilliMeter Wave Radar

unique millimeter wave radar that was developed for the project is the heart of this system, as well as the subsequent successful field implementations of the ACFR. The flatbed is 15 m long, 2.9 m wide, and 1.6 m high; it weights 17.5 tonnes and can carry a container load of 60 tonnes. The vehicle has front and rear steer geometry a diesel-hydraulic drive and steering systems. To maintain mechanical invariance for the forward and backward motion the vehicle was designed diagonally symmetric, with one driving and one encoder-instrumented wheel on each axis. GPS does not operate reliably in the container yard due to strong multipath from the large metal surfaces and complete satellite occlusion in the aisles. A MMWR was developed to sense trihedral markers with a physical area of 20 cm^2 [27] up to a distance of approximately 200 m. The large operating range and the excellent detection rate (80%) allow for a relatively sparse marker placement and reliable range and bearing measurements. The localization is achieved in the Kalman filter framework by fusion of the radar absolute measurements with the model of the vehicle (DR) driven by odometry[28] input supplied by wheel encoders and steer encoders. Centimeter-level localization accuracy is consistently achieved by the system.

The sensor suites of the aforementioned commercial robots always consisted of the relative (wheel encoders) and absolute (compass, GPS, Hall effect transducers, laser rangefinder, ultrasonic transducers, video camera) sensors. There are devices already present on the robots, but not presently used for localization – infrared transmitter, RF Ethernet modem – that could be incorporated into the localization sensor suite for greater sensing redundancy and thus increased reliability and accuracy of localization. HelpMate, AutoVac, and Automation Kit contain the most typical sensors and attain the centimeter-level localization accuracy of the best academic research platforms discussed in the next section.

[27]The apparent radar cross section of the 20 cm^2 Retroreflective trihedral is 100 m^2. A special polarizing grid on the trihedrals allows them to be distinguished from each other by the radar. Thus the return signal strength and ambiguity resolution are embedded in the design of this marker system.

[28]Inertial sensors are not used on the vehicle.

FIGURE 2.7. The Autonomous Guided Vehicle [42]

3.2. Research Platforms. S. Scheding *et.al.* describe the development and experimental validation of a guidance system for an **autonomous Load, Haul and Dump truck** (LHD) [95]. A typical articulated vehicle is shown on Figure 33. The localization sensor suite [96] is composed of the relative (proprioceptive) and absolute (exteroceptive) localization sensor groups. The relative sensors of the LHD are discussed below. The odometry group of sensors includes a potentiometer and wheel encoders. The articulation angle of the platform is directly measured by a potentiometer, and the encoders measure the wheel velocities - the cheapest way of obtaining the DR. The strap-down[29] INS sensor suit is composed of sealed sensors, well suited for the dusty underground environment, and consists of a triaxial accelerometer and four gyroscopes. The gyroscopes are dissimilar; the more accurate units measure the critical, for terrestrial navigation, yaw rate, and the less accurate ones (with

[29]The strap-down system is attached to the vehicle directly and follow its rotations. Thus the attitude of the gyros and accelerometers changes continuously with respect to the navigation reference frame and a "software gimbal" - the algorithm that would maintain the orientation of the navigation reference frame - is required to determine the body's roll and pitch with respect to the gravity vector and to discriminate between the linear and angular accelerations. In difference to the strap-down system, the gimbaled system is actively stabilized so that its attitude remains constant with respect to the navigation reference frame. The gyros and accelerometers mounted in such a system will preserve their orientation irrespective of the rotations of the vehicle, which in turn simplifies the navigational calculations. The downside of such an arrangement is its complexity and resulting lower reliability. [9, 54]

higher drift) measure the roll and pitch. The initialization of the INS is accomplished when the platform is stationary by determining the pitch and roll of the vehicle with respect to the navigation reference frame by means of the accelerometers installed on the platform. Since the sensors drift with time, temperature and are affected by the engine-induced vibrations a calibration filter needs to be implemented to reduce the attitude errors. The proposed filtering scheme is similar to the complimentary filter [9] discussed in Section 2. Here the low-frequency attitude is obtained from the low-pass filtered accelerometer data, while the high frequency attitude is provided by the gyros. Shaping filter may be used to model and reject the low frequency errors in the gyro information [95]. The absolute sensors of the LHD are discussed below. Two time-of-flight (TOF) range and bearing laser scanners: the rotating 360^o Guidance Control Systems (GCS) laser [30] and two solid state SICK 180^o -sweeping time-of-flight rangefinders arranged to cover 270 degrees with 90 degree overlap. The out-of-plane laser arrangement together with the forward motion results in a 3-D model of the environment, potentially useful for obstacle avoidance [96, 41] Two sets of ultrasonic sensors detect gross changes in the environment and can be used to detect side tunnels, for example. These sensors have short range and are suitable for wall following or obstacle detection at close range only (usually less than 10 meters). The data from each sensor is individually time stamped so that asynchronous measurements could be correctly fused in time by the extended Kalman filter. The experiments revealed that the no-slip assumption is not valid for the heavy underground vehicle and that a kinematic model that explicitly account for the slip by including an unobservable front and rear slip angles into the estimated state gives consistent results. The authors also note that the effective wheel radius is a variable parameter for the vehicle, that depends on the loading and tire wear [31]. The variation of the effective radius can also be attributed to slip. The dynamic evaluation of the unobservable slip angle and effective wheel radius results in overall improvement of localization accuracy.

[30]Retroreflective tape markers are used in conjunction with the GCS laser scanner.

[31]Loading and tire wear are just some of the parameters affecting the effective wheel radius; soil sinkage, vehicle velocity, and attitude are other important factors. [47, 93, 58]

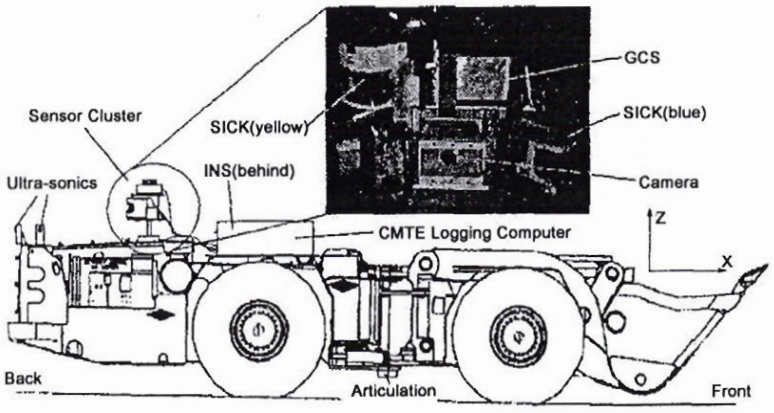

(a) LHD used for the trials

(b) A Typical LHD: Atlas Copco Wagner ST1510

FIGURE 2.8. LHD and its sensor suit [96, 1]

The **Polar Bear** [97] shown in Figure 2.9 on page 21 is an all-terrain spooler platform that employs visual and ultrasonic SONAR sensors to follow a person outdoors at speeds of up to 5 km/h. The robot determines the range and bearing to the person's distinctly coloured vest and SONAR beacon array. The system's behaviour is similar to that of *Intellecady* (see page 14) pursuer.

The **Navigation Test Vehicle** (NTV) of the University of Florida [73] is a Kawasaki Mule ATV shown in Figure 2.10 on page 21. The accurate position and orientation are obtained via a Kalman filter that integrates the INS (Honeywell MAPS) with the Differential Global Positioning System (Ashtec RTKGPS) (RTKGPS) [32]. The position data is accurate to within 6 cm (1 σ) at a rate of 10 Hz. The positional

[32]The localization system costs approximately US $130,000 in 2000.

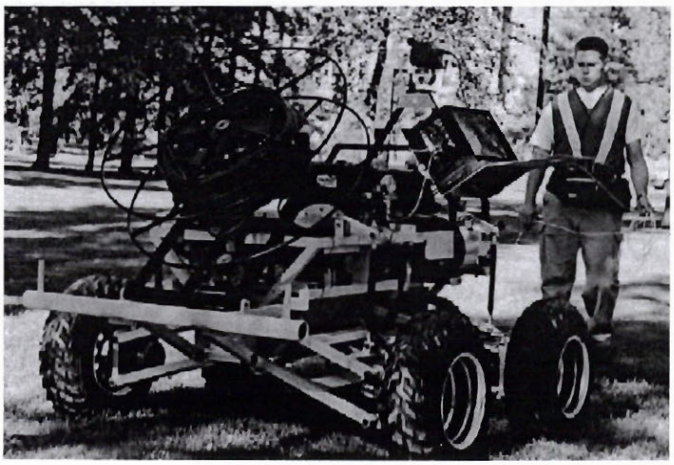

FIGURE 2.9. The Polar Bear in pursuit [97]

accuracy is maintained for a short period of time when the DGPS signal is lost due to satellite occlusion by a tree or a tall building.

FIGURE 2.10. Navigation Test Vehicle, University of Florida [73]

Jay A. Farrell describes a **Magnetometer and DGPS aided INS** system [113] for structured highway environment augmented by magnetic beacons. The robust lateral control of the vehicle is achieved in the Kalman filter framework using a strap-down INS, DGPS, and Magnetometer. A series of 2.5 cm in diameter and 10 cm long ceramic magnetic bars were buried vertically at 1.2 m intervals in the field tests. The magnetic guide path tracking is robust and gives measurement error of less than 2 cm at high speed cruising (up to 135 km/h). Since the beacons are laid along the

desired path, it is not necessary to know the exact location of each beacon. The error vector to the path is obtained form the magnetometer data and allows the correction of the heading of even angularly non-accelerating vehicle. It is noted that in the urban canyon environment the accuracy of GPS signal is non-uniform and strongly depends on the geometry of the visible sky window[33]. For example, GPS position estimate uncertainty along the trajectory is low enough for the Kalman filter to weigh it so that the measurement complements the INS. At the same time GPS position estimate uncertainty transverse to the trajectory is high due to satellite occlusion by the buildings on both sides of the roadway and thus the measurement is weighted out by the filter. Due to localization system redundancy the author suggests that beacon density can be decreased[34] in the areas with the good GPS signal reception, while in the areas with unreliable or no GPS reception (in a tunnel, for example) the density should be increased back to the nominal value.

Ulf Larson *et. al.* describe localization of an autonomous articulated **CALMAN Lawn Mower**[64] shown in Figure 2.11. The number of sensors is kept to an absolute minimum with no redundancy for neither relative nor absolute localization: the wheel encoders are used for the DR and the laser scanner supplies angle-only measurements to surveyed beacons. Centimeter-level accuracy is achieved at the speed of 0.3 m/s. The reported tests are done on a parking lot, and therefore are not representative of the localization system performance on the soft turf [58, 93].

An autonomous harvester that uses vision to track the crop line is reported in the work of Ollis *et.al.*[78]. A vision based crop line tracking technique is demonstrated on the example of the automated harvester in the work of Mark Ollis and Anthony Stentz. The boundary between the cut and uncut crop is detected by the vision system and is used as an absolute reference path. An end-of-row detector is used to trigger the dead reckoning controlled turning behavior of the harvester. The

[33]This is in addition to usual ionospheric error, satellite geometry, and multipath errors.
[34]It is important to be able to estimate the effect of the localization system configuration changes on the overall navigation accuracy. A localization system model can be used to this end.

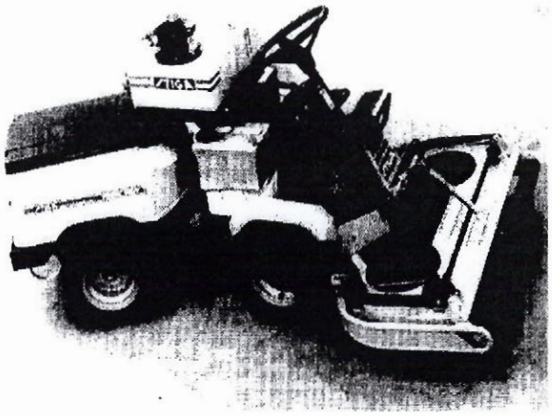

FIGURE 2.11. The Autonomous Articulated Lawn Mower CALMAN [63]

crop line tracking is resorted to during the GPS outages when no other absolute measurement is available to the harvester.

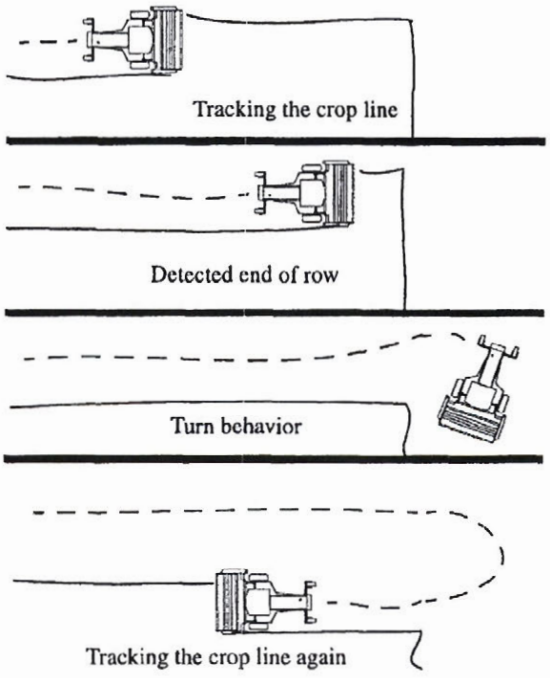

FIGURE 2.12. The Autonomous Harvester: Crop Line Tracking [78]

4. Summary

From the previous account of the sensors, localization techniques, and existing systems autonomous robot requires relative, as well as absolute sensing modalities in order to localize accurately, with bounded pose uncertainty, and at a frequency sufficiently high for control purposes. The relative localization can be realized using the odometry and INS, while the absolute localization - by an artificial landmark sensing setup. An extended Kalman filter can be designed to fuse the high frequency measurements from the INS with the low frequency measurements from the absolute localization system (GPS, for example.)

CHAPTER 3

The Vehicles

1. The Mowers in the Experiments

Three Toro company mower platforms were used in the localization experiments: the Groundsmaster 3500-D[1] (Hal), the Greensmaster 3250-D (Toby), and the Greensmaster 3200 (Toby-2)[2] golf course mowers. The photograph of the Hal and Toby autonomous mowers and Toby-2 localization testbed is shown in Figure 3.1 on page 24.

The diesel-hydraulic powered Hal and Toby are 3-wheel drive (all wheel drive, in their case) platforms, while Toby-2 is a gasoline-hydraulic powered front wheel drive platform. The mowers have an inverted tricycle configuration. The back steering wheel (see Figure 3.2 on page 25) has no vertical offset[3] and is driven by a hydraulic ram with a lock[4] of $\pm 45^o$. The vehicles have no suspension and rely on their pneu-

[1]"D" designates diesel powerplant.
[2]Toby and Hal are the autonomous platforms developed by TORO and CMU, Toby-2 is a standard TORO platform outfitted with the localization sensor suit and a portable computer for data logging.
[3]Zero vertical offset allows to turn the steering wheel in place without changing the orientation of the mower.
[4]The vehicles transmission design does not impose limit on the maximum steering angle allowing virtually differential drive maneuverability. The 45^o limit makes the rear wheel track within the radius of the front wheel while turning and prevents from accidentally dropping the rear wheel in a sand bunker that has been cleared by the front wheels. The Toro Company named this configuration *the Perfect Triangle Wheel Stand* [106].

(a) Toby and Hal autonomous mowers

(b) Toby-2 the localization testbed

FIGURE 3.1. The mower platforms used in the experiments.

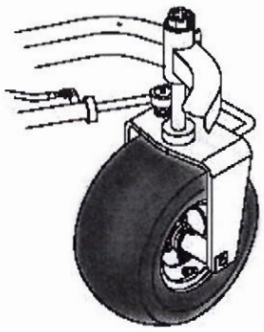

FIGURE 3.2. The steering wheel and fork assembly [104]

matic tires for shock absorption[5]. The three platforms differ in size and power but can be viewed as scaled versions of the same mechanical design; in the following discussion no distinction will be made between them unless clarity is compromised. The hydrostat of the transmission is driven directly by the internal combustion engine. The flow to the hydraulic constant displacement direct-drive motors (see Figure 3.3) determines the speed and direction of rotation and is controlled by the operator[6] through the swash plate of the hydrostat. Equal torque is developed by both front

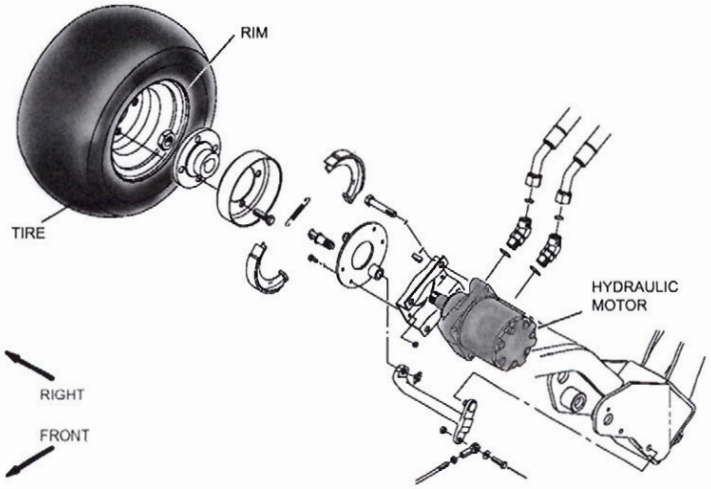

FIGURE 3.3. Front wheel assembly drawing. [104]

hydraulic motors regardless of the rotational speed owing to their parallel connection

[5]The vehicles have sturdy steel frames, which, given the small size of the platforms will not contribute to smoothness of the ride.

[6]Operator input is replaced by the computer-controlled servo action in the autonomous versions.

and provides for turning without wheel slippage[7]. The rotational speed of the steering wheel (third) motor is equal to the average of the rotational speeds of the front motors due to its parallel connection[8] to the front motors. This arrangement provides superior traction to the mower and results in virtually no wheel slippage even on wet grass[9]. The schematic of the hydrostatic transmission of the Greensmaster 3200 is shown in Figure 3.4 on page 26. The dimensions of the mowers relevant to

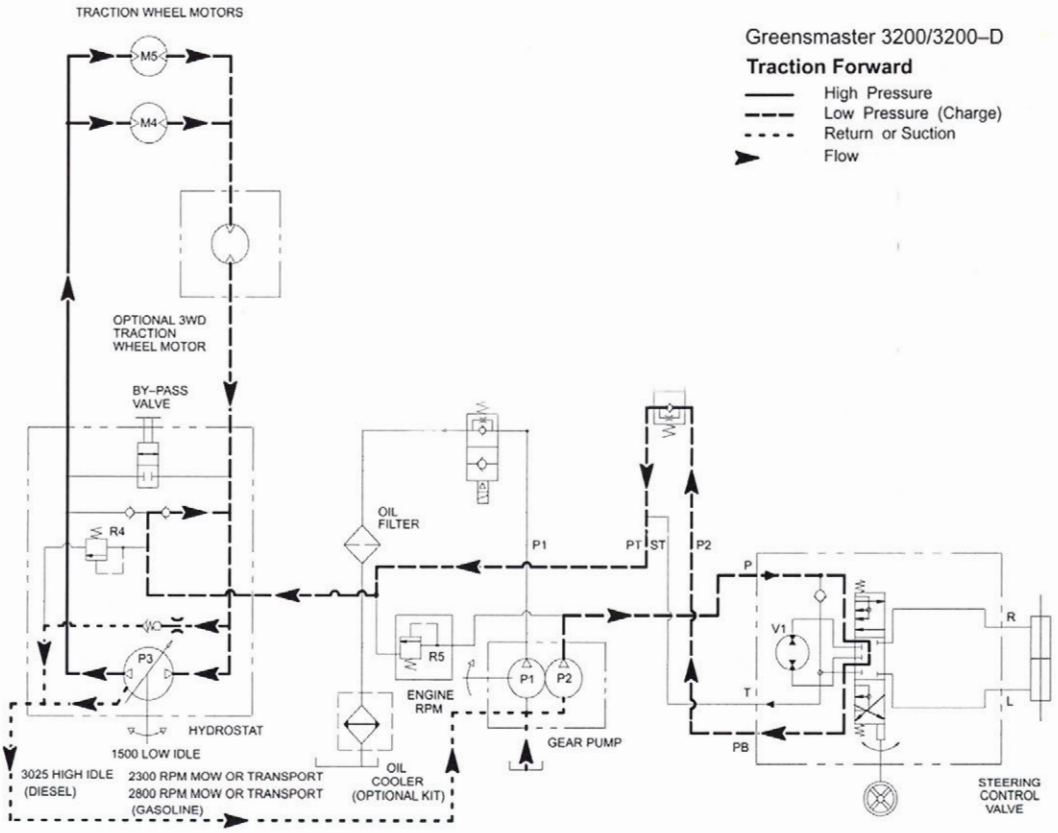

FIGURE 3.4. The hydrostatic transmission. [104]

the kinematic analysis are given in the Table 3.1 on page 26. The autonomous mower

[7]Same effect is achieved in the gear differentials of mechanical transmissions.
[8]Hence The Toro Company's **Series/Parallel** hydrostatic transmission.
[9]The mower operates at slow speed ($2\ m/s$) on the straight portions of the path and is slowed down on the turns. Therefore the side-slip is excluded from the further discussion. A no-slip nonholonomic model will be developed.

	Hal	*Toby*	*Toby-2*
Wheel Thread, m	1.410	1.280	1.280
Wheel Base, m	1.480	1.280	1.280
Wheel Radius, m	0.250	0.210	0.210

TABLE 3.1. The nominal mower dimensions.

low-level control is accomplished using The Toro Company's PID control boards and electro-mechanical servovalves, while the high-level control and obstacle avoidance software and supporting hardware were developed by the project's collaborators from CMU[12, 13, 14, 15, 41] in cooperation with The Toro Company.

2. Kinematic Model

There is no standard approach for choosing a vehicle model for a localization algorithm [51, 68]. Most of the mobile robot localization research to date uses kinematic modeling for low speed "non-dynamic" applications; dynamic models are used for highly dynamic high speed applications [51]. The more complete models are more accurate only if their parameters closely correspond to those of the vehicle[62] and these parameters may be difficult to estimate[10]. Given low ($2\ m/s$) mowing speed of the vehicles and slower cornering speed (about $1\ m/s$) at the end of each swath and complexity of modeling the hydraulic drive train [42], the dynamic effects are neglected. A kinematic model of the *nonholonomic*[11] system represents the vehicle in the localization algorithm. The mower operates in flat, as well as in hilly, terrain. It was decided however, that a planar system (dead reckoning) model is adequate for precise localization in three dimensions. The updates from the absolute sensors

[10]Force or torque sensing may be required in addition to quadrature encoders sufficient for the kinematic approach. The pressure and flow measurements (by pressure transducers and turbine flow meters) in the hydraulic system are analogous to the voltage and current measurements in the electrical system.

[11]The constraints to a motion of a mechanical system part can be categorized as geometrical and kinematic. Geometrical constraints restrict the possible configurations of a system (a hard stop in a robot joint, for example). Kinematic constraints restrict the velocities of the system parts, and are precipitated by the geometrical constraints (and system dynamics.) Yet kinematic constraints do not always impose geometric constraints, as in the rigid body rolling without sliding on a surface. Mathematically these constraints are characterized by their nonintegrability. Therefore, a mechanical system with nonintegrable kinematic constraints is called nonholonomic [49].

allow to correct for the errors due to planar approximation of the three-dimensional terrain. Alternatively, the more complete three-dimensional dead reckoning requires full attitude sensing in real time and shows no significant accuracy improvement in comparison to the two-dimensional dead reckoning [32] [12]. The absolute latitude and longitude GPS estimate, for example, can be viewed as a projection of the 3D position onto a 2D map, in which the robot is localized. The robot is brought to the desired 3D location by a tracking algorithm that operates in 2D and continuously corrects for the inaccuracy of the 2D DR modeling using the absolute (GPS) measurements. However, it is important to know the vehicle attitude in the navigation reference frame to compensate for the absolute sensor position (a high-mounted GPS antenna, for example, see Figure 3.5.) Since the mid-track velocity of the mower is directly

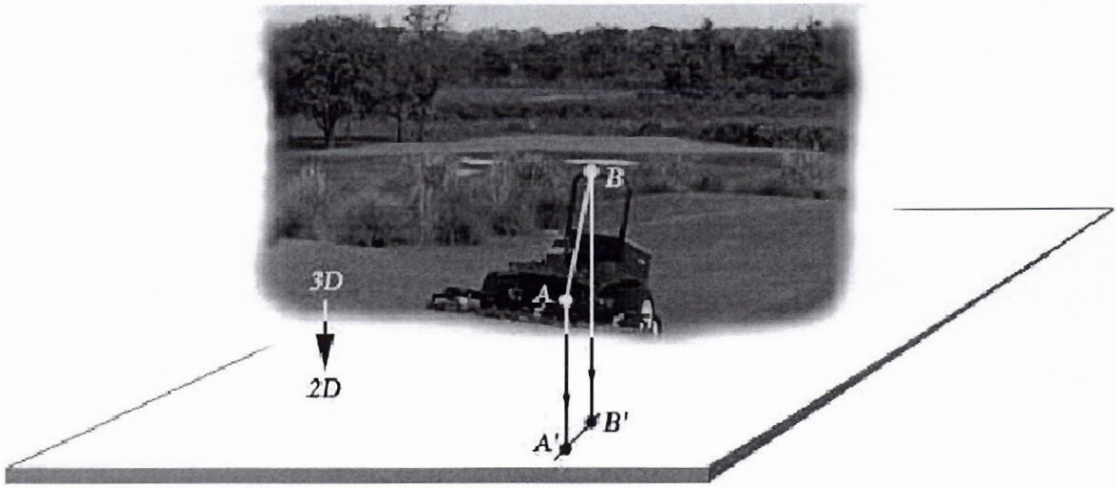

FIGURE 3.5. Three-dimensional localization using two-dimensional map. Point A is the platform reference point; the Line AB is vertical in the mower frame. If a GPS antenna is at point B, the projection $A'B'$ of the three-dimensional line AB onto the plane is the correction that has to be applied to the GPS measurement of the 2D location of point A. Thus it is desirable to have magnitude of AB as small, as possible to reduce error due to inaccurate attitude estimation.

available from the encoders, the mid-track point is chosen as a *platform reference point* for the vehicle motions. The vehicle is right-hand Cartesian coordinate system

[12]The experiments on the hard concrete, sandy ground, and even hard incline showed no significant difference between the 2D and 3D estimates. On cratered sandy ground a 0.9% accuracy improvement was achieved by the 3D DR over 2D DR[32].

is fixed at the mid-track with the x-axis pointing forward and the y-axis pointing to the left[13].

The mower's pose in a global planar Cartesian coordinate system is described by the coordinates (x, y) of the platform reference point (front mid-axis) and its heading (ϕ). The kinematic equations of motion are given by

$$V_A = \frac{V_R + V_L}{2} \tag{3.1}$$

$$\dot{x} = V_A \cdot cos(\phi) \tag{3.2}$$

$$\dot{y} = V_A \cdot sin(\phi) \tag{3.3}$$

$$\dot{\phi} = \frac{V_R - V_L}{b} \tag{3.4}$$

Where V_R and V_L are the right and left wheel velocities, and ϕ is the mower heading[14]. The mower kinematic diagram is shown in Figure 3.6.

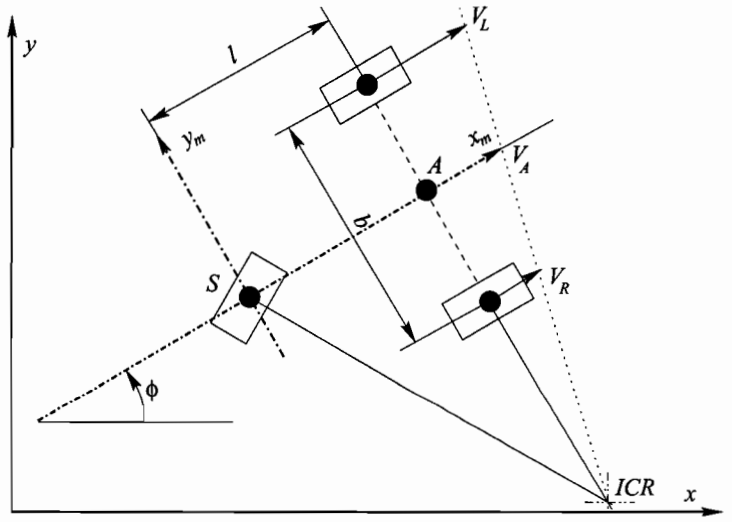

FIGURE 3.6. The Mower Kinematic Diagram in the horizontal plane. b is the effective wheel thread, l is the wheel base.

[13]This convention does not follow the usual navigational x – forward and y –to the right convention. The present choice is deeply rooted in the project's history and is not known to the author.

[14]The steering angle and steering wheel velocities are measured for the control purposes of the mower,but are not accurate enough for the localization and therefore are included neither in the above equations, nor in the following discussion.

The next section describes the localization system sensors and the sensor fusion algorithm.

CHAPTER 4

The Localization System

The relative (DR) and absolute sensors are used in the mower localization. The central localization data fusion algorithm is an extended Kalman filter [9, 81, 3, 19] that uses the sensor data to arrive at the vehicle's pose estimate. The process model describes the time evolution of the system and the measurement model provides the link between the measurements and the system state.

1. Localization Sensors

The sensors for the autonomous golf course mower must provide mower localization within 10 cm in the direction transverse to the direction of motion [1] at a mowing speed of 2 m/s, preferably in all weather and lighting conditions.

1.1. Relative Sensors. Encoders, gyroscopes, and accelerometers were considered as possible candidates for the dead reckoning system of the mower. Barshan and Durrant-Whyte [16] determined that orientation information from the INS is far better than its position information. Thus it was decided to use the wheel encoders for the position estimation and not to use accelerometers. A single axis gyroscope would provide the heading rate either fused with the encoder-derived heading rate, or as a sole source of heading information.

[1] Oscillations from the course larger than 5 cm become visually noticeable. On the other hand, positioning accuracy along the direction of motion is not critical; 10 - 15 cm will be sufficient since the edges of the field are mown during the initial perimeter cut.

Two digital interface (Open Collector) DYNAHER CONTROLS Inc. DYNAPAR brand H20-series [29] (H230300104203[2]) quadrature encoders with unbreakable code disks are used to measure the rotary displacement of the front wheels. The encoder flanges are bolted to the spring-steel mounting brackets on the mower frame. Metal rims with molded rubber tires are held by set screws on the encoder shafts and roll on the outer surfaces of the tires as shown in figure 4.1.

FIGURE 4.1. The encoder mounted on the mower in contact with the wheel.

A strap-down open loop[3] single axis[4] fiber optical gyroscope (FOG) [50] KVH Industries, Inc E-Core RD2060 [61] is used to measure the yaw rate of the platform. The unit costs US $2500.00 and has a maximum specified drift[5] of $0.0012^o/s = 0.072^o/min = 4.32^o/hr$ (see Table 4.1.)

[2]Some of the information coded in the designation **H23-0300**-1-0-4-2-**0-3**: model – H23; pulses per revolution – 300; electrical (0) – 5-26 V DC in, 7406 Open Collector output; termination (3) – 7-pin side mount connector

[3]open loop gyroscopes provide no feedback to a frequency or phase shifting element to cancel the rotationally induced Sagnac phase shift [50].

[4]It is desirable to have a three-axis gyroscope on an outdoor platform, however, the cost of such a device is prohibitive for the application. The E-Core RD2060, on the other hand, is insensitive to rotation and acceleration in other axes [60].

[5]Bias drift is a slowly changing error in the rate of rotation. Non-zero bias drift results in the non-zero angular rate reading by a stationary gyro. This is not related to the rotation of the Earth. The *nonlinearity of the scale factor with respect to angular rate* and *nonlinearity of the scale factor with respect to temperature* are secondary error sourses after the bias drift. No error compensation is provided in the unit; custom temperature compensation table for the gyro was provided by KVH at a later date; custom scale factor compensation with respect to rate tables (or empirical formulas) are not available from KVH. Nowadays, however, E-Core 2000 series gyroscopes can be purchased with both compensations built-in.

TABLE 4.1. Technical specifications for the KVH E-Core RD2060 [61]

Performance		RD2060
Input Rate (max)	$\pm^o/s$	±60
Rate Resolution	$^o/s$	0.004
Scale Factor	$^o/bit$	0.000183
Nonlinearity	% rms	4
Full Temp.	% rms	1
Bias Stability		
Constant Temperature	$^o/s\ 1\sigma$	0.0012
Full Temperature	$^o/s\ p-p$	0.24
Angle Random Walk	$^o/hr/\sqrt{Hz}$	5
Bandwidth	Hz	100

A proprietary elliptical polarization-maintaining optical fiber insures that in the absence of rotation the two counter-propagating beams follow identical paths and thus insures repeatability of light propagation speed through the fiber. Bias stability of $2^o/hr$ and bias driftof $5-10^o/hr$ are attained. The gyroscope (in short: "gyro") is mounted inside the electronics enclosure shown in Figure 4.6 on page 43. Thus the dead reckoning is provided by the combination of the two front wheel encoders and a single-axis strap-down gyroscope.

1.2. Absolute Sensors. A Kalman filter for dead reckoning alone can substantially reduce the localization error, but since the actual position and heading are unobservable [11, 16, 79] the filter will inevitably diverge. The absolute measurements are necessary to bind the dead reckoning localization error[6].

A **ground-mounted magnetic marker grid in conjunction with a magnetometer** was initially considered, but rejected because of the short detection range of the magnetic markers. Circular (sprinkler head mountable) magnetic markers cut out of 3M's *Magnetic Lateral Warning and Guidance Tape* [2] and a mower-mounted **Magnetic Guidance Sensor** by Safety Technologies Inc. [92] were tested (see Figure 4.2.) The markers were detectable only within 0.15 m which is ample for the uninterrupted magnetic tape guidance, but is insufficient for the sparse a marker

[6]Some of the causes of dead reckoning errors are the gyro drift, wheel slippage, tread wear, and improper tire inflation.

placement on the golf course. The required localization accuracy demands a marker density too high to be practical[7]. On the other hand, golf courses are mostly open spaces with good GPS[8] reception.

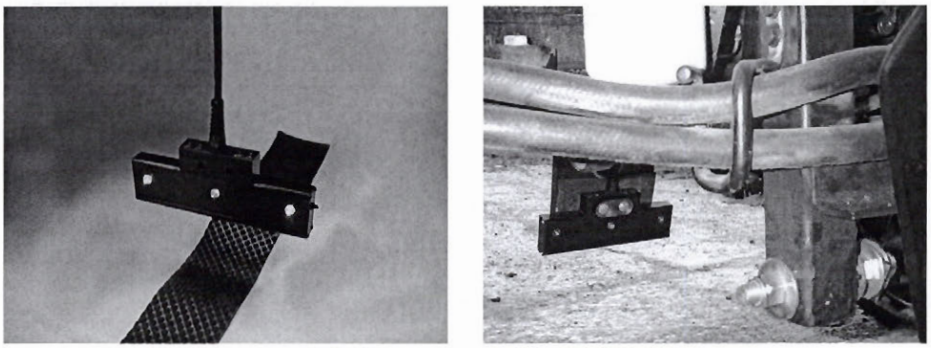

(a) Safety Technologies Magnetic Guidance Sensor over 3M tape.

(b) The Magnetic Guidance Sensor on Toby-2.

FIGURE 4.2. Safety Technologies Magnetic Guidance Sensor [92] over 3M tape.

A high-performance 2 *cm* accuracy **NovAtel ProPack RTKGPS** [76] [9] based localization system of Hal[10] maintained 97% of the tracking error below the target value of 10 *cm* [89]. GPS provides a convenient way to initialize the localization algorithm and bind its error. The simulation in Section **??** suggests that a sub-meter accuracy DGPS can be used as an absolute sensor in the localization system capable of maintaining lateral error below 10 *cm*. A sub-meter **CSI Wireless SX-I** WAAS enabled DGPS [25] card (shown in Figure 4.3) was integrated into the navigation system as described in Appendix E.

However, a GPS-only solution for the absolute localization is unsatisfactory due possible GPS signal loss as a result of line of site obstruction by foliage, nearby buildings or due to unfavorable satellite configuration.

[7]Sports field marking could be accomplished though by dense (in the order of 0.1 m) placement of the strong magnetic rods along the desired trajectory [113].
[8]See Appendix A for the description of various GPS modes (DGPS, RTKGPS).
[9]The RTK system cost is over US $21,000.
[10]Hal's sensor suite includes the fiber-optic gyroscope, the wheel encoders, and the RTKGPS for localization.

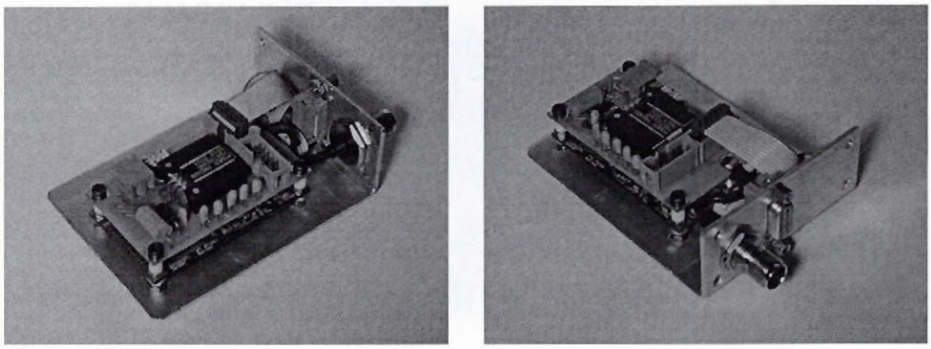

(a) View from the back of the mounting frame.

(b) View at the frontof the mounting frame

FIGURE 4.3. The CSI Wireless SX-I card with the custom interface board stacked on top and mounted on a frame. The GPS antenna connector and the serial connectors are bolted to the frame.

Ground-based pseudo satellites (pseudolites) that transmit a regular L1-band GPS signal seem to be the immediate remedy to the GPS coverage problem since they can be positioned anywhere (even indoors) to augment the constellation directly [20]. However they cannot be readily integrated with the standard GPS receivers due to software and hardware incompatibilities. The pseudolites stay put on the surface of the earth, while the GPS satellites move along their elliptical trajectories in space. The GPS format was designed to describe the motion of navigation satellites in *orbital parameters* and is unsuitable for the description of the stationary ground-based objects. Since the pseudolite position is known before taking the measurement, the GPS receiver software has to be modified so that it accepts static pseudolite positions and disregards the position information in the pseudolite's GPS message. Pseudolites also have to be added to the GPS almanac "manually" in order for a receiver to detect them. On the hardware side, it is common for GPS antennas to reject measurements with elevation angles less than 10 to 15 degrees to mitigate the ionospheric delay and multipath. The GPS antenna has to be redesigned or the pseudolites have to be positioned within the vision field of the antenna to be detected. The pseudolite signal in the *near-field* is also orders of magnitude stronger than the GPS signal and

can jam the receiver. Time Division Multiple Access (TDMA) communication has to be applied in the near field of the pseudolite[20, 109].

Still, DGPS does provide the desired absolute localization solution most of the time, but is expected to fail under tree cover or when less than six satellites are in its antenna's direct line of sight. It is proposed to fuse *absolute heading sensor* data with the rest of the sensory information to maintain the desired orientation at GPS blackouts. Maintaining the desired orientation is essential for staying within the lateral error margin.

The **Honeywell HMR3000 digital electronic compass** with three orthogonal Magnetoresistive (MR) [44, 43] sensors and a liquid filled two-axis tilt sensor[11] provides a tilt-compensated heading measurement. The sensor is shown in Figure 4.4 on page 34. Changes in the sensors' resistance under the action of the Earth's magnetic field are converted to a digital NMEA 0813 formatted RS-232 signal.

GPS can also be augmented by vision-based local positioning system (LPS): the *Motion from Structure* (MFS) [94] monocular visual navigation approach is used to extract the vehicle's motion from the images of known environmentally fixed distinctive landmarks. Since the appearance of a golf course cannot be modified, the landmarks for the vision system must be unobtrusive. The density of the visual marker grid depends on the effective camera range and quality of the dead reckoning system that has to maintain pose estimation accuracy until the external camera measurements become available. Finding an optimal placement of a minimal number of markers is an open-ended problem in general [80], however a particular solution for a fixed marker grid geometry and regular mowing pattern is given in Section 5.2. It is shown that marker grid based on the existing sprinkler system does not provide sufficient coverage to maintain the desired localization accuracy. Thus the visual marker has to meet the following requirements: it has to be self-contained so that it can be placed where additional coverage is most needed; it has to be flush with the ground

[11]The sensor should neither be stored nor operated at an angle exceeding 75 degrees to avoid its temporary accuracy loss. The fluid in the bubble should remain approximately level most of the time.

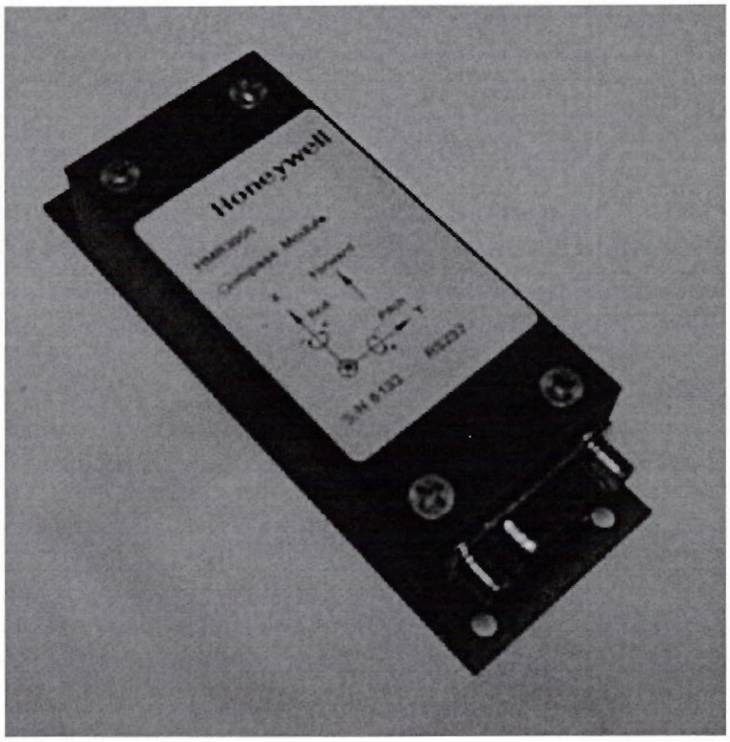

FIGURE 4.4. The Honeywell Magnetoresistive compass/inclinometer

and have a small footprint in order not to obstruct the view; it must be visible out of the grass enough to be detected by the mower camera(s); the marker must retract to avoid the mower blades. The design of a hiding visual beacon is outlined in Appendix F. Proof-of-concept visual marker LPS experiments were performed with two SONY DFW-VL500 IEEE1394 cameras mounted on the mower (Hal), one in the front and one in the back, as shown in Figure 6.1 on page 51. Red computer mouse pads were used as visual marker mock-ups.

2. Data Logging and Auxiliary Devices

The system architecture[12] consists of three major components: a dead reckoning system, the absolute localization system, and a data-logging computer. The block

[12]The architecture of Toby-2's localization sensor suit is given here. Sensors and hardware used in the experiments with Toby and Hal are described in the subsequent sections along with the pertaining data analysis.

diagram of the system is shown in Figure 4.5. **The dead reckoning system** is composed of the DYNAPAR H230300104203 wheel encoders with Open Collector outputs and the E-Core RD2060 fiber-optic gyroscope with RS-232 serial output connected to a TERN Aengine microprocessor [102] and P100 expansion [103] boards stack, **The absolute localization system** consists of the HMR3000 Magnetoresistive compass/inclinometer and SX-I WAAS DGPS board with custom built power and RS-232 interface[13]. **The data-logging computer** is IBM 380ED Pentium 166 MHz laptop running Linux[14] and Windows 2000. Data logging and code development is done in Linux, while Windows-exclusive sensor calibration and testing programs provided by the hardware manufacturers are run in Windows 2000. Figure 4.5 on page 36 shows that the computer must accept three RS-232 connections while only one RS-232 port is available on the laptop; a Quatech QSP-100 PCMCIA to quad

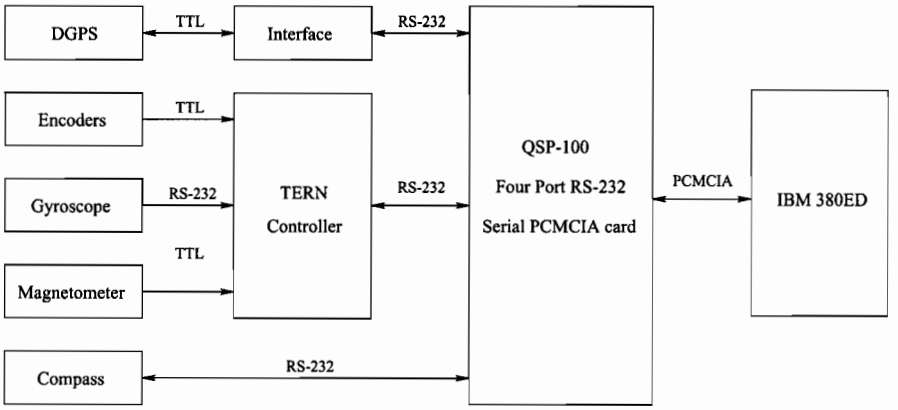

FIGURE 4.5. Overall Localization System Hardware Architecture

serial card [15] is used to provide the required connections. The actual implementation on the mower is shown in Figure 4.7.

[13]The details of SX-I integration are provided in Chapter E.
[14]RedHat distribution 7.0 with kernel recompiled form sources to version 2.4.19.
[15]The card is supported in the Linux kernel 2.4.19; no driver module is required. The card is also supported under Windows 2000

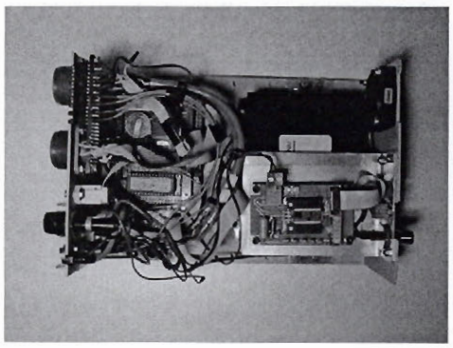

(a) The top view on the open electronics box. The SX-I DGPS is installed.

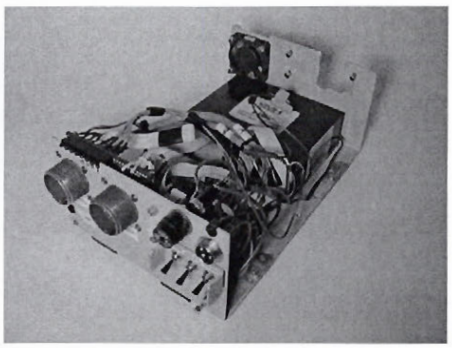

(b) A view on the open eletronics box with the DGPS removed.

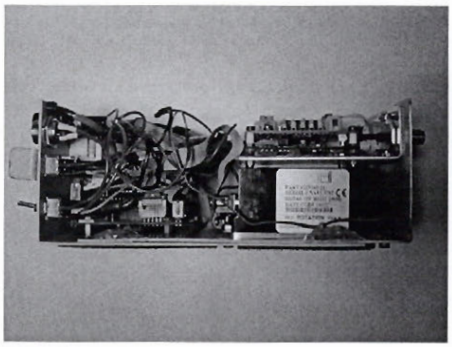

(c) Side view on the open electronics box. The SX-I DGPS is installed.

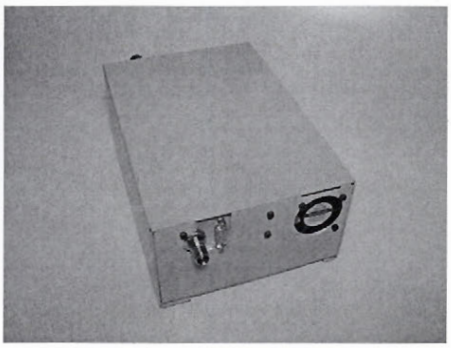

(d) The back view on the electronics box with the cover bolted on. The back cover bears the DGPS antenna and serial connectiors.

FIGURE 4.6. The electronics box containing the TERN computer, SX-I with the interface board on top, and a RD2060 fiber optical gyroscope.

3. The Localization Algorithm

The most common use of linear filtering is for nonlinear analysis.

– H.W.Sorenson [46]

The main localization data fusion algorithm is a **discrete extended Kalman filter** (EKF)[9, 81, 3] that uses the kinematics of the mower driven by the relative sensor observations [16] and observations from the absolute sensors to arrive at the vehicle's

[16]If DR is unavailable, a motion model is assumed [35]; separate motion models are used[10, 8] for quiescent and maneuvering situations – a model for straight flight, a model for coordinated turn, *et cetera*. The predictions from the models are combined[111] or switched between[88] based on

FIGURE 4.7. The screen support serves as the QSP-100 serial connectors holder.

pose estimate[17]. A total state space or *direct formulation*[81] of the filter was chosen (in difference to the error state space or *indirect formulation*[79]) so that all available information is weighted by the EKF-optimized time-varying gains.

The computational flow for one cycle of a discrete extended Kalman filter is shown in a flowchart in Figure 4.8 on page 44. This representation of the EKF follows one given by Bar-Shalom [9] with the modifications appropriate for the system. It is assumed that the process noise $\mathbf{v}(k)$, input noise $\boldsymbol{\gamma}(k)$, and the measurement noise

the target observation. Thus, even though the relative sensor measurements are subjected to drift in time, they provide valuable high bandwidth information about the vehicle motion that is more accurate than the information inferred from the infrequent absolute measurements.

[17]EKF is chosen due to its proven track record in localization.

$\mathbf{w}(k+1)$, are additive, zero mean, white, and mutually uncorrelated [9, 3]:

$$E(\mathbf{v}(k)) = \mathbf{0} \tag{4.1}$$

$$E(\boldsymbol{\gamma}(k)) = \mathbf{0} \tag{4.2}$$

$$E(\mathbf{w}(k)) = \mathbf{0} \tag{4.3}$$

$$E(\boldsymbol{w}(k)\boldsymbol{v}(j)^T) = \mathbf{0}, \forall k, j \tag{4.4}$$

$$E(\boldsymbol{v}(k)\boldsymbol{\gamma}(j)^T) = \mathbf{0}, \forall k, j \tag{4.5}$$

$$E(\boldsymbol{w}(k)\boldsymbol{\gamma}(j)^T) = \mathbf{0}, \forall k, j \tag{4.6}$$

$$E(\boldsymbol{v}(k)\boldsymbol{v}(j)^T) = \mathbf{Q}\delta_{kj}, \forall k, j \tag{4.7}$$

$$E(\boldsymbol{w}(k)\boldsymbol{w}(j)^T) = \mathbf{R}\delta_{kj}, \forall k, j \tag{4.8}$$

$$E(\boldsymbol{\gamma}(k)\boldsymbol{\gamma}(j)^T) = \boldsymbol{\Gamma}\delta_{kj}, \forall k, j \tag{4.9}$$

Where δ_{kj} is the Kronecker delta function. This section concentrates on the development of the process and measurement models for the mowers.

3.1. The Process Model. The process model plays a critical role in the localization system performance since the robot's localizations relies on it and the dead reckoning measurements entirely while absolute observations are not available. The following kinematic model [17, 108, 62] is found to be an adequate discretized version of the kinematic equations:

$$f_x(k) = x_{k+1} = x(k) + \Delta D(k) \cdot cos(\phi(k) + \frac{\Delta\phi(k)}{2}) \tag{4.10}$$

$$f_y(k) = y_{k+1} = y(k) + \Delta D(k) \cdot sin(\phi(k) + \frac{\Delta\phi(k)}{2}) \tag{4.11}$$

$$f_\phi(k) = \phi(k+1) = \phi(k) + \Delta\phi(k) \tag{4.12}$$

Where $\Delta D(k)$ is the distance travelled by the mid-axis point given the values that the right and the left wheels have traveled, $\Delta D_R(k)$ and $\Delta D_L(k)$ respectively (see

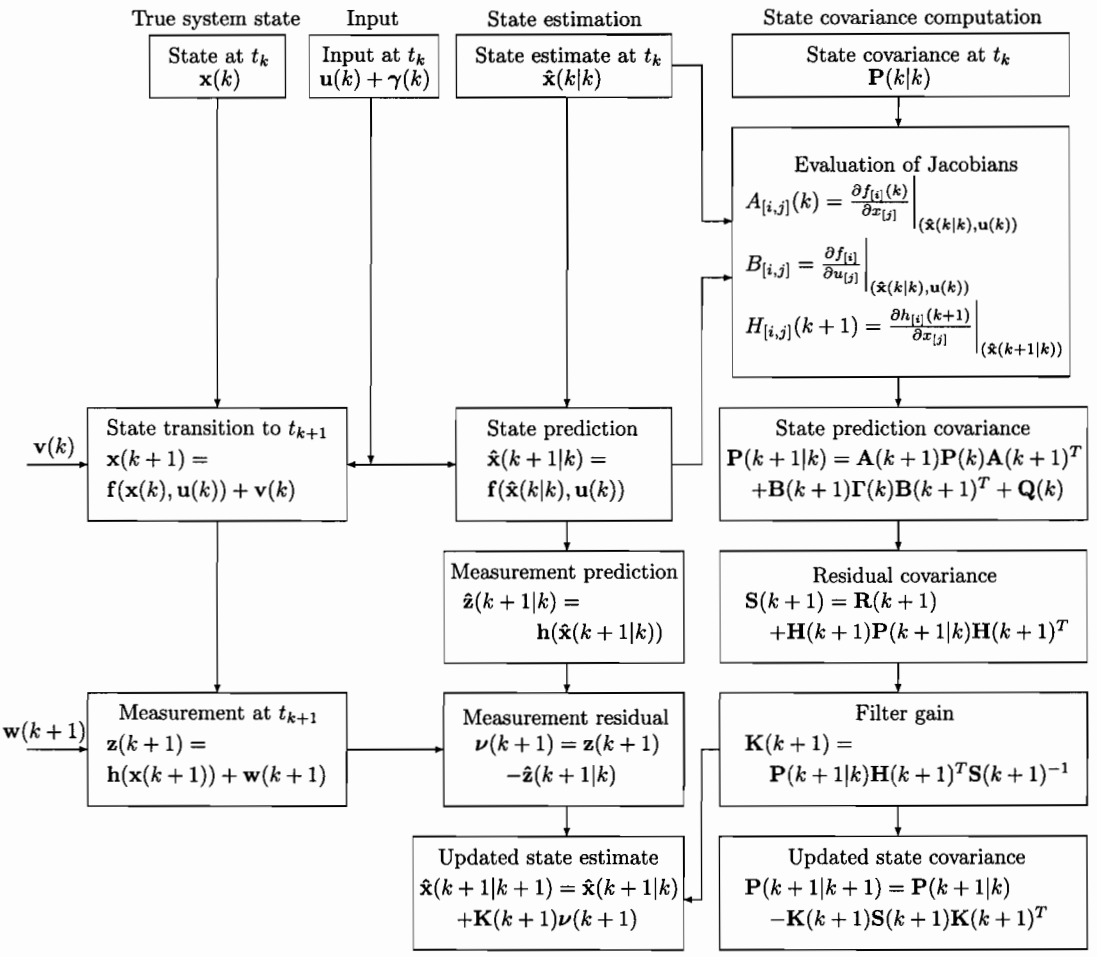

FIGURE 4.8. The Extended Kalman Filter Computational Flow. The two parallel computations: the state estimation and the state covariance estimation are shown in the parallel columns.

Figure 4.9 on page 44:

$$\Delta D(k) = \frac{\Delta D_R(k) + \Delta D_L(k)}{2} \tag{4.13}$$

The incremental change in the orientation $\Delta\phi(k)$,can be obtained from odometry given the effective width of the mower b:

$$\Delta\phi(k) = \frac{\Delta D - R(k) - \Delta D_L(k)}{b} \tag{4.14}$$

Thus the system state vector may be written as $\mathbf{x}(k) = [x(k)\ y(k)\ \phi(k)]^T$, the input vector as $\mathbf{u}(k) = [\Delta D(k)\ \Delta\phi(k)]^T$ represents odometer and the gyroscope measurements[18], and the system function $\mathbf{f}(\mathbf{x}) = [f_x\ f_y\ f_\phi]^T$ where the function components are represented by the Equations 4.10-4.12. The system matrix ($\mathbf{A}(k)$) and input gain matrix ($\mathbf{B}(k)$) are represented by the following Jacobians:

$$\mathbf{A}(k) = \begin{bmatrix} \frac{\partial f_x}{\partial x(k)} & \frac{\partial f(x)}{\partial y(k)} & \frac{\partial f_x}{\partial \phi(k)} \\ \frac{\partial f_y}{\partial x(k)} & \frac{\partial f_y}{\partial y(k)} & \frac{\partial f_y}{\partial \phi(k)} \\ \frac{\partial f_\phi}{\partial x(k)} & \frac{\partial f_\phi}{\partial y(k)} & \frac{\partial f_\phi}{\partial \phi(k)} \end{bmatrix}_{\mathbf{x}(k)} = \begin{bmatrix} 1 & 0 & -\Delta D(k) \cdot \sin(\phi(k) + \frac{\Delta\phi(k)}{2}) \\ 0 & 1 & \Delta D(k) \cdot \cos(\phi(k) + \frac{\Delta\phi(k)}{2}) \\ 0 & 0 & 1 \end{bmatrix}_{\mathbf{x}(k)} \quad (4.15)$$

$$\mathbf{B}(k) = \begin{bmatrix} \frac{\partial f_x}{\partial \Delta D(k)} & \frac{\partial f_x}{\partial \Delta\phi(k)} \\ \frac{\partial f_y}{\partial \Delta D(k)} & \frac{\partial f_y}{\partial \Delta\phi(k)} \\ \frac{\partial f_\Phi}{\partial \Delta D(k)} & \frac{\partial f_\phi}{\partial \Delta\phi(k)} \end{bmatrix}_{\mathbf{x}(k)} = \begin{bmatrix} \cos(\phi(k) + \frac{\Delta\phi(k)}{2}) & -\frac{\Delta D(k)}{2}\sin(\phi(k) + \frac{\Delta\phi(k)}{2}) \\ \sin(\phi(k) + \frac{\Delta\phi(k)}{2}) & \frac{\Delta D(k)}{2}\cos(\phi(k) + \frac{\Delta\phi(k)}{2}) \\ 0 & 1 \end{bmatrix}_{\mathbf{x}(k)} \quad (4.16)$$

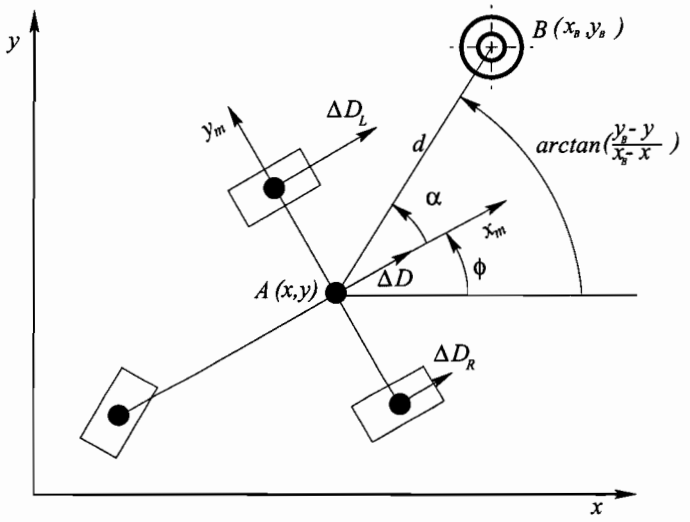

FIGURE 4.9. The system schematic (the bird's eye view.) The blocks represent the mower wheels and the concentric circles represent a marker.

[18]Heading rate $\Delta\phi(k)/\Delta t$ from both the odometry and the gyroscope can be fused in the EKF. However the heading rate from the odometry is much less reliable for the outdoor platform than that from the gyroscope and is always outweighed by the later.

3.2. The Measurement Model. The azimuth α_i with respect to the mower x-axis and the elevation η_i with respect to the mower x–y plane (observed from the mid-axis point at the distance μ form the ground-plane) angles to the i-th marker are obtained by the absolute measurement system a time instant k (see Figure 4.9 on page 44.) The measurement vector for a single marker measurement is defined as $\mathbf{z}_i(k) = [\alpha_i(k)\ \eta_i(k)]^T$. The absolute measurement angles are related to the system state variables $x(k)$, $y(k)$, and $\Phi(k)$ by the followiing nonlinear measurement equation:

$$\alpha_i = h_{\alpha i}(\mathbf{x}(k)) = \arctan(\frac{y_{Bi} - y(k)}{x_{Bi} - x(k)}) - \phi_k \tag{4.17}$$

$$\eta_i = h_{\eta i}(\mathbf{x}(k)) = -\arctan(\mu / d_i(\mathbf{x}(k)) \tag{4.18}$$

$$d_i(\mathbf{x}(k)) = \sqrt{(x_{Bi} - x(k))^2 + (y_{Bi} - y(k))^2}$$

and the measurement matrix $H(k)$ is given by the Jakobian:

$$\mathbf{H}_i(k) = \begin{bmatrix} \frac{\partial h_{\alpha i}}{\partial x(k)} & \frac{\partial h_{\alpha i}}{\partial y(k)} & \frac{\partial h_{\alpha i}}{\partial \phi(k)} \\ \frac{\partial h_{\eta i}}{\partial x(k)} & \frac{\partial h_{\eta i}}{\partial y(k)} & \frac{\partial h_{\eta i}}{\partial \phi(k)} \end{bmatrix}_{\mathbf{x}(k)} \tag{4.19}$$

$$\frac{\partial h_{\alpha i}}{\partial x(k)} = \frac{y_{Bi} - y(k)}{(x_{Bi} - x(k))^2 + (y_{Bi} - y(k))^2} \tag{4.20}$$

$$\frac{\partial h_{\alpha i}}{\partial y(k)} = \frac{-x_{Bi} + x(k)}{(x_{Bi} - x(k))^2 + (y_{Bi} - y(k))^2} \tag{4.21}$$

$$\frac{\partial h_{\alpha i}}{\partial \phi(k)} = -1 \tag{4.22}$$

$$\frac{\partial h_{\eta i}}{\partial x(k)} = \frac{\mu(x_{Bi} - x(k))}{\sqrt{(x_{Bi} - x(k))^2 + (y_{Bi} - y(k))^2}(\mu^2 + (x_{Bi} - x(k))^2 + (y_{Bi} - y(k))^2)} \tag{4.23}$$

$$\frac{\partial h_{\eta i}}{\partial y(k)} = \frac{\mu(y_{Bi} - y(k))}{\sqrt{(x_{Bi} - x(k))^2 + (y_{Bi} - y(k))^2}(\mu^2 + (x_{Bi} - x(k))^2 + (y_{Bi} - y(k))^2)} \tag{4.24}$$

$$\frac{\partial h_{\eta i}}{\partial \phi(k)} = 0 \tag{4.25}$$

Multiple measurements are accommodated by stacking the $\mathbf{H}_i(k)$ matrices and corresponding measurement vectors $\mathbf{z}_i(k)$ as follows:

$$\mathbf{H}(k) = [\mathbf{H}_i(k)^T \, \mathbf{H}_{i+1}(k)^T \, \mathbf{H}_{i+2}(k)^T \ldots \mathbf{H}_N(k)^T]^T, \qquad i = 1, 2, \ldots, N \tag{4.26}$$

$$\mathbf{z}(k) = [\mathbf{z}_i(k)^T \, \mathbf{z}_{i+1}(k)^T \mathbf{z}_{i+2}(k)^T \ldots \mathbf{z}_N(k)^T]^T, \qquad i = 1, 2, \ldots, N \tag{4.27}$$

3.3. Time Propagation of Process Errors. The extended Kalman filter keeps track of its estimates accuracy by propagating the state error covariance matrix[19] in time based on the variances of the individual measurements it receives from the sensors. Such sensors as GPS receivers usually contain an internal Kalman filter and are able to report on the quality of the data they provide. Non-computerized sensors do not offer this facility and call for the measurement error estimation. It is assumed that the constant measurement biases are calibrated out, so that the error variances alone can be used to model the goodness of the measurements for the EKF. There exist different approaches[20] to modeling the process noise covariances [31, 42, 108, 57]. In the present EKF implementation the process noise is modeled is taken along the lines proposed by Chenavier and Crowley [31]:

$$\mathbf{Q}(k) = \begin{bmatrix} Q_{11}(k) & 0 & 0 \\ 0 & Q_{22}(k) & 0 \\ 0 & 0 & Q_{33}(k) \end{bmatrix} \tag{4.28}$$

[19]This matrix is not a covariance, but rather a mean square error (MSE) matrix because the estimated state is not the exact conditional mean for the EKF [9].

[20]One of the popular approaches is a trial-and-error tuning of the process noise covariance values to achieve somewhat acceptable filter performance. Even though every system error modeling technique requires explicit assumptions to be made at some point of the algorithm, a methodology is helpful in the filter development. On the other hand, more accurate system state error propagation and resulting more optimal operation of the Kalman filter will not help improve the localization accuracy in the long run if the absolute sensors cannot provide sufficiently accurate and numerous measurements for the fusion. (Moreover, Kalman Filters in general do not recover well from large errors[38] and therefore large state error operation is not acceptable from both practical and theoretical perspectives.) Thus a compromise – evidence-based heuristic and tuning – state error modeling technique should be adequate for our system.

The process errors are assumed to be uncorrelated so that the time-varying process noise matrix $\mathbf{Q}(k)$ is diagonal with the following entries:

$$\mathbf{Q}_{11}(k) = K_{ss}|\Delta D cos\phi| \tag{4.29}$$

$$\mathbf{Q}_{22}(k) = K_{ss}|\Delta D sin\phi| \tag{4.30}$$

$$\mathbf{Q}_{33}(k) = K_{s\phi}|\Delta D| + K_{\phi\phi}|\Delta\phi| \tag{4.31}$$

where K_{ss} is the odometry drifting coefficient along the distance traveled with respect to incremental distance ΔS; $[K_{ss}] = m^2/m$, $K_{s\phi}$ is the odometry drifting coefficient along the heading with respect to incremental distance ΔS; $[K_{s\phi}] = rad^2/m$, and $K_{\phi\phi}$ is the odometry drifting coefficient along the heading with respect to incremental heading Δphi; $[K_{\phi\phi}] = rad^2/rad$ The authors experimentally tuned the above coefficients for their mobile robot.

3.4. Measurement Gate. Real world measurements even from reliable and robust sensors such as Millimeter Wave Radar[42] contain fair amount of noise. The regular sensor noise is accounted for by the measurement error covariance matrix **R**. Meanwhile sporadic erroneous measurements are not described by the covariance-only error model of the Kalman filter and the additional processing is called for in order not to allow them degrade the filter state estimate. Since INS measurements normally are not subjected to large measurement errors a measurement *validation gate* is applied to the absolute measurements only. Smaller validation gate values apply stricter acceptance criteria to measurements, while larger validation gate values accept measurements liberally. The compromise between high landmark detection rate and rejection of the erroneous measurements is made by tuning the gate value according to the overall uncertainty of the state estimation, so that smaller values of the gate are applied when the filter is confident in its estimate, while larger values will be applied when the localization is less certain and therefore greater tolerance should be exercised towards the nonconformist measurements that appear to be erroneous to the drifting model. Filter optimality follows from filter *consistency*, that is its ability

to maintain an unbiased state estimate along with its proper covariance[21] value, and is preserved by introduction of a measurement gate. The actual consistency test is implemented as follows[9]. The *normalized innovation squared* (NIS) of a consistent filter

$$\epsilon_\nu(k) = \nu(k)^T S(k)^{-1} \nu(k) \tag{4.32}$$

has a chi-square distribution with the degrees of freedom equal to the dimension of the measurement. The higher and lower bounding values of the gate corresponding to the dimension of the measurement are read from the chi-square table. A measurement passes the test if its calculated $\epsilon_\nu(k)$ value remains within the gate, otherwise it is discarded as erroneous.

3.5. The treatment of asynchronous measurements. The EKF time step must not be fixed; the algorithm allows to process asynchronous data at different rates[18]. Thus the inertial navigation system steadily outputs measurements at 100 Hz, the NovaTel RTKGPS – at approximately 20 Hz, the low-cost SX-I GPS – at 1 Hz, and the visual measurements are obtained with the frequency 0.5 to 2 Hz. It is important to align arriving data in time, according to their time stamp for proper data fusion. For the real time operation this requires temporary storage of the INS measurements for a period of a typical absolute measurement delay, so that once the new, but already outdated absolute measurement arrives it is properly fused at the time of its time stamp with the INS data. Once the past measurement is incorporated, the state is propagated through the INS data buffer to the present. A timing schematic for the localization filter is shown in Figure 4.10. Present work does not take into the consideration the real-time issues; the real data is aligned for post-processing by the localization algorithm off-line.

[21] Wrong covariances produce wrong Kalman gain and suboptimal measurement weighting.

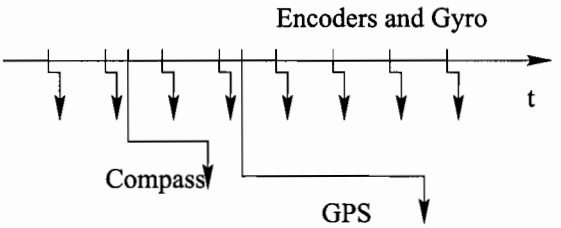

FIGURE 4.10. Real Time Timing Sequence of the Localization Filter. The arrows represent measurements; they start at the measurement insant and extend their heads to the time of their availability to the filter.

CHAPTER 5

The Landmark Density Evaluator

The Landmark Density Evaluator (LDE) is developed in Matlab® environment and calculates and plots the characteristic localization statistics based on the odometer, gyroscope, and absolute sensor measurements. The desired landmark density and sensing noise are supplied to the estimator as parameters. The LDE can operate on the simulated, experimental or mixture of the simulated and experimental data in order to estimate the expected localization accuracy and precision with the given INS and absolute sensor parameters. The absolute sensing from distance and bearing, bearing only, and direct position observation (GPS-like) is accommodated for both simulated and actual data. A graphical user interface of the LDE shown in Figure 5.1 allows to change the system error parameters, choose the sensing mode, load the optional data files, close the unwanted figures and stop the program execution on the flight, if desired. The schematic diagram of the LDE is shown on Figure 5.2 on page 46. The operation of LDE is covered in Appendix B on page 67. This section concentrates on the development of equations for the process noise matrix $\mathbf{Q}(k)$ and optimized marker placement.

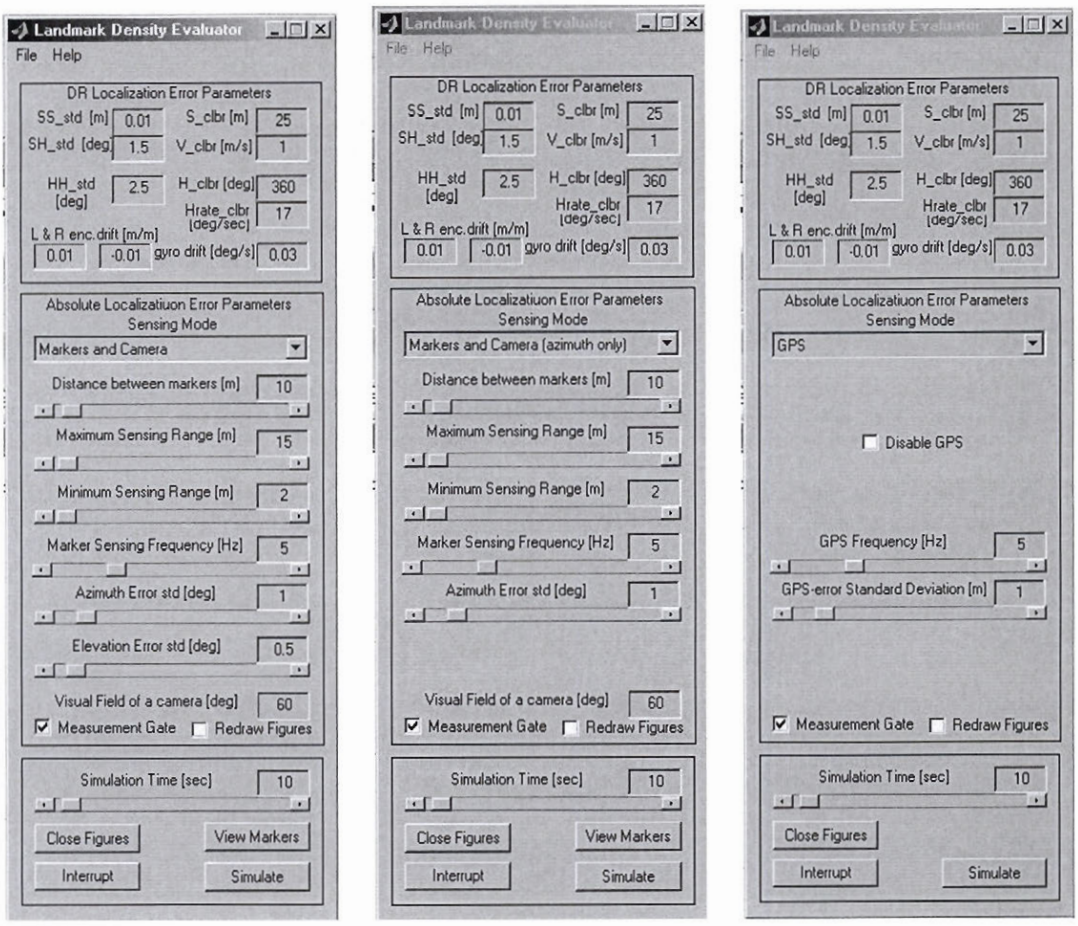

(a) Range and bearing absolute measurement mode.

(b) Bearing-only absolute measurement mode.

(c) Direct position measurement (GPS mode).

FIGURE 5.1. The Modes of the Landmark Density Evaluator

1. The Process Noise

The process noise for the extended Kalman filter is calculated as proposed by Chenavier and Crowley [31]:

$$\mathbf{Q}(k) = \begin{bmatrix} Q_{11}(k) & 0 & 0 \\ 0 & Q_{22}(k) & 0 \\ 0 & 0 & Q_{33}(k) \end{bmatrix} \tag{5.1}$$

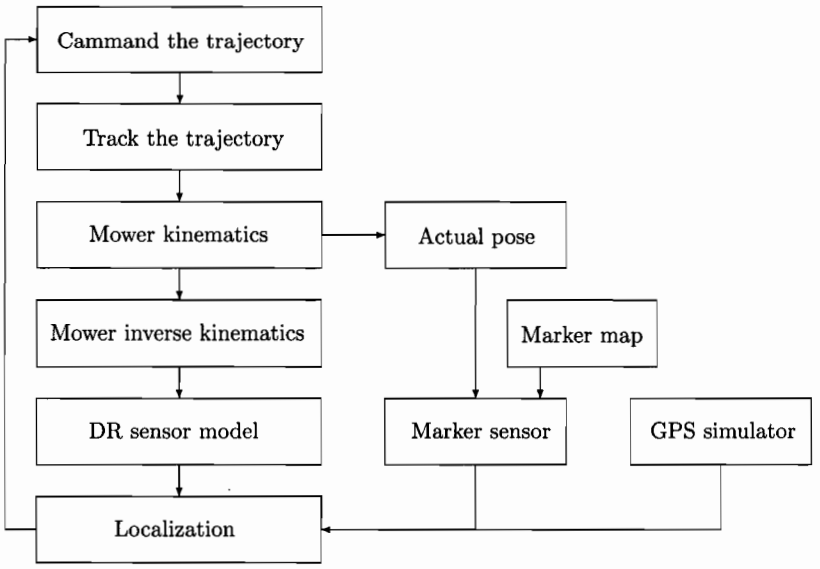

FIGURE 5.2. The Schematic of the Landmark density Evaluator

where

$$\mathbf{Q}_{11}(k) = K_{ss}|\Delta D cos\phi| \tag{5.2}$$

$$\mathbf{Q}_{22}(k) = K_{ss}|\Delta D sin\phi| \tag{5.3}$$

$$\mathbf{Q}_{33}(k) = K_{s\phi}|\Delta D| + K_{\phi\phi}|\Delta\phi| \tag{5.4}$$

However, instead of tuning the coefficients $[K_{ss}] = m^2/m$, $[K_{s\phi}] = rad^2/m$, and $[K_{\phi\phi}] = rad^2/rad$ outright, it is proposed to derive their values from the overall *system* [6] dead reckoning performance expressed in more physically meaningful quantities than the coefficients themselves. From Equations 5.2, 5.3, and 5.4:

$$K_{ss} = \frac{\sigma_{ss}^2}{|\Delta s|} \tag{5.5}$$

$$K_{s\phi} = \frac{\sigma_{s\phi}^2}{|\Delta s|} \tag{5.6}$$

$$K_{\phi\phi} = \frac{\sigma_{\phi\phi}^2}{|\Delta\phi|} \tag{5.7}$$

Where σ_{ss}^2, $\sigma_{s\phi}^2$ are the user-supplied distance and angular error variances obtained from the straight line runs of length Δs; $\sigma_{\phi\phi}^2$ is the angular error variance obtained from the circular unidirectional runs with the total travel angle $\Delta\phi$.

The noise contributions of the odometers $\Delta\sigma_D$ and the gyroscope $\Delta\sigma_{\dot{\phi}}$ at each iteration are obtained as follows:

$$\Delta\sigma_D = \frac{\sigma_{ss}^2}{\frac{\Delta s \cdot \Delta t}{V_n}} \tag{5.8}$$

$$\Delta\sigma_{s\phi} = \frac{\sigma_{s\phi}^2}{\frac{\Delta s \cdot \Delta t}{V_n}} \tag{5.9}$$

$$\Delta\sigma_{\phi\phi} = \frac{\sigma_{\phi\phi}^2}{\frac{\Delta \phi \cdot \Delta t}{\omega_n}} \tag{5.10}$$

$$\Delta\sigma_{\phi} = \sqrt{(\Delta\sigma_{s\phi})^2 + (\Delta\sigma_{\phi\phi})^2} \tag{5.11}$$

$$\Delta\sigma_{\dot{\phi}} = \sqrt{2 \cdot \left(\frac{\Delta\sigma_{\phi}}{\Delta t}\right)^2} \tag{5.12}$$

Where V_n is the nominal speed during the calibration runs, ω_n is the nominal turning rate during the circular runs, and Δt is the nominal time step of the iteration.

2. The Optimized Marker Placement

The geometry of the marker placement affects the absolute position estimation accuracy. An optimal absolute marker placement is an open-ended problem in the general case, however few attempts to optimize marker placement for specific scenarios were done. Armingol *et al.* [55] described two approaches to marker positioning. The first approach uses an a priori marker placement with density high enough so that each path can be fully covered. Once a path is chosen, only the markers that are visible from the path remain, to reduce the infrastructure cost. The second approach selects a path through the regions of good marker coverage for a given marker map. Beacon patterns suitable for a given trajectory were considered by McGillem *et al.* [74], while Durrant-Whyte [42] found that a triangular grid provides the maximum accuracy and coverage.

The following is an attempt to optimize the marker placement for a predefined path - mowing pattern - so that required overall localization accuracy (INS and absolute positioning system combined) give the required localization accuracy with a minimum number of markers. A marker grid with triangular cells is oriented along the swaths (see Chapter 6, Section 2.2.1.) The marker placement consept is illustrated in Figure 5.3. The open loop (dead reckoning only) localization system precision is used

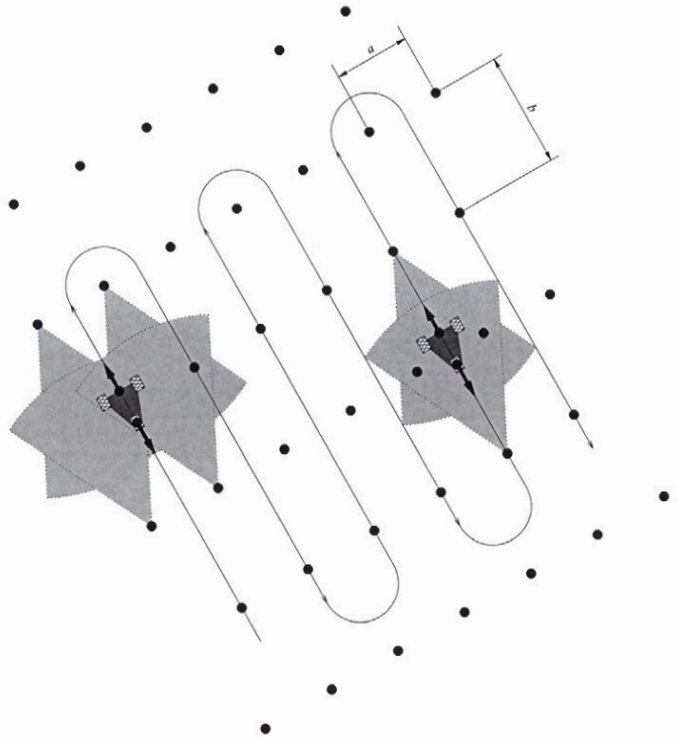

FIGURE 5.3. Optimized Marker Placement Concept. The dark filled circles in the triangular pattern represent the markers; the lighter filled circular segments show the marker visibility in the mower orientation shown; the arrows in the front and back of the mower point in the directions of the camera vision fields. The parameters a and b of the triangular cell are maximized so that the desired localization accuracy is achieved with a minimal number of markers.

to estimate the parameters of the asymmetric triangular marker grid. The system's dead reckoning precision is determined experimentally on the straight line paths. The

localization error covariance provided by the Kalman filter is also indicative of the estimation precision [75]. Marker visibility at the edges of the field ensures proper alignment of the mowing pattern. Absolute corrections at the beginning of the swath minimize the heading error incurred during the turn by the INS, while corrections at the end of the swath, prior to entering the turn, allow to minimize the absolute error by correcting the mower localization prior to entering the straight segment.

CHAPTER 6

Localization Implementation and Validation

This chapter describes the experimental results for the work conducted for this thesis. The localization experiments are performed in the open-loop mode on the Toby-2 localization testbed and on the autonomous Toby and Hal without the feedback to the control system. The localization error should be calculated with respect to the ground truth (GT). One of the main difficulties in the validation of the localization outdoors is the absence of a ground truth for the vehicle motion. Comparing the estimated and actual GT positions in the fixed points on the trajectory is a representative but not reliable localization performance characteristic since dead reckoning (DR) error depends on the trajectory[1]. The use of NovAtel 2 *cm* accuracy real time kinematic GPS (RKTGPS) as the absolute sensor for the ground truth extended Kalman filter (EKF)[2] allows to directly evaluate the performance of the vision-based localization system.

[1]Odometry errors virtually cancel over symmetric trajectories, for example a mowing pattern consisting of an equal number of left and right turns and equal distances traveled in both directions [57]. Gyro drift depends not only on the temperature, but also on the turning rate, thus trajectories with many sharp turns result in higher gyro drift and worse localization than mostly straight line or slightly curved trajectories. At high turning rates gyro output becomes highly nonlinear and requires polynomial curve fitting for adequate measurement interpretation [77]

[2]Use of Vulcan 3D laser-based precision Measurement System manufactured by Arc Second [5] as a ground truth for a 30 m by 60 m testing area was considered, but the system's cost was prohibitive.

1. The Visual Markers Experiment

The experimental setup is shown in Figure 6.1. Two DFW-VL500 [98] digital camera modules are mounted on the mower, one in the front and the back. The markers are scattered at about $10\,m$ distance from each other. The GPS signal in the testing area provides $2\,cm$ accuracy absolute localization, which is fused with the odometry in the localization extended Kalman filter of the mower gives high-quality ground truth position estimate. The accuracy and precision (error standard devi-

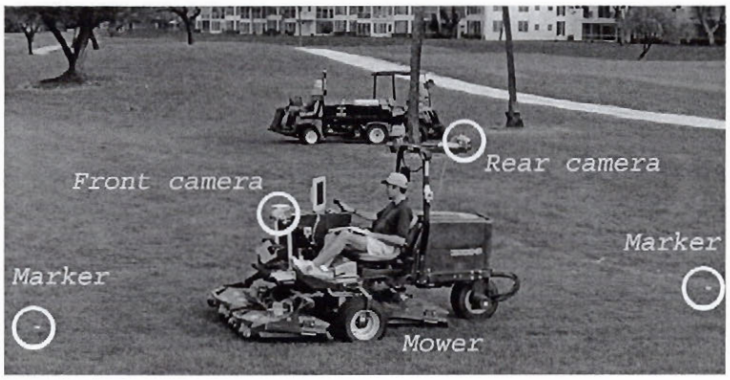

FIGURE 6.1. The experimental setup: the mower (foreground) is equipped with the cameras in the front and in the back; the markers are seen in the front and in the back of the mower. The mower is manually driven.

ation) of the cameras' measurements are obtained by comparison with the ground truth. The biases and standard deviations are given in Table 6.1 and the corresponding error distributions are shown in Figure 6.2 on page 52. The measurements are debiassed prior to being used in the EKF. The local marker approach is general, so the results of the experiments estimate the localization accuracy obtainable by a marker-based system irrespective of the actual hardware implementation. The cardioidal and mowing pattern path experiments are described in this section.

1.1. The Cardioidal Path. The cardioidal path is composed of a clockwise turning maneuvers in a $40\ m \times 40\ m$ area with marker positioned in a square pattern every $10\ m$. The localization quality based on the experimental data is summarized in Table 6.2.

TABLE 6.1. The camera's biases and precision.

	Front Camera	Back Camera
Azimuth		
Bias	1.10^o	-2.50^o
Standard Deviation	0.67^o	0.67^o
Elevation		
Bias	0.15^o	-0.12^o
Standard Deviation	0.16^o	0.15^o

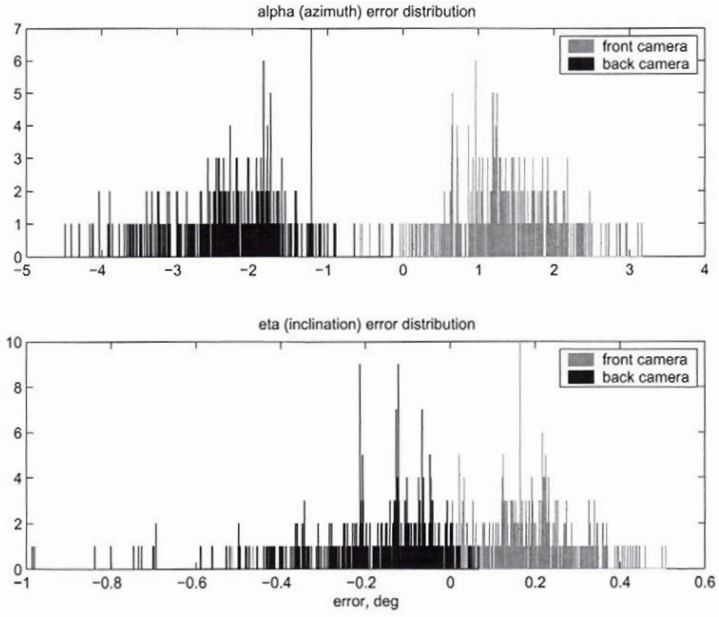

FIGURE 6.2. The absolute measurement error distribution of visual measurements.

TABLE 6.2. The cardioidal path localization performance.

	Transverse Error	Tangential Error	Heading Error
Expected	-0.002 m	0.006 m	0.083^o
Maximum	0.233 m	0.866 m	1.894^o
Standard Deviation	0.089 m	0.202 m	0.430^o

In summary, the cardioidal localization transverse errors are below 10 cm with 90% probability, the tangential errors are below 10 cm with 80% probability, and below 18 cm with 90% probability (see Figures 6.4 (a) and (b) on page 56.)

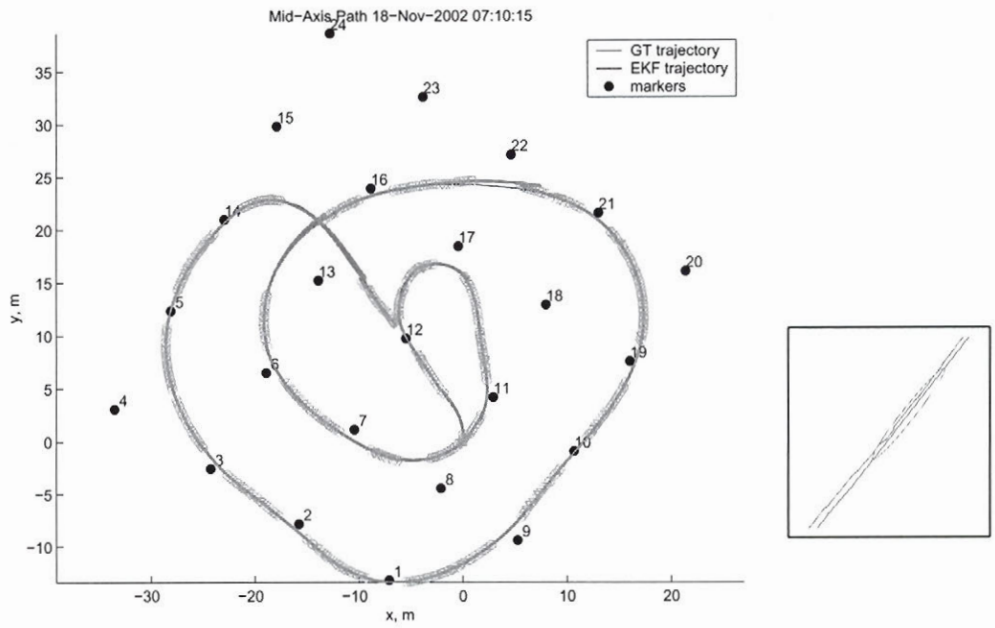

FIGURE 6.3. The cardioidal path and the zoom-in to a covariance ellipse of the localization uncertainty.

1.2. The Mowing Pattern Path. A section of a regular mowing pattern with visual marker measurements is analyzed in this experiment. It is essential to maintain the localization accuracy on the straight sections of the pattern (Figure 6.5 on page 57), while the accuracy on the curved "hairpin" U-turns is not as important.

TABLE 6.3. The straight sections of the mowing pattern localization performance.

	Transverse Error	Tangential Error	Heading Error
Expected	0.110 m	0.272 m	-0.008^o
Maximum	0.220 m	0.540 m	0.884^o
Standard Deviation	0.064 m	0.157 m	0.101^o

In summary, the localization transverse errors are below 7 cm with 90% probability, the tangential errors are below 8 cm with 80% probability (see Figures 6.7 (a) and (b) on page 59.)

2. Simulated Localization

The following localization scheme evaluation is performed on the Landmark Density Evaluator (LDE) based on the combined experimental and simulated data.

2.1. Simulated Measurements and Experimental Trajectory. The experimental mower trajectory is combined with the simulated optimized triangular pattern marker placement and measurements. The marker sensor is assumed to be unbiased with the azimuth measurement error standard deviation (*std*) of 1^o, and the elevation measurement error *std* of 0.5^o, in accordance with the precision characteristics of the experimental camera measurements. The localization is evaluated for two marker sensing frequencies: 2 Hz and 5 Hz.

TABLE 6.4. The simulated 2 Hz and 5 Hz measurements and experimental trajectory localization performance.

	Transverse Error	Tangential Error	Heading Error
	2 Hz Absolute Measurements		
Expected	0.117 m	0.243 m	-0.066^o
Maximum	0.233 m	0.483 m	2.139^o
Standard Deviation	0.068 m	0.141 m	0.682^o
	5 Hz Absolute Measurements		
Expected	0.050 m	0.125 m	-0.049^o
Maximum	0.099 m	0.249 m	2.091^o
Standard Deviation	0.029 m	0.073 m	0.583^o

In summary, the localization transverse errors for the 2 Hz absolute measurements are below 6.5 cm with 90% probability, the tangential errors are below 8.5 cm with 90% probability (see Figures 6.8 (a) and (b) on page 60.) The 5 Hz absolute measurements are below 6.2 cm with 90% probability, the tangential errors are below 7.4 cm with 90% probability (see Figures 6.9 (a) and (b) on page 61.) The higher bandwidth (5 Hz) absolute sensor provides the desired transverse localization accuracy for the system configuration considered here.

3. Summary

The analysis of the experimental data of the visual absolute marker experiment showed that on the straight sections of the mowing pattern the localization transverse errors are below 7 *cm* with 90% probability, the tangential errors are below 8 *cm* with 80% probability, which is close to the desired 10 *cm* transverse accuracy. Transverse to the direction of motion localization errors in excess of 10 *cm* occur with a probability of 8% with a maximum error of 22 *cm*. The larger errors are due to insufficient marker coverage of the test area at the U-turns where a large localization uncertainty is accumulated. With the extended absolute measurement coverage and optimized marker positioning in the Landmark Density Evaluator the localization errors transverse to the direction of motion reduced to below 6.2 *cm* with 90 % probability. The errors tangential to the direction of motion reduced to 7.4 *cm* with 90 % probability. The innovation sequence generally remains within the one-sigma bound and is unbiased. It is concluded that the filter is consistent, that is its covariances correspond to the inaccessible covariances of the actual process. The behavior of the innovation sequence indicates that this is the case.

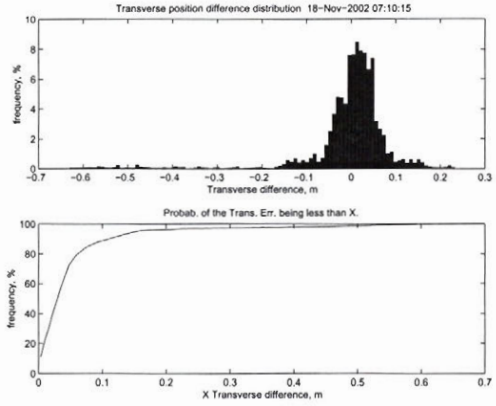

(a) Transverse error distribution.

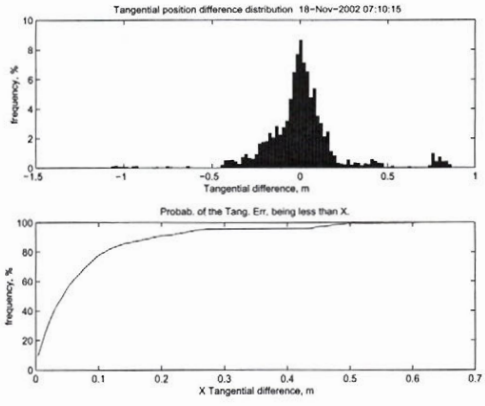

(b) Tangential error distribution.

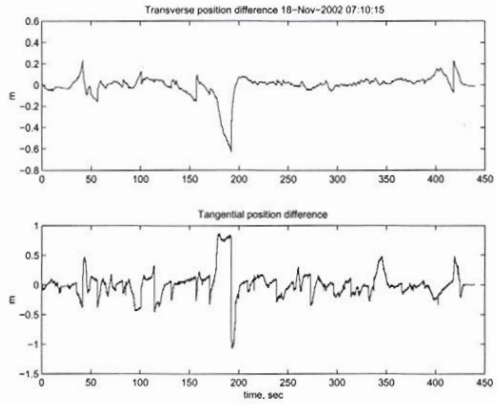

(c) Transverse and tangential errors.

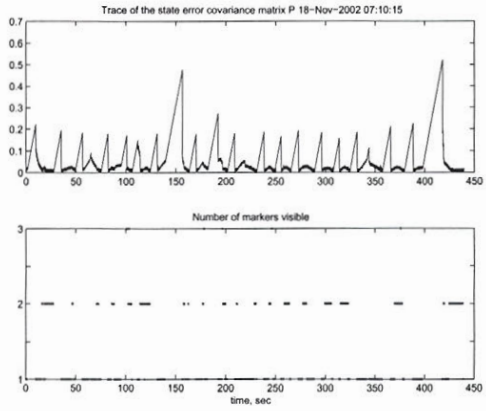

(d) Trace of P and number of visible markers.

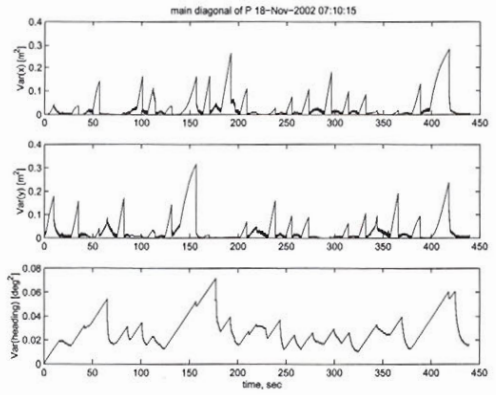

(e) Values of the main diagonal of P.

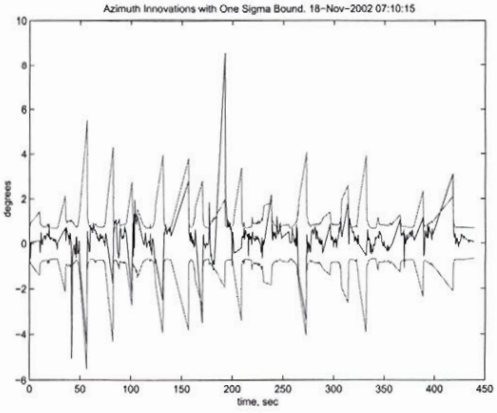

(f) Azimuth innovation and its 1 σ bound.

FIGURE 6.4. The visual representations of the cardioidal experiment data.

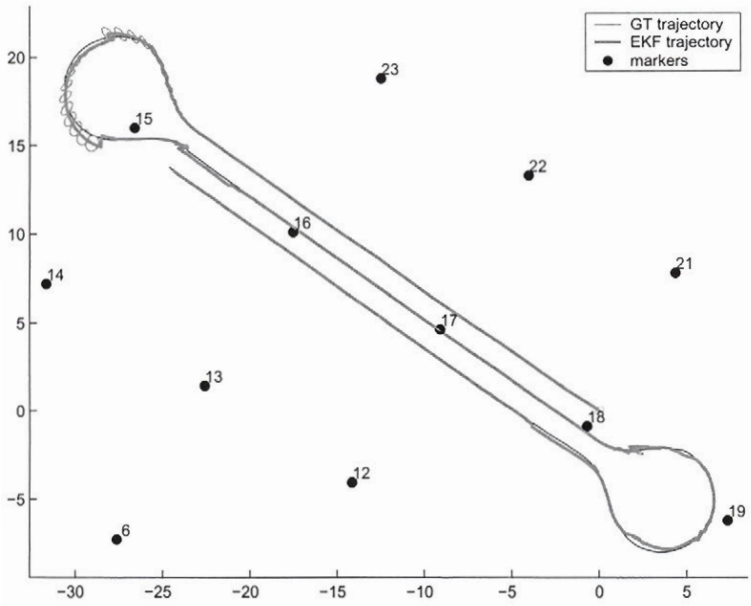

FIGURE 6.5. The two swaths path.

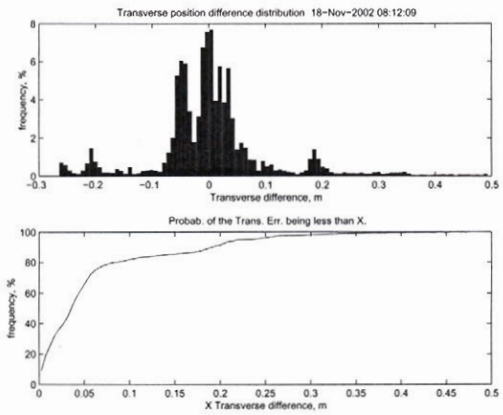

(a) Transverse error distribution.

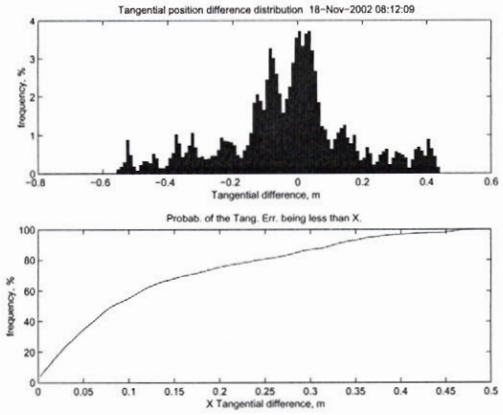

(b) Tangential error distribution.

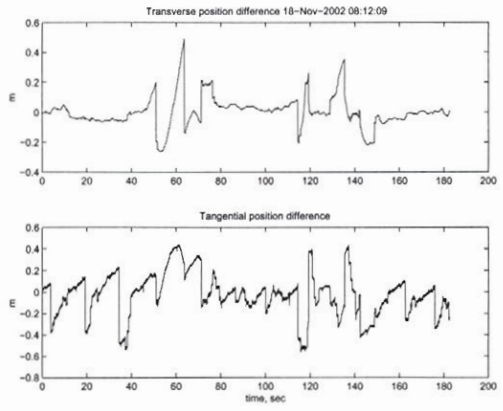

(c) Transverse and tangential errors.

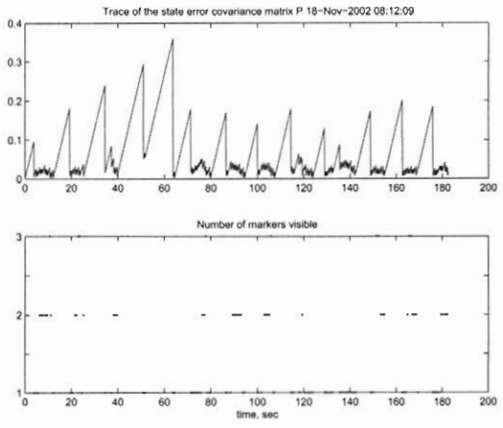

(d) Trace of P and number of visible markers.

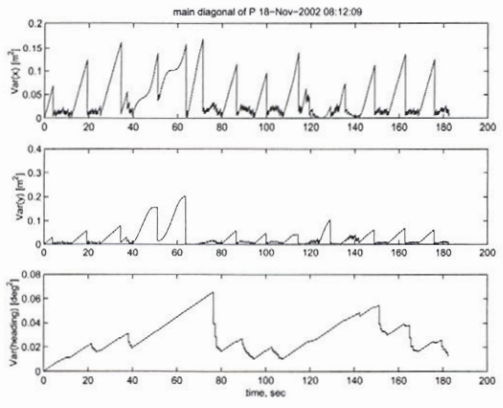

(e) Values of the main diagonal of P.

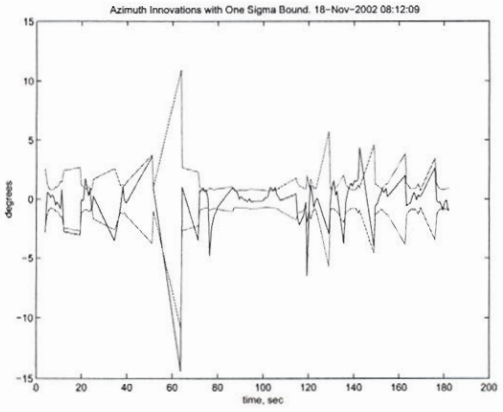

(f) Azimuth innovation and its 1 σ bound.

FIGURE 6.6. The visual representations of the two swaths segment data.

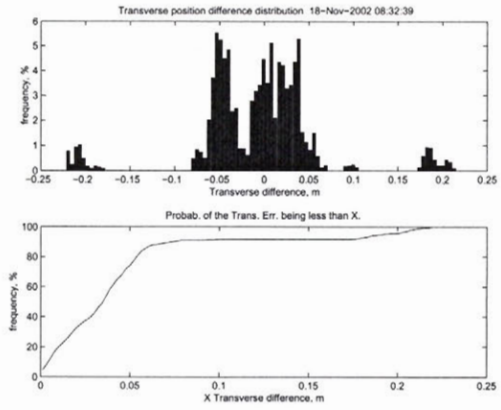

(a) Transverse error distribution.

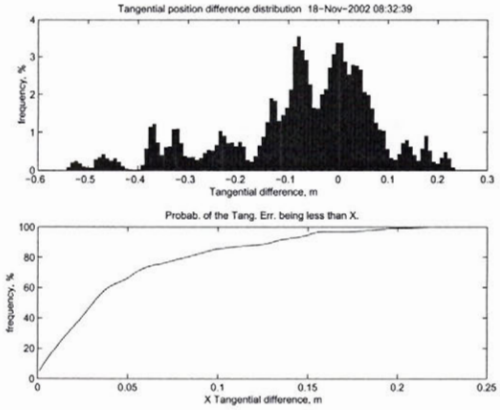

(b) Tangential error distribution.

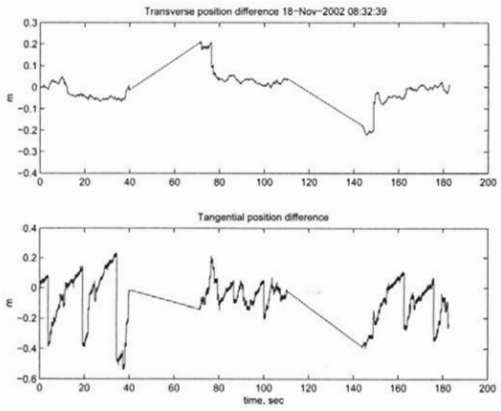

(c) Transverse and tangential errors.

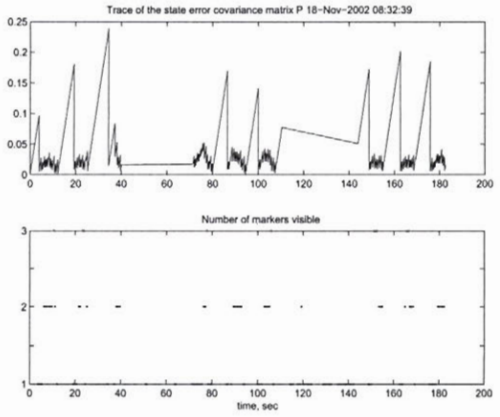

(d) Trace of P and number of visible markers.

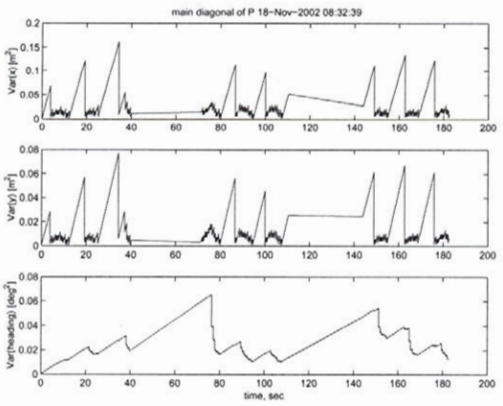

(e) Values of the main diagonal of P.

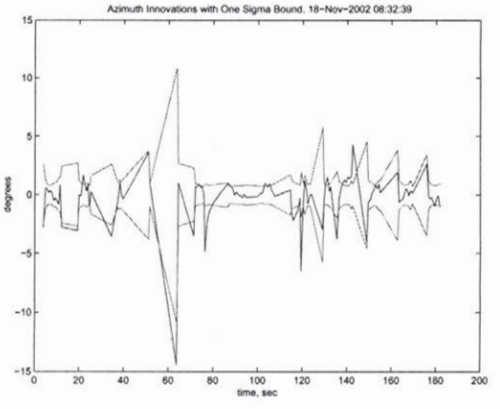

(f) Azimuth innovation and its 1 σ bound.

FIGURE 6.7. The visual representations of the two swaths segment data.

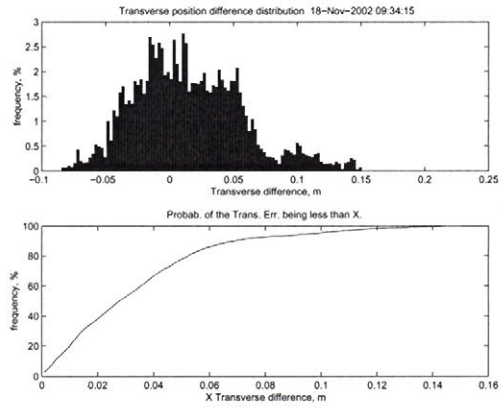

(a) Transverse error distribution.

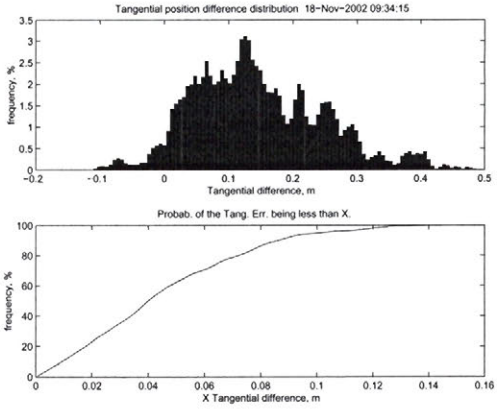

(b) Tangential error distribution.

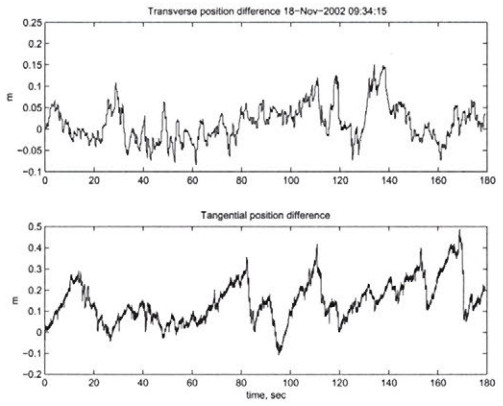

(c) Transverse and tangential errors.

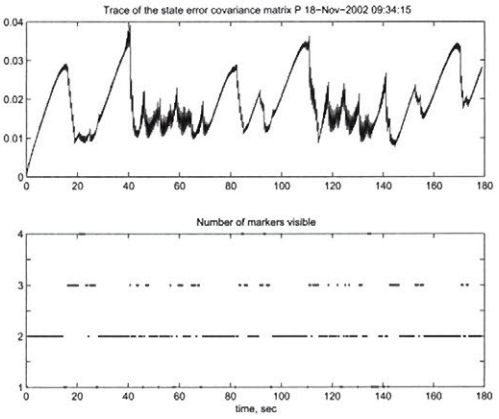

(d) Trace of P and number of visible markers.

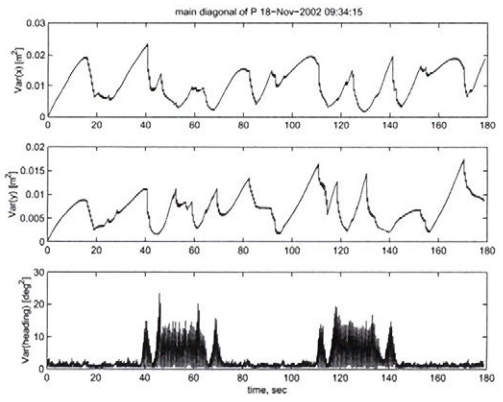

(e) Values of the main diagonal of P.

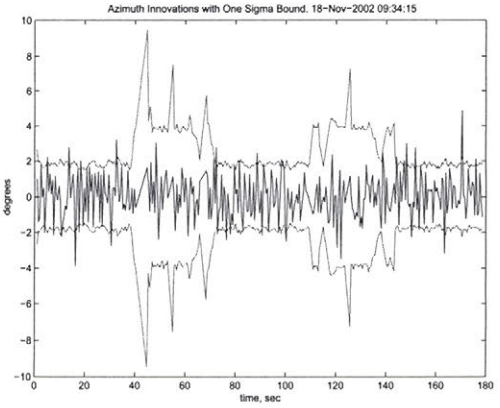

(f) Azimuth innovation and its 1 σ bound.

FIGURE 6.8. The visual representations of the 2 Hz simulated measurements and experimental trajectory data.

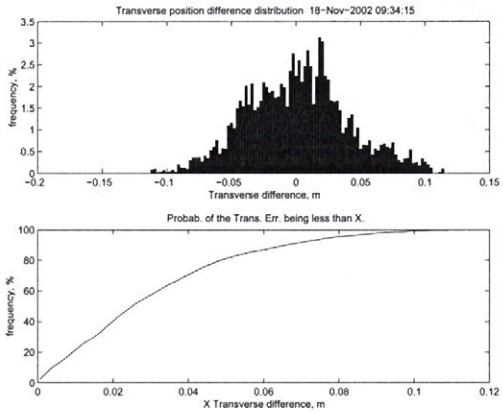

(a) Transverse error distribution.

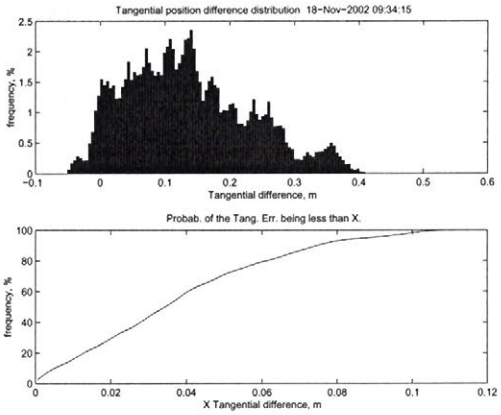

(b) Tangential error distribution.

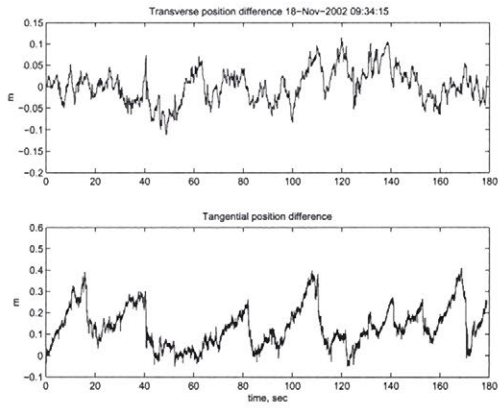

(c) Transverse and tangential errors.

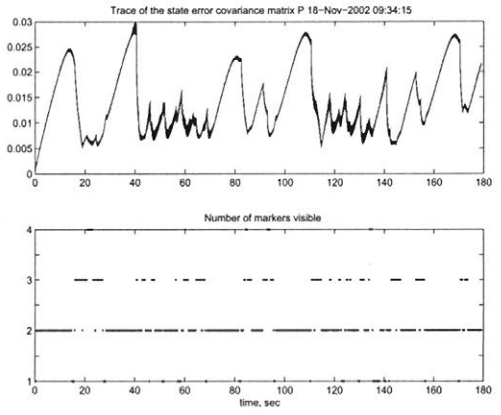

(d) Trace of P and number of visible markers.

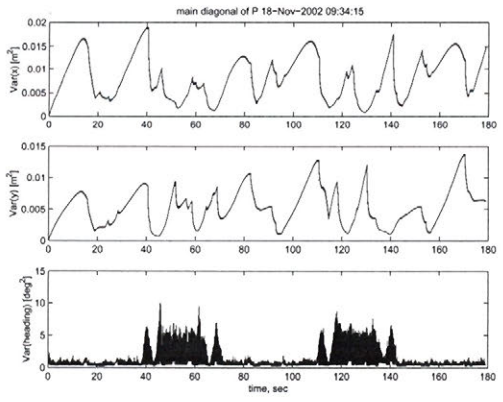

(e) Values of the main diagonal of P.

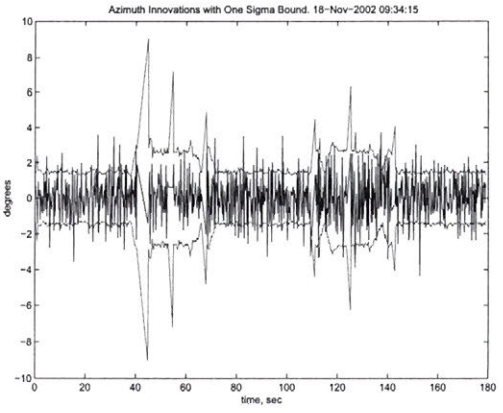

(f) Azimuth innovation and its 1 σ bound.

FIGURE 6.9. The visual representations of the 5 Hz simulated measurements and experimental trajectory data.

CHAPTER 7

Conclusions

This thesis outlines the problem of outdoor autonomous robot localization. The Kalman filtering methodology is used in conjunction with the chi-square gaiting technique for a robust localization using real as well as simulated measurements. The test results showed that the set goal of lateral position error is attainable, but requires additional investigation and sensor development. As in the numerous examples of terrestrial localization this system requires both the dead reckoning and the absolute localization in real time. It is suggested that the fusion of dead reckoning, low-cost (1 m precision) DGPS and another relatively low-cost absolute sensor – the electronic compass – will solve the absolute measurement starvation problem encountered in INS and GPS-only systems when the navigation satellites are occluded. The magnetic compass, being an absolute sensor, will supply the most important information for terrestrial navigation: the absolute heading. The current localization system relying on the sensors described above attains up to 8 cm accuracy overall in the direction perpendicular to the direction of motion. The parallel error stayed within 15 cm, which is acceptable for the application. The availability of affordable, compact sensors, computing and communications equipment allows application of the new technologies in the environments previously inaccessible. (Low-cost 1 m precision DGPS, Wave LAN, fast computers available for image processing, for example.)

Future Work. The future work would include integration of the additional sensors (wave LAN radio modem, for example) to further increase the redundancy of the measurements and thus the robustness of the system. Monte-Carlo localization (MCL) and combined KF/MCL techniques could be implemented to improve the robustness of the localization with the noisy sensors and uncertain initial conditions. The robust and accurate integrated navigation system could be implemented on a vehicle.

APPENDIX A

The Global Positioning System

The Global Positioning System (GPS) consists of the space-based[1] and the ground-based parts. The space-based part of the GPS constellation consists of 24 satellites (21 + 3 spares) on six elliptical orbital planes. The satellites transmit on two L-band carrier frequencies: L1 = 1227.6 MHz, and L2 = 1575.42 MHz. Since the ionospheric time delay is proportional to the square of the transmitter frequency, dual L1 and L2 band receivers (military grade) can calculate the delay directly and compensate for it. Single L1 band consumer GPS compensate for up to 50% of the ionospheric time delay in software. The ground-based part of the GPS system consists of four monitor stations that invert the navigation solution to track the satellites. Since the introduction of GPS[69] service in the beginning of eighties it has been used for military marine, air and land navigation, land surveying followed by civilian navigation, Geographic Information Systems (GIS), vehicle tracking and agriculture field guidance[2]. In the mid-1990s, Russia added the Glonass positioning

[1]Ground-based navigational aids like Loran, and Omega [54] use low frequency modulation for their signals so that they reflect from the ionosphere and provide broader coverage. Unfortunately, low frequency carrier waves can be modulated with little navigation information, which results in inaccurate localization – about 7400 m 2σ for Omega, for example. The high frequency signals, on the other hand will penetrate the ionosphere and can only be used in the direct line of sight coverage area from the transmitter. A dense antenna tower grid (one antenna for about 150 km^2) would be required for worldwide coverage. Placing the high frequency transmitter high in space solves both the area coverage and signal modulation problems.

[2]Transit - the first satellite navigation (satnav) system -introduced in 1973 was used for global satellite navigation before the GPS era. Transit is still operational, but it is unlikely that the dying satellites will be replaced, because of the system's significantly lower accuracy (about 457 m, 1σ)

system that can be exploited in combination with GPS[3]. By the year 2007, Europe's civilian (in contrast to the military-run GPS and Glonass) Galileo positioning system, fully compatible with GPS will be operational, providing additional redundancy for the safety-critical services. [69, 45] The weak GPS signals require direct line of sight (LOS) for reception. Four to five satellites have to be visible to obtain a low-accuracy three-dimensional position estimate; six to eight satellites in view give good GPS position.

1. Differential GPS

Differential GPS (DGPS) uses a correction signal from a beacon-receiver positioned at a known location in the operating region. Ground-based (radiobeacon stations) or space-based (satellites) networks providing the differential corrections are called *augmentation systems.* Temporary loss of the base correction (differential) signal leads to rapid degradation of position accuracy and to termination of the differential mode.

2. Space-Based Augmentation System

There exist three fully compatible Space-Based Augmentation Systems (SBAS) that provide subscription-free differential correction signal: WAAS (USA), EGNOS (Europe), MSAS (Japan). North America is covered by the WAAS system that comprises a grid of 25 ground reference stations in the USA. Two master stations on each coast process the data from all the slave stations and generate a correction (differential) signal broadcast through one of the two geostationary satellites. The satellite transmitters allow use of the unmodified GPS message structure for the correction signal, standard GPS antennas and receivers with WAAS-enabled software.

---

and measurement update rate (once every 1.5 hours or so) [69] than, progressively more affordable, GPS.

[3]Due to principal differences between GPS and Glonass (polar vs. Cartesian space representations, elliptical vs. circular satellite orbits, for example) merging the two systems is a nontrivial task; a typical dual receiver is the Ashtec GG24.

3. Real Time Kinematic GPS

Real Time Kinematic GPS (RTKGPS) is a DGPS in which a rover station is initialized at a surveyed position. RTK mode requires continuous GPS lock maintained[69].

APPENDIX B

Auxiliary Derivations

1. The Dynamic Model (Lagrangian Approach)

The Lagrangian approach was used to derive the equations of motion of the tricycle platform:

$$\mathbf{M}(\mathbf{q})\ddot{\mathbf{q}} + \mathbf{V}(\mathbf{q}, \dot{\mathbf{q}}) = \mathbf{E}(\mathbf{q})\boldsymbol{\tau} - \mathbf{A}^T\boldsymbol{\lambda} \tag{B.1}$$

where $\mathbf{M}(\mathbf{q})$ is the inertia matrix , $\mathbf{V}(\mathbf{q}, \dot{\mathbf{q}})$ is the vector of position and velocity dependent forces, $\mathbf{E}$ is the input transformation matrix, $\boldsymbol{\tau}$ is the input vector, $\mathbf{A}$ is the constraint matrix , and $\boldsymbol{\lambda}$ is the vector of Lagrange multipliers [36, 85]. For the three-wheel platform of the mower the following state vector was chosen:

$$\mathbf{q} = [x \;\; y \;\; \phi \;\; \theta_S \;\; \gamma \;\; \theta_L \;\; \theta_R]^T \tag{B.2}$$

where x, y are the Cartesian coordinates of the point of interest, and ϕ is the orientation of the platform; θ_S, θ_L, θ_R are the wheel axial rotation angles – S-steering wheel, L-left, R-right wheel[1], γ is the steering angle. The driving (τ_ω) and steering (τ_γ) torques compose the input vector:

$$\boldsymbol{\tau} = [\tau_\omega \;\; \tau_\gamma]^T \tag{B.3}$$

[1]Kinetic energies of the wheels were taken into account

The Lagrangian is calculated assuming negligible changes in the altitude, so that potential energy is constant and set to zero. $\mathbf{M(q)}$ and $\mathbf{V(q,\dot{q})}$ are obtained from the Lagrangian by taking the acceleration coefficients and the rest of the terms respectively.

$$\mathbf{M(q)} \tag{B.4}$$

$$= \begin{bmatrix} m_p{+}3m_w & 0 & (f(m_p+2m_w)-2m_wc)sin\phi & 0 & 0 & 0 & 0 \\ 0 & m_p{+}3m_w & -(f(m_p+2m_w)-2m_wc)cos\phi & 0 & 0 & 0 & 0 \\ 0 & 0 & J_p{+}3J_v{+}f^2m_p{+}\frac{1}{2}m_w(b^2{+}4(c{+}f)^2 & 0 & J_v & 0 & 0 \\ 0 & 0 & 0 & J_a & 0 & 0 & 0 \\ 0 & 0 & J_v & 0 & J_v & 0 & 0 \\ 0 & 0 & 0 & 0 & 0 & J_a & 0 \\ 0 & 0 & 0 & 0 & 0 & 0 & J_a \end{bmatrix}$$

$$\mathbf{V(q,\dot{q})} \tag{B.5}$$

$$= [\dot{\phi}^2(f(m_p{+}2m_w){-}2m_wc)cos\phi \;\; \dot{\phi}^2(f(m_p{+}2m_w){-}2m_wc)sin\phi \;\; 0 \;\; 0 \;\; 0 \;\; 0 \;\; 0]^T$$

where m_p is the platform mass, m_w is the wheel mass, J_p is the platform's moment of inertia about the vertical axis ($z-axis$), J_v and J_a are the moments of inertia of the wheel about the vertical axis and about its own axis; the dimensions b, c,and f are shown in Figure B.1 on page 69. 3.6. There are five independent nonholonomic constraints (three for the front wheels and two for the steering wheel) arising from no free-spinning and no side-sliding conditions. These conditions written in the matrix form for the state vector of the system become:

$$\mathbf{A\dot{q}} = \mathbf{0} \tag{B.6}$$

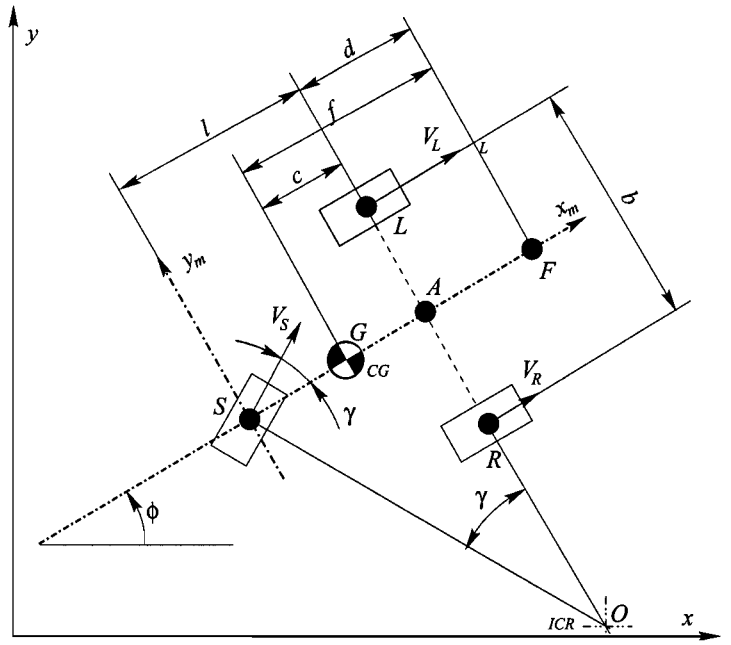

FIGURE B.1. Schematic of the mower platform

$$\mathbf{A} = \begin{bmatrix} cos\phi & sin\phi & -b/2 & 0 & 0 & -r & 0 \\ cos\phi & sin\phi & b/2 & 0 & 0 & 0 & -r \\ sin\phi & -cos\phi & d & 0 & 0 & 0 & 0 \\ cos(\phi+\gamma) & sin(\phi+\gamma) & 0 & -r & 0 & 0 & 0 \\ sin(\phi+\gamma) & -cos(\phi+\gamma) & 0 & 0 & 0 & 0 & 0 \end{bmatrix} \tag{B.7}$$

The Null Space(S-matrix) of the constraint matrix A can be used to avoid calculation of the Lagrange multipliers:

$$\mathbf{S^T A^T = 0} \tag{B.8}$$

S transforms the vector of independent velocities into the vector of the generalized velocities and was obtained as follows:

$$\mathbf{A_{5\times 7}\dot{q} = 0} \quad \longrightarrow \quad \begin{bmatrix} \mathbf{A_{15\times 3}} & \mathbf{A_{25\times 2}} & \mathbf{A_{35\times 2}} \end{bmatrix} \begin{bmatrix} \mathbf{\dot{q}_1} \\ \mathbf{\dot{q}_2} \\ \mathbf{\dot{q}_3} \end{bmatrix} = \mathbf{0} \tag{B.9}$$

$$\dot{\mathbf{q}}_1 = \begin{bmatrix} \dot{x} & \dot{y} & \dot{phi} \end{bmatrix}^T \tag{B.10}$$

$$\dot{\mathbf{q}}_2 = \begin{bmatrix} \dot{\theta_S} & \dot{\gamma} \end{bmatrix}^T \tag{B.11}$$

$$\dot{\mathbf{q}}_3 = \begin{bmatrix} \dot{\theta_L} & \dot{\theta_R} \end{bmatrix}^T \tag{B.12}$$

$$\mathbf{A_1}\dot{\mathbf{q}}_1 + \mathbf{A_2}\dot{\mathbf{q}}_2 + \mathbf{A_3}\dot{\mathbf{q}}_3 = 0 \quad \longrightarrow \quad \begin{bmatrix} \mathbf{A_1} & \mathbf{A_3} \end{bmatrix} \begin{bmatrix} \dot{\mathbf{q}}_1 \\ \dot{\mathbf{q}}_3 \end{bmatrix} = -\mathbf{A_2}\dot{\mathbf{q}}_2 \tag{B.13}$$

$$\begin{bmatrix} \dot{\mathbf{q}}_1 \\ \dot{\mathbf{q}}_3 \end{bmatrix} = -\begin{bmatrix} \mathbf{A_1} & \mathbf{A_3} \end{bmatrix}^{-1} \mathbf{A_2}\dot{\mathbf{q}}_2 \tag{B.14}$$

$$\dot{\mathbf{q}} = \mathbf{S}\dot{\mathbf{q}}_2 \tag{B.15}$$

$$\mathbf{S} = -\begin{bmatrix} \mathbf{A_1} & \mathbf{A_3} \end{bmatrix}^{-1} \mathbf{A_2} = \begin{bmatrix} r \cdot cos(\phi+\gamma) & 0 \\ r \cdot sin(\phi+\gamma) & 0 \\ r \cdot sin(\gamma)/d & 0 \\ 1 & 0 \\ 0 & 1 \\ cos\gamma-(b \cdot sin\gamma)/(2d) & 0 \\ cos\gamma+(b \cdot sin\gamma)/(2d) & 0 \end{bmatrix} \tag{B.16}$$

Premultiplication of Equation B.1 by the S-matrix makes the term containing the Lagrange multipliers vanish:

$$\mathbf{S^T}[\mathbf{M(q)}\ddot{\mathbf{q}} + \mathbf{V(q,\dot{q})} = \mathbf{E(q)}\boldsymbol{\tau} - \mathbf{A}^T\boldsymbol{\lambda}] \tag{B.17}$$

$$\mathbf{S^T M(q)}\ddot{\mathbf{q}} + \mathbf{S^T V(q,\dot{q})} = \mathbf{S^T E(q)}\boldsymbol{\tau} - \mathbf{S^T A}^T\boldsymbol{\lambda} \tag{B.18}$$

$$\mathbf{S^T M(q)}\ddot{\mathbf{q}} + \mathbf{S^T V(q,\dot{q})} = \mathbf{S^T E(q)}\boldsymbol{\tau} \tag{B.19}$$

Using the S-matrix Equation B.16 to rewrite the equations of motion in terms of the independent coordinates:

$$\boldsymbol{\nu} = \dot{\mathbf{q}}_2 \tag{B.20}$$

$$\dot{\mathbf{q}}_2 = \mathbf{S}\nu \quad \longrightarrow \quad \ddot{\mathbf{q}} = \dot{\mathbf{S}}\nu + \mathbf{S}\dot{\nu} \tag{B.21}$$

$$\mathbf{S^T M(q)S}\dot{\nu} + \mathbf{S^T M(q)}\dot{\mathbf{S}}\nu + \mathbf{S^T V(q,\dot{q})} = \mathbf{S^T E(q)}\boldsymbol{\tau} \tag{B.22}$$

$$\mathbf{S^T M(q)S}\dot{\nu} + \mathbf{S^T}(\mathbf{M(q)}\dot{\mathbf{S}}\nu + \mathbf{V(q,\dot{q})}) = \mathbf{S^T E(q)}\boldsymbol{\tau} \tag{B.23}$$

Thus for the implementation the last equation is written in the following form:

$$\dot{\boldsymbol{\nu}} = (\mathbf{S^T M(q)S})^T[\boldsymbol{\tau} - \mathbf{S^T}(\mathbf{M(q)}\dot{\mathbf{S}}\nu + \mathbf{V(q,\dot{q})}] \tag{B.24}$$

$$\dot{\boldsymbol{\nu}} = [\ddot{\theta}_S \;\; \ddot{\gamma}]^T \tag{B.25}$$

Steering angle and the drive speed are obtained from the control law and converted to the required torque inputs (see Equation B.3) by a PD controller.

2. The Adaptation of the Zhang Tracker

This chapter describes the adaptation of the tracking algorithm for differentially driven platforms developed by Y.L. Zhang *et.al.* [114] for tricycle platforms.

The tracking algorithm translates the difference between the desired and actual positions of the point of interest of the differentially driven platform into the desired platform wheel velocities:

$$[\theta_{Ldes} \;\; \theta_{Rdes}]^T = \mathbf{G}^{-1}\left[[\dot{x}_{ref} \;\; \dot{y}_{ref}]^T - \mathbf{K_p}\left([x \;\; y]^T - [x_{ref} \;\; y_{ref}]^T\right)\right] \tag{B.26}$$

where $[\boldsymbol{\theta_{Ldes}} \;\; \boldsymbol{\theta_{Rdes}}]^T$ is the vector of desired angular speeds, $[x \;\; y]^T$ is the sensed position of the platform, and $[\dot{x}_{ref} \;\; \dot{y}_{ref}]^T$ is the refrence position on the trajectory.

The proportional gain matrix $\mathbf{K_p}$ is chosen to be diagonal[2]:

$$\mathbf{K_p} = \begin{bmatrix} k_x & 0 \\ 0 & k_y \end{bmatrix} \tag{B.27}$$

The Jacobian $\mathbf{G}$ transforming the rotational wheel velocities into the Cartesian velocities is:

$$[\dot{x} \;\; \dot{y}]^T = \mathbf{G}\,[\theta_L \;\; \theta_R]^T \tag{B.28}$$

$$\mathbf{G} = \frac{r}{2b} \begin{bmatrix} 2d \cdot sin\phi + b \cdot cos\phi & -2d \cdot sin\phi + b \cdot cos\phi \\ -2d \cdot cos\phi + b \cdot sin\phi & 2d \cdot cos\phi + b \cdot sin\phi \end{bmatrix} \tag{B.29}$$

Due to non-homogeneity of the kinematic state vector $\left[\dot{\theta_S} \;\; \dot{\gamma}\right]^T$ of a steered vehicle it is not possible to obtain a Jacobian similar to G in the Equation B.29 . However, the steering angle and steering wheel velocity can be expressed in terms of the front wheel velocities so that the control law of the Equation B.26 can be used [59].

Referring to Figure B.1 on page 69 the following geometrical relations take place:

$$\frac{V_L}{\|\vec{OL}\|} = \frac{V_R}{\|\vec{OR}\|} = \frac{V_S}{\|\vec{OS}\|} = -\dot{\phi} \tag{B.30}$$

$$\|\vec{OS}\| = \frac{l}{sin\gamma}; \qquad \|\vec{OA}\| = \frac{l}{tan\gamma} \tag{B.31}$$

$$\|\vec{OL}\| = \|\vec{OA}\| + b/2; \quad \|\vec{OR}\| = \|\vec{OA}\| - b/2; \tag{B.32}$$

The velocities of the front wheels can be related to the velocity, orientation of the steering wheel and platform geometry as follows:

$$V_R = \frac{\|\vec{OR}\|}{\|\vec{OS}\|} V_S = \frac{\|\vec{OA}\| - b/2}{\frac{l}{sin\gamma}} V_S = \frac{\frac{l}{tan\gamma} - b/2}{\frac{l}{sin\gamma}} V_S = \left(cos\gamma - \frac{b \cdot sin\gamma}{2l}\right) V_S \tag{B.33}$$

[2]The K values are tuned. Zhang *et.al* suggest $k_x = k_y = 3$. Values in the range of 2 to 24 give good tracknig depending on the trajectory curvature. Gain scheduling allows to change the gains depending on the tracking error. For x or y tracking error in excess of 0.8m gain of 2 is used, for 0.5m $\rightarrow$ 7, for 0.15m $\rightarrow$ 20, and 24 otherwise.

Similarly the relation for the left wheel velocity is:

$$V_L = \left(cos\gamma + \frac{b \cdot sin\gamma}{2l} \right) V_S \tag{B.34}$$

From the Equations B.33 and B.34 the expression for the steering angle and steering wheel linear speed are obtained in terms of the front wheel linear speeds:

$$\gamma = arctan\left(\frac{V_L - V_R}{V_L + V_R} \cdot \frac{2l}{b} \right) \tag{B.35}$$

$$V_S = \frac{V_L + V_R}{2cos\gamma} \tag{B.36}$$

Assuming identical wheel radii for all wheels the Equation B.36 can be written in term of the angular velocities:

$$\gamma = arctan\left(\frac{\dot{\theta}_L - \dot{\theta}_R}{\dot{\theta}_L + \dot{\theta}_R} \cdot \frac{2l}{b} \right) \tag{B.37}$$

$$\dot{\theta}_S = \frac{\dot{\theta}_L + \dot{\theta}_R}{2cos\gamma} \tag{B.38}$$

The performance of the modified tracker is comparable to that of the *pure pursuit* tracker [90]. The pure pursuit tracker will be used in the simulator due to its relative simplicity and robustness.

APPENDIX C

Other Absolute Localization Modalities

A development of a reliable, accurate and inexpensive local positioning system (LPS) for the areas with no or poor GPS coverage for forest, urban canyon, underground, or capacious indoor environments is still an open research problem. The use of the infrared identification tags (IRID) attempted in the nineties did not lead to a development of a robust LPS [112, 110]. The first promising LPS for the autonomous robot localization use custom hardware: the range and bearing MilliMeter Wave Radar (MMWR)[42] and the range only radar [56]. The radio frequency (RF) navigation aids are desirable for the absolute localization since they operate robustly around the clock and at various atmospheric conditions [54].

RADAR absolute Local Positioning System (LPS) localization system presented by Paramvir Bahl and Venkata N. Padmanabhan[7] is outstanding by its use of common off the shelf hardware only – the Radio Frequency (RF) wireless Digital RoamAbout^{TM}WaveLAN cards (based on Lucent's WaveLAN^{TM}). The positioning and dynamic tracking is done by triangulation on the basis of the LAN card antenna signal strength. Four computers : three base stations running FreeBSD 3.0 and a Pentium-based Windows laptop all equipped with the wireless Network Interface Card (NIC) were used in the experiments. WaveLan NIC makes available the signal strength (SS) and the signal-to-noise ratio (SNR). FreeBSD WaveLAN driver extracts

the SS and SNR information every time a packet of information is received. The information is subsequently processed by a localization algorithm. The system was tested indoors and accuracies of 1m and 3.5m were obtained for static and dynamic localization respectively. Outdoor experiments would reveal how well the system can localize in the line-of-site environment. Use of regular wireless cards for the localization adds value to such a network and makes a fuller use of its capabilities.

APPENDIX D

Image Processing at CMU

The image processing was done at Carnegie Mellon University (CMU), by Parag Batavia and Jeff Mishler. The following account is included here for completeness of the visual absolute marker experimet description. Figure D.1 shows a typical camera

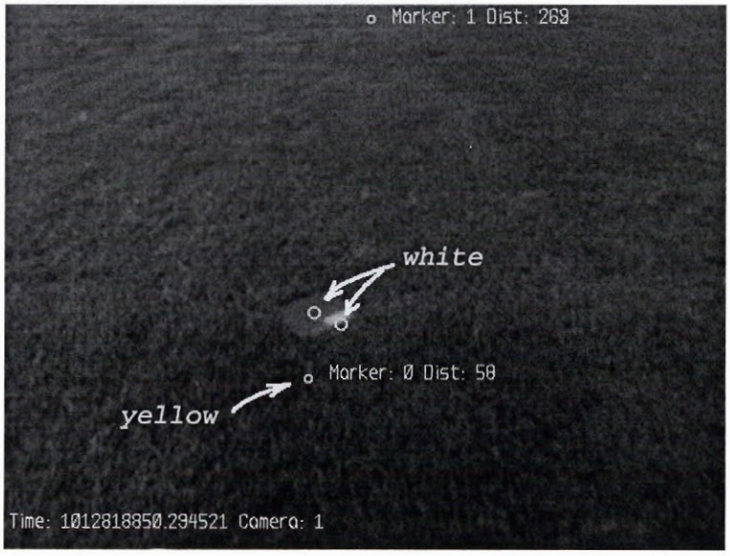

FIGURE D.1. A typical frame taken by the on-board camera. The colors of the circles are indicated in the figure.

image collected by a Sony DFW-VL500 [98] FireWire CCD camera mounted on the mower.

The mower was driven on a spiral pattern on a field with 28 markers placed at roughly six meter intervals. During the motion 181 image points were extracted and

181 sets of angles are produced using the estimated pose, extracted image points, camera intrinsic and extrinsic parameters, and the marker map.

- The image name, camera ID, and time stamp are written to a text file as images are obtained and time stamped.
- The position information is logged with a time stamp as well, but the image and position time stamps are not identical. To associate the position information with the image, the first position time stamp which is greater or equal to the image time stamp is taken. This gives a reasonable approximation because the position data is obtained more frequently (about 100 Hz versus 0.5 Hz) than the image data.
- The images are run through a segmentation process to obtain the observed marker positions, which correspond to the white circles in the images. They should always line up with the marker in the image, but depend on the quality of the segmentation and may include false positives or missed targets.
- The identity of the markers observed in the image is established. To identify the markers and determine where the target should appear in the given image the information about the vehicle's location, the marker locations, and the camera locations is used. This involves projecting the 3D marker position onto the camera's image plane, and corresponds to the yellow circles in the images. If all the data were perfect (segmentation, vehicle position, marker location, camera extrinsic and intrinsic parameters) the yellow circle would be inside the white circle. Our data is not perfect, so the yellow circles do not fall exactly on the white circles. The marker ID of the closest yellow circle (that is less than 64 pixels away from the white circle) is associated with this image observation. (This step can be eliminated if we have barcodes or other means of performing this data association.)
- If there is a successful match, the angles to this marker are computed and stored along with the time stamp in the "Marker angles" file.

APPENDIX E

SX-I Interface

CSI SX-I DGPS card requires TTL to RS-232 level conversion, 3.3 V for DGPS circuitry, 12 V for the antenna, and 3.3 V backup power. To meet these requirements in a compact package a plug-in interface was designed to fit directly over the DGPS card. The board scematic and the printed circuit board layout are shown in Figures E.1, E.2 The interface board parts and their prices as of October 2002 are given in Table E.1. The interface board has the same physical size as the DGPS card and is stacked on top of it and secured by four bolts as shown in Figure E.3 on page 82.

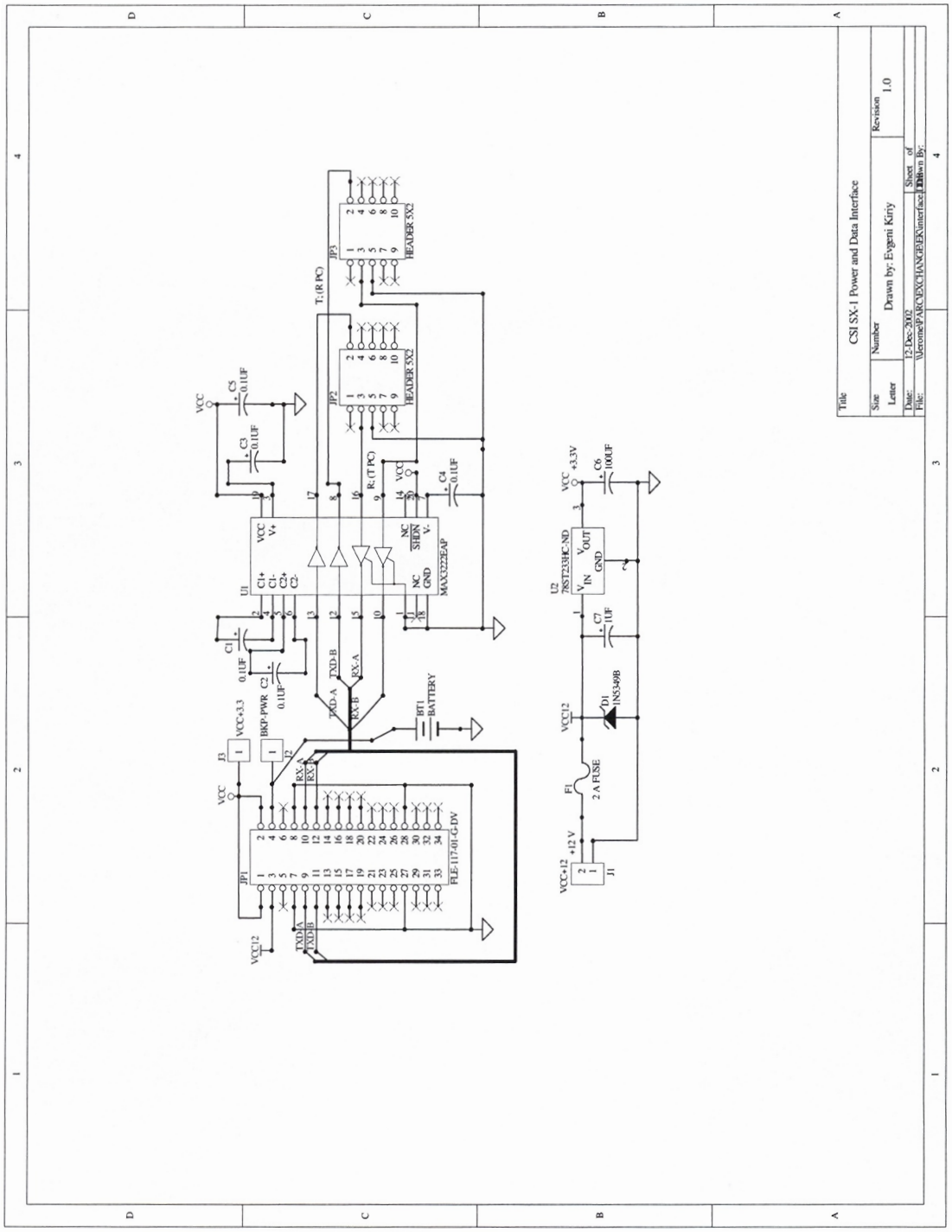

FIGURE E.1. Schematic of the interface card.

TABLE E.1. Bill of Materials for the SX-I interface.

SX-I interface board components					
	Description	DigiKey PN	Unit price	Quantity	Total
1	TIA/EIA-232-F (RS232) D/R	296-13086-1-ND	3.38	1	3.38
2	C1-C4 (0.1 mF) bypass cap.	399-1439-ND	0.45	4	1.80
3	switching regulator (3.3V 2A)	78ST233HC-ND	18.42	1	18.42
4	tantalum cap. C1 (1 mF)	399-1337-ND	0.41	1	0.41
5	tantalum cap. C2 (100 mF)	399-1475-ND	4.14	1	4.14
6	Fuse block (2 A)	F1224CT-ND	1.89	1	1.89
7	FFSD-series 34-pin connector	FLE-117-01-G-DV	13.32	1	13.32
8	MCX antenna connector	919-103P-51AX	32.00	1	32.00
9	Coin cell battery holder	103K-ND	1.91	1	1.91
10	Coin Lihtium battery 20 *mm*	P186-ND	2.29	1	2.29
11	Silicon Zener diod (12V, 5W)	1N5349BMSCT-ND	0.80	1	0.80
12	10-pin 2.54 × 2.54 header	MHB10K-ND	1.33	2	2.66
12	Term. block 5.08 *mm* Header	ED2427-ND	1.10	1	1.10
12	Term. block 5.08 *mm* Plug	ED1717-ND	1.05	2	2.10
15	interface PCB	SX-1 INTERFACE	71.30	1	71.30
				Total per board (CAD)	157.52

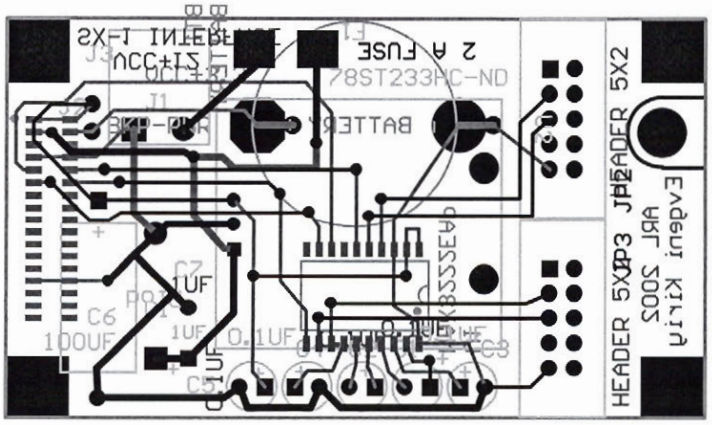

FIGURE E.2. Printed Circuit Board Layout of the interface card.

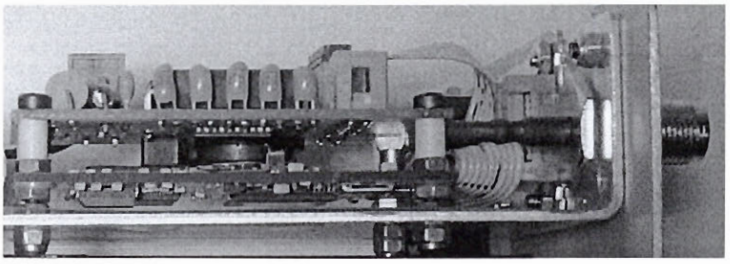

(a) The side view

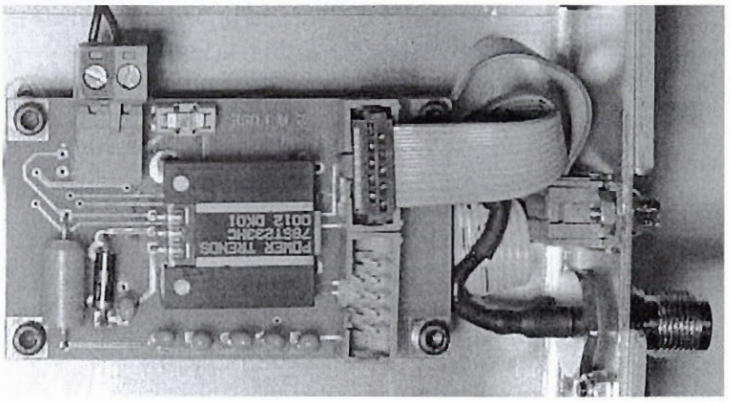

(b) The top view

FIGURE E.3. The CSI SX-I and the interface board with connections.

APPENDIX F

Hiding Visual Beacon

The visual beacon mentioned in Subsection 1.2 of Chapter 4 has to meet the following requirements:

- it has to be flush with the ground and have a small footprint in order not to obstruct the view when not in use;
- it must be visible out of the grass to be detected by the mower camera(s);
- the beacon must hide from the mower blades.

The proposed beacon can be enclosed in an emptied sprinkler head housing. The beacons can be remotely commanded to extract out of their housings at the beginning of the mowingn the grass) once the mower approaches the beacon and the beacon is no longer in the field of view of the mower, the beacon retracts to avoid the mower blades. The retraction occurs as a response to an elevated noise level near the mower: the beacon would have a noise-sensor calibrated to the noise level at 2-3 m from the mower. The retraction speed should be approximately: t_{min}=(2 m)/(6 m/s)=0.11 s (minimal hiding time); for height up to 15 cm = 0.15 m the servo max. velocity should be (0.15 m)/(0.11 s)=1.36 m/s; the retraction can be performed faster if a recoil spring is used and the servo motor only raises the marker. Raising speed is not a critical factor, though the faster the marker reappears in the camera vision field, the better the localization will be.

APPENDIX G

Data Sheets

GPS Sensor Specifications

Receiver Type:	L1, C/A code, with carrier phase smoothing
Channels:	12-channel, parallel tracking (10-channel when tracking WAAS)
WAAS Tracking:	2-channel, parallel tracking
Update Rate:	5 Hz max
Horizontal Accuracy:	<1 m 95 confidence (DGPS*) <5 m rms confidence** (no SA)
Cold Start:	60 s (no almanac or RTC***)
Warm Start 1:	45 s (valid almanac, no RTC)
Warm Start 2:	35 s (valid almanac and RTC)
Hot Start:	20 s (valid almanac, RTC, and < 2 hours since last fix):
Reacquisition:	< 1 s
Maximum Speed:	1607 kph (999 MPH)
Maximum Altitude:	18,288 m (60,000 ft)

Communications

Serial ports:	2 full duplex RS-232
Baud Rates:	4800, 9600, 19200
Correction I/O Protocol:	RTCM SC-104
Data I/O Protocol:	NMEA 0183, SLX binary
Timing Output:	1 PPS (HCMOS, active low, rising edge sync, 10 kΩ, 10 pF load)
Event Marker Input:	HCMOS, active low, falling edge sync, 10 kΩ, 10 pF load

Environmental

Operating Temperature:	-30°C to +70°C
Storage Temperature:	-40°C to +85°C
Humidity:	95% non-condensing
Shock:	EP 455
Vibration:	EP 455

Power

Input Voltage:	3.3 VDC +- 5%
Power Consumption:	700 mW nominal
Current Consumption:	210 mA nominal
Antenna Voltage Input:	15 VDC maximum
Antenna Short Circuit Protection:	Yes
Antenna Gain Input Range:	10 to 40 dB
Antenna Input Impedance:	50 Ω

Mechanical

Dimensions:	<71.1 mm L x <40.6 mm W x <12 mm H (<2.8" L x <1.6" W x <0.5" H)
Weight:	<113 g (<4 oz)
Status Indication:	4 surface-mount LED's indicating power, GPS lock, Differential lock, and DGPS position
Power/Data Connector:	34-pin male header, 0.05" pitch
Antenna Connector:	MCX, female, straight (right angle available)

Pin-out

Pin 1	Power in (3.3 VDC +-5%)	**Pin 2**	Power in (3.3 VDC +-5%)
Pin 3	Antenna power 15 VDC max[1]	**Pin 4**	Backup Power[2]
Pin 5	Do not connect	**Pin 6**	Do not connect
Pin 7	Ground	**Pin 8**	Ground
Pin 9	TXD Port A[3]	**Pin 10**	RX Port A[3]
Pin 11	TXD Port B[3]	**Pin 12**	RX Port B[3]
Pin 13	TXD Port C[3]	**Pin 14**	RX Port C[3]
Pin 15	1 PPS output	**Pin 16**	Manual mark input[4]
Pin 17	GPS lock indicator[4]	**Pin 18**	Differential lock indicator[4]
Pin 19	DGPS position indicator[4]	**Pin 20**	ARM boot select
Pin 21	Do not connect	**Pin 22**	Do not connect
Pin 23	Do not connect	**Pin 24**	Do not connect
Pin 25	DSP boot select	**Pin 26**	Do not connect
Pin 27	Ground	**Pin 28**	Ground
Pin 29	Do not connect	**Pin 30**	Do not connect
Pin 31	Do not connect	**Pin 32**	Do not connect
Pin 33	Do not connect	**Pin 34**	Do not connect

Notes:
1. 100 mA max
2. 2.7 to 5 VDC, 10 uA consumption nominal
3. Transmit and receive referenced to the receiver
4. 1 mA max, requires external buffering

* SVs > 5, HDOP < 2, RTCM SC-104 correction data from a dual frequency reference station, short baseline, and low multipath environment.

** Dependent upon ionospheric activity and multipath

*** Real-time clock

FIGURE G.1. CSI Wireless SX-I WAAS DGPS data sheet [25]. Note: The correctness of the pinout in the above data sheet was verified; there exist versions of SX-I data sheet with a different pinout.

REFERENCES

[1] *Atlas Copco Wagner LHD ST1810*, http://www.atlascopcowagner.com/vehicles/, November 2002.

[2] 3M, http://www.3m.com/us/safety/tcm/contact/index.jhtml, *Magnetic Lateral Warning and Guidance Tape*, 2001.

[3] A.Gelb, J.F.Kasper, R.A.Nash, C.F.Price, and A.A.Sutherland, *Applied optimal estimation*, The MIT Press, Cambridge, Massachusetts, 1974.

[4] A.Papoulis, *Probability, Random Variables, and Stochastic Processes*, McGraw-Hill Series in Systems Science, McGraw-Hill Book Company, Inc., New York, USA, 1965.

[5] Arc Second, http://www.arcsecond.com/products/products.php, *Vulcan 3D Measurement System*, November 2002.

[6] Viktor P. Astakhov, *Metal cutting mechanics*, Crc Press, 1999.

[7] Paramvir Bahl and Venkata N. Padmanabhan, *RADAR: An In-Building RF-based User Location and Tracking System*, Proceedings of the IEEE Infocom 2000 (Tel-Aviv, Israel), vol. 2, IEEE, March 2000, pp. 775–784.

[8] Y. Bar-Shalom, K. C. Chang, and H. A. P. Blom, *Tracking a Maneuvering Target Using Input Estimation vs. the Interacting Multiple Model Algorithm*, IEEE Transactions on Aerospace and Electronic Systems **25** (1989), 296–300.

[9] Yaakov Bar-Shalom, X. Rong Li, and Thiagalingam Kirubarajan, *Estimation with Applications to Tracking and Navigation*, 2001.

[10] Yaakov Bar-Shalom and Xiao-Rong Li, *Multitarget-Multisensor Tracking: Principles and Techniques*, YBS, 1995.

[11] Billur Barshan and Hugh F.Durrant-Whyte, *An Inertial Navigation System for Mobile Robot*, Proceedings of the 1993 IEEE/RSJ International Conference on Intelligent Robots and Systems (Yokohama, Japan), IEEE/RSJ, 26-30 July 1993, pp. 2243–2248.

[12] Parag Batavia, Stephan Roth, and Sanjiv Singh, *Automated turf management progress report: Q4 2000*, Tech. report, Carnegie Mellon University, National Robotics Engineering Consortium, 2000.

[13] ———, *Preliminary report on obstacle detectioon for coverage operations*, Tech. report, Carnegie Mellon University, National Robotics Engineering Consortium, 5000 Forbes Avenue, Pittsburgh, PA, USA, March 2000.

[14] ———, *Automated turf management progress report: Q4 2001*, Tech. report, Carnegie Mellon University, National Robotics Engineering Consortium, 11 April 2001.

[15] ———, *Automated turf management progress report: Q4 2001*, Tech. report, Carnegie Mellon University, National Robotics Engineering Consortium, 9 January 2001.

[16] Billur Barshan and Hugh F. Durrant-Whyte, *Inertial navigation systems for mobile robots*, IEEE Transactions on Robotics and Automation **11** (1995), no. 3.

[17] Philippe Bonnifait and Gaetan Garcia, *A Multisensor Localization Algorithm for Mobile Robots and its Real-Time Experimental Validation*, Proceedinds of the 1996 IEEE International Conference on Robotics and Automation (Minneapolis, USA), IEEE, April 1996, pp. 1395–1400.

[18] Mohammad Bozorg, Eduardo M.Nebot, and Hugh F.Durrant-Whyte, *A Decentralised Navigation Architecture* , Proceedings of the 1998 IEEE International Conference on Robotics and Automation (Leuven, Belgium), IEEE, May 1998, pp. 3413–3418.

[19] Alison Brown, Neil Gerein, and Keneth Taylor, *Modeling and Simulation of GPS Using Software Signal Generation and Digital Signal Reconstruction*, Proceedings of the ION National Technical Meeting (Anaheim, CA, USA), ION, January 2000.

[20] Ip Ki Choi, *Pseudolite Research at UNSW*, 1st Hong Kong Symposium on Satellite Positioning System Applications (Hong Kong), 11 December 1999.

[21] The Toro Company, Toro Advantage (2001), no. 2.

[22] ———, Toro Advantage (2002), no. 4.

[23] ———, Toro Advantage (2002), no. 5.

[24] Fabio Cozman and Eric Krotkov, *Robot localization using a computer vision sextant*, IEEE International Conference on Robotics and Automation, vol. 1, May 1995, pp. 106–111.

[25] CSI wireless, http://www.csi-wireless.com, *SX-I Compact, submeter GPS and SBAS module*, February 2002.

[26] A. Doucet, N.de Freitas, and N. Gordon, *Sequential Monte Carlo Methods in Practice*, Springer-Verlag New Yourk, Inc., New Yourk, USA, 2001.

[27] Gregory Dudek and Michael Jenkin, *Computational Principles of Mobile Robotics*, no. ISBN: 0521568765, Cambridge University Press, May 2000.

[28] Hugh Durrant-White, *Australian Centre for Field Robotics Annual Report*, Tech. report, The University of Sydney, 2001.

[29] Dynaher Corporation, http://www.dynapar-encoders.com, *Dynapar encoder series H20 data sheet.*

[30] F.Lu and E.Milios, *Robot pose estimation in unknown environments by matching 2d range scans*, Journal of Intelligent and Robotic Systems **18** (1997), 249–275.

[31] James L. Crowley Frédéric Chenavier, *Position Estimation for Mobile Robot Using Vision and Odometry*, IEEE International Conference on Robotics and Automation (Nice, France), IEEE, May 1992.

[32] Yasutaka Fuke and Eric Krotkov, *Dead Reckoning for a Lunar Rover on Uneven Terain*, Proceedings of the 1996 IEEE International Conference on Robotics and Automation (Minneapolis, USA), vol. 1, IEEE, April 1996, pp. 411–416.

[33] Jakov Gelfandbein, *Ieee senior member*, 2002, personal communication.

[34] Puneet Goel, Stergios I.Roumeliotis, and Gaurav S.Sukhtme, *Robust Localization Using Relative and Absolut Position Estimates*, Proceedings of the 1999 IEEE/RSJ Intenational Conference on Intelligent Robots and Systems, vol. 2, IEEE/RSJ, 1999, pp. 1134–1140.

[35] G.Petryk and M.Buehler, *Dynamic Object Localization via Proximity Sensor Network*, Proceedings of the IEEE/SICE/RSJ International Conference on Multisensor Fusion and Integration for Intelligent Systems, IEEE, SICE, RSJ, 1996, pp. 337–341.

[36] Donald T. Greenwood, *Principles of dynamics*, second ed., Prentice-Hall, Inc., Englewood Cliffs, New Jersey 07632, 1988.

[37] Jens-Steffen Gutman, Wolfram Burgard, and Dieter Fox Kurt Konolige, *An Experimental Comparison of Localization Methods*, International Conference on Intelligent Robots and Systems, IROS'98, October 1998.

[38] J.-S. Gutmann and D. Fox, *An Experimental Comparison of Localization Methods Continued*, IEEE/RSJ International Conference on Intelligent Robots and Systems (IROS'02) (Lausanne, Switzerland), IEEE/RSJ, (to appear) 2002.

[39] Jens-Steffen Gutmann, *Digital creatures laboratory, sony corporation*, personal communication, 16 August 2002.

[40] Yoshiro Hada, Kunikatsu Tkase, and Kouji Ohgaki, *Indoor NAvigation of Multiple Mobile Robots in a Dynamic Environment Using iGPS*, Proceedings of the 2002 IEEE Interanational Conference on Robotics and Automation (Washington, DC, USA), IEEE, May 2002, pp. 2682–2688.

[41] Parag H.Batavia, Stephan A.Roth, and Sanjiv Singh, *Autonomous Coverage Operations In Semi-Structured Outdor Environment*, Proceedings of the 2002 IEEE/RSJ International Conference on Intelligent Robots and Systems, IROS 2002 (Lausanne, Swiss), IEEE/RSJ, October 2002.

[42] H.F.Durrant-Whyte, *An autonomous guided vehicle for cargo handling applications*, The International Journal of Robotics Research **15** (1996), no. 5, 407–440.

[43] Honeywell, http://www.ssec.honeywell.com/magnetic/datasheets/hmr3000.pdf, *HMR3000 data sheet*, 1999.

[44] H.R.Everett, *Sensors for mobile robots: Theory and application*, A K Peters, Ltd., 289 Linden Street, Wellesley, MA 02181, USA, 1995.

[45] Ian Humphrey and Christopher Reynolds, *Vehicle Integrated Navigation Sytem*, The Satellite Division of the Institute of Navigation 14^{th} International Technical Meeting (Salt-Lake City, Utah), Fibersense Technology Corporation, Institute of Navigation, September 2001.

[46] H.W.Sorenson, *Kalman Filtering: Theory and Application*, IEEE Press, New York, USA, 1985.

[47] Karl Iagnemma and Steven Dubowsky, *Mobile robot Rough-Terrain Control (RTC)for Planetary Exploration*, Proceedings of the 2000 ASME IDETC/CIE: 26th Biennial Mechanisms and Robotics Conference, DETC 2000 (Baltimore, Maryland), ASME, 10-13 Septembef 2000.

[48] Stergio I.Roumeliotis and George A.Bekey, *Bayesian estimation and kalman filtering: a unified framework for mobile robot localization*, Proceedings of the Iternational Conference on Automation anf Robotics (San Francisco, CA, USA), IEEE, April 2000, pp. 2985–2992.

[49] Neimark Urii Isaakovitch and Fufaev Nikolai Alekseevich, *Dynamics of nonholonomic systems*, Translations of Mathematical Monographs, vol. 33, AMS, Providence, Rhode Island, 1972, translated from the Russian by J.R. Barbour.

[50] J.Borenstein, H.R.Everett, and L.Feng, *Navigating mobile robots: Systems and techniques*, A.K.Peters, Ltd.,, 289 Linden Street, Wellesley, MA 02181, 1996.

[51] Simon J.Julier, *Process Models for the Navigation of High-Speed Land Vehicles*, Ph.D. thesis, Robotics Research Group, Department of Engineering Svience,Wadham College, University of Oxford, United Kingdom, 1997.

[52] Simon J.Julier and Hugh F.Durrant-Whyte, *On the Role of Process Models in Autonomous Land Vehicle Navigation Systems.*

[53] John J.Leonard and Hugh F.Durrant-Whyte, *Mobile Robot Localization by Tracking Geometric Beacons*, IEEE Transactions on Robotics and Automation **7** (1991), no. 3, 376–382.

[54] J.L.Farrell, *Integrated aircraft navigation*, Academic Press, Inc., San Diego, California, 1976.

[55] J.M.Armingol, L.Moreno, A.de la Escalera, and M.A.Salichs, *Landmark perception Planning for Mobile Robot Localization*, Proceedings of the 1998 IEEE Intenational Conference on Robotics and Automation (Leuven, Belgium), IEEE, May 1998, pp. 3425–3430.

[56] George Kantor and Sanjiv Singh, *Preliminary Results in Range-Only Localization and Mapping*, Proceedings of the 2002 IEEE International Confernce on Robotics and Automation (Washington, DC, USA), IEEE, May 2002, pp. 1818–1823.

[57] Alonzo Kelly, *General Solution for Linearized Error Propagation in Vheicle Odometry*, Proceedings of the 2002 IEEE International Symposium of Robotics Research (Maui, Hawaii), IEEE, 9-12 November 2001.

[58] K.Iagnemma and S.Dubowsky, *Terrain Estimation for High-Speed Rough-Terrain Autonomous Vehicle Navigation*, Proceedings of the SPIE Conference on Unmanned Ground Vehicle Technology IV (Orlando, Florida), vol. 4715, IEEE, 1-5 April 2002.

[59] Evgeni Kiriy and Martin Buehler, *Automated Turf Management Progress Report Q1, 2001*, Tech. report, McGill University, Montreal, Canada, 30 April 2001, Internal document.

[60] KVH Industries, Inc., *KVH E-Core 2000 brochure*, 1998.

[61] KVH Industries, Inc., http://www.kvh.com/Products/Product.asp?id=39, *KVH E-Core 2060 data sheet*, 2000.

[62] Thomas Dall Larsen, MArtin Bak, Nils A.Andersen, and Ole Ravn, *Location Estimation for an Autonomously Guided Vehicle Using an Augmented Kalman Filter to Autocalibrate the Odometry*, International Conference on Multisource-Multisensor Information Fusion (Las Vegas, NV,USA), CSREA Press, 6-9 July 1998.

[63] Ulf Larsson, Johan Forsberg, and Ake Wernersson, *Mobile Robot Localization: Integrating Measurements from a Time-of-Flight Laser*, IEEE Transactions on Industrial Electronics **43** (1996), no. 3, 422–431.

[64] Ulf Larsson, Caj Zell, Kalevi Hyyppa, and Ake Wernersson, *Navigating an Articulated Vehicle and Reversing with a Trailer*, Proceedings of the 1994 IEEE International Conference on Robotics and Automation (San Diego), IEEE, May 1994, pp. 2398–2404.

[65] James L.Crowley, *Mathemtical Foundations of Navigation and perception for an Autonomous Mobile Robot*, Workshop on Reasoning with Uncertainty in Robotics (Netherlands), University of Amsterdam, 4-6 December 1996.

[66] Don Lerro and Yaakov Bar-Shalom, *Tracking With Debiased Consistent Converted Measurements Versus EKF*, IEEE Transactions on Aerospace and Electronic Systems **29** (1993), no. 3, 1015–1022.

[67] Lennart Ljung and Torsten Soderstrom, *Theory and practice of recursive identification*, The MIT Press, Cambrige, Massachusetts, 1983.

[68] L.Ljung, *Modeling of dynamic systems*, Prentice-Hall Information and System Science Series, PTR Prentice Hall, Englewood Cliffs, NJ, 1994.

[69] Tom Logsdon, *Understanding the Navstar GPS, GIS and IVHS*, second ed., Van Nostrand Reinhold, 1995.

[70] Jim Louderback, Annaliza Savage, and Patrick Norton, *Golfpro international intelecady*, http://www.techtv.com/freshgear/products/story/0,23008,2119274,00.html, July 1998.

[71] Feng Lu and Evangelos Milios, *Robot Pose Estimation in Unknown Environments by Matching 2D Range Scans*, Journal of Intelligent and Robotic Systems **18** (1997), 249–275.

[72] Raj Madhavan, Hugh Durrant-Whyte, and Gimini Dissanayake, *Natural Landmark-Based Autonomous Navigation Using Curvature Scale Space*, Proceedings of the 2002 IEEE International Conference on Robotics and Automation (Washington, DC, USA), IEEE, May 2002, pp. 3936–3941.

[73] Rommel E. Mandapat, *Performance Comparison of the MAPS/Astech position system versus the Novatel Beeline GPS system using CIMAR's Navigation Test Vehicle*, Tech. report, University of Florida, 2000.

[74] McGillem, *Comparison of Two-Sensor Tracking Methods Based on State Vector Fusion and Measurement Fusion*, IEEE Transactions on Aerospace and Electronic Systems **24** (1988), no. 4, 447–457.

[75] Randall Smith nd Peter Cheeseman, *On the Representation and Estimation of Spatial Uncertainty*, The International Journal of Robotics Research **5** (Winter 1986), no. 4, 56–68.

[76] NovAtel Inc., http://www.novatel.com/Documents/Papers/Rt-2.pdf, *NovAtel ProPack data sheet*, 2000.

[77] Lauro Ojeda, Hakyoung Chung, and Johann Borenstein, *Precision-Calibration of Fiber-Optics Gyroscopes for Mobile Robot Navigation*, Proceedings of the 2000 IEEE International Conference on Robotics and Automation (San Francisco, CA, USA), IEEE, 24-28 April 2000.

[78] Mark Ollis and Anthony Stentz, *Vison-Based Perception for an Automated Harvester*, Proceedings of the 1997 IEEE/RSJ International Conference on Intelligent Robotic Systems, IEEE/RSJ, September 1997.

[79] Kyu Cheol Park, Dohyoung Chung, Hakyoung Chung, and Jang Gyu Lee, *Dead Reckoning Navigation of a Mobile Robot Using an Indirect Kalman Filter*, International Conference on Multisensor Fusion and Integration for Intelligent Systems (Washington D.C. USA), IEEE/SICE/RSJ, IEEE, December 8-11 1996, pp. 132–138.

[80] Cedric Pradalier and Sepanta Sekhavat, *"Localization Space": a Framework for Localization and Planning, for Sytems Using a Sensor/Landmarks Module*, Proceedings of the 2002 IEEE International Conference on Robotics and Automation (Washington, DC, USA), IEEE, May 2002, pp. 708–713.

[81] P.S.Maybeck, *Stochastic Models, Estimation, and Control*, Mathematics in Science and Engineering: A Series of Monographs and Textbooks, vol. 141, Academic Press, Inc., New York, USA, 1979.

[82] Pyxis Corporation, http://www.pyxis.com/products/helpmate.asp, *HELPMATE ®, the Trackless Robotic Courier*, November 2002.

[83] R.E.Kalman, *A New Approach to Linear FIltering and Production Probems*, Journal od Basic Engineering (1960), 35–45.

[84] Ioannis Rekleitis, *Cooperative Localization and Multi-Robot Exploration*, Ph.D. thesis, McGill University, Montreal,Canada, 2002.

[85] Murray R.M., Li Z., and Sastry S.S., *A Mathematical Introduction to Robotic Manipulation*, CRC Press, 1994.

[86] ROBOSOFT, http://www.robosoft.fr/SERVICE/01_FloorCR/01AutovacC6/AutovacC6.ht *Automation Kit for a cleaning machine*, November 2002.

[87] ROBOSOFT, http://www.robosoft.fr/SERVICE/01_FloorCR/01AutovacC6/AutovacC6.ht *AutoVacC 6: the autonomous industrial vacuum cleaner*, November 2002.

[88] J.A. Roecker and C.D. McGillem, *Target tracking in Maneuver-Centered Coordinates*, IEEE Transactions on Aerospace and Electronic Systems **25** (1989), no. 6, 836–843.

[89] Stephan Roth, Parag Batavia, and Sanjiv Singh, *Palm Aire Data Analysis*, report, February 2002.

[90] Stephan A Roth and Parag Batavia, *Evaluating path tracker performance for outdoor mobile robots*, Automation Technology for Off-Road Equipment, July 2002.

[91] Andrew Russell, David Thiel, and Alan Mackay-Sim, *Sensing Outdoor Trails for Mobile Robot Navigation*, Proceedings of the 1994 IEEE Conference on Robotics and Automation (San Diego, USA), IEEE, 1994, pp. 2672–2677.

[92] Safety Technologies, Inc., http://www.autoflagger.com/mag_sensor.htm, *Magnetic Guidance Sensor*, January 2001.

[93] Tony Sandberg, *Heavy Truck Modeling for Fuel Consumption Simulations and Measurements*, Ph.D. thesis, Division of Vehicular Systems, Department of Electrical Engineering, Linkoping University, Linkoping, Sweden, 2001.

[94] S.Chandrashekhar and R.Chellappa, *Passive Navigation in a Partially Known Environment*, IEEE Workshop on Visual Motion (Princeton, NJ), IEEE, October 1991, pp. 2–7.

[95] S. Scheding, G. Dissanayake, E. Nebot, and H. Durrant-Whyte, *Slip Modelling and Aided Inertial Navigation of an LHD*, IEEE International Conference on Robotics and Automation, 1997.

[96] Steve Scheding, E. Nebot, M. Stevens, H. Durrant-Whyte, J. Roberts, P. Corke, J. Cunningham, and B. Cook, *Experiments in autonomous underground guidance*, Proceedings of the IEEE Int. Conf. on Robotics and Automation, 1997.

[97] James Andrew Smith, *A Tracking System for a Seismic Surveying Mobile Robot*, Master's thesis, University of Alberta, 2001.

[98] Sony, http://www.sony.co.jp/en/Products/ISP/pdf/catalog/DFWV500E.pdf, *Sony DFW-VL500 Digital Camera Module data sheet.*

[99] S.Scheding, E.M.Nebot, and H.F.Durrant-Whyte, *High integrity navigation: A frequency-domain approach*, IEEE Transaction on Control Systems Technology **8** (2000), no. 4, 676–694.

[100] S.Thrun, *Bayesian landmark learning for mobile robot localization*, Machine Learning **33** (1998), no. 1, 41–76.

[101] Kenji Tashiro, Jun Ota, Yeuan C.Lin, and Tamio Arai, *Design of the Otimal Arrrangement of Artificial Landmarks*, Proceedings of the 1992 IEEE International Confernce on Automation and Robotics, vol. 1, IEEE, June 1995, pp. 407–413.

[102] Tern Inc., http://www.tern.com, *AE-40 (40MHz)*, 2001.

[103] Tern Inc., http://www.tern.com, *P100*, 2001.

[104] The Toro Company, *Greensmaster®3200/3200-D Service Manual*, 1997.

[105] The Toro Company, *Precision Turf Management*, 1999, CD-ROM.

[106] The Toro Company, http://www.toro.com/golf/mower/green/ride/feature_design.html, *Greensmaster®Riding Mowers: Features: Perfect Triangle Wheel Stand Design*, November 2002.

[107] The Toro Company, http://www.toro.com/home/mowers/imow/, *Toro iMow*, November 2002.

[108] C. Ming Wang, *Localization estimation and uncertainty analysis for mobile robots*, IEEE Int. Conf. on Robotics and Automation (Philadelphia), April 1988.

[109] Jinling Wang, Liwen Dai, Toshiaki Tsujii, and Chris Rizos, *GPS/INS/Pseudolite Integration: Concepts, Simulation and Testing*, http://www.gmat.unsw.edu.au/snap/publications/wang_etal2001d.pdf, 5 March 2002.

[110] Andy Ward, Alan Jones, and Andy Hopper, *A New Location Technique for the Active Office*, IEEE Personal Communications (1997), 42–47.

[111] W.D.Blair and Y.Bar-Shalom, *Tracking Maneuvering Targets with Multiple Sensors: Does More Data Always Mean Better Estimates?*, IEEE Transactions on Aerospace and Electronic Systems **32** (1996), no. 1, 450–456.

[112] Jay Werb and Colin Lanzl, *Designing a Positioning System for Finding Things and People Indoors*, IEEE Spectrum (1998), 71–78.

[113] Yunchun Yang and Jay A. Farrell, *Magnetometer and Differential Carrier Phase GPS aided INS for Advanced Vehicle Control* , 2001 National Technical Meetings Proceedings: Look at the Changing Landscape of Navigation Technology (Long Beach, California), ION, 22-24 January 2001.

[114] Y.L.Zhang and X.Feng, *On the Tracking Control of Differentially Steered Wheeled Mobile Robots*, Journal of Dynamic Systems, Measurement, and Control **119** (1997), 455–461.

Index

Document Log:

Manuscript Version 0

Typeset by $\mathcal{AMS}$-LaTeX — 5 February 2003

Evgeni Kiriy

Ambulatory Robotics Lab, McGill University, 3480 University St., Montréal, Québec, Canada, H3A 2A7

Typeset by $\mathcal{AMS}$-LaTeX